NASA Contractor Report 204149

Low Speed, 2–D Rotor/Stator Active Noise Control at the Source Demonstration

John C. Simonich, Ken A. Kousen, Anthony C. Zander, and Michael Bak
United Technologies Research Center
East Hartford, Connecticut

David A. Topol
Pratt & Whitney
East Hartford, Connecticut

September 1997

Prepared for
Lewis Research Center
Under Contract NAS3–26618

National Aeronautics and
Space Administration

Table of Contents

Summary

Wake/blade-row interaction noise produced by the Annular Cascade Facility at Purdue University has been modeled using the LINFLO analysis. Actuator displacements needed for complete cancellation of the propagating acoustic response modes have been determined, along with the associated actuator power requirements. As an alternative, weighted least squares minimization of the total far-field sound power using individual actuators has also been examined. Attempts were made to translate the two-dimensional aerodynamic results into three-dimensional actuator requirements. The results lie near the limit of present actuator technology.

In order to investigate the concept of noise control at the source for active rotor/stator noise control at the source, various techniques for embedding miniature actuators into vanes were examined. Numerous miniature speaker arrangements were tested and analyzed to determine their suitability as actuators for a demonstration test in the Annular Cascade Facility at Purdue. The best candidates demonstrated marginal performance.

An alternative concept to using vane mounted speakers as control actuators was developed and tested. The concept uses compression drivers which are mounted externally to the stator vanes. Each compression driver is connected via a tube to an air cavity in the stator vane, from which the driver signal radiates into the working section of the experimental rig. The actual locations and dimensions of the actuators were used as input parameters for a LINFLO computational analysis of the actuator displacements required for complete cancellation of tones in the Purdue experimental rig. The actuators were designed and an arrangement determined which is compatible with the Purdue experimental rig and instrumentation. Experimental tests indicate that the actuators are capable of producing equivalent displacements greater than the requirements predicted by the LINFLO analysis. The acoustic output of the actuators was also found to be unaffected by the presence of air flow representative of the Purdue experimental rig.

A test of the active noise control at the source concept for rotor/stator active noise control was demonstrated. This 2-D test demonstrated conclusively the simultaneous reduction of two acoustic modes. Reductions of over 10 dB were obtained over a wide operating range.

Introduction

Rotor/stator interaction tone noise is an important part of the total noise produced by a turbofan engine. One technique which can be used to reduce these tones is active noise control.

The objective of this study was to demonstrate an active noise control application in gas turbines. The approach considered here was to mount the anti noise actuators as close as possible to the noise source. This approach seeks to achieve global noise reduction by canceling noise at the source. This concept involves embedding actuators in the fan exit guide vanes. It has been shown by Kousen and Verdon (ref. 1,2) that it is theoretically possible to completely cancel the noise of a given set of modes by employing a single actuator per acoustic mode. This approach to rotor/stator active noise control has been patented by UTC (ref. 3). Kousen and Verdon (ref. 2) developed a computational model based on the linearized unsteady flow analysis LINFLO. The model considered blade surface mounted pistons as a source of anti-sound. Complete cancellation of all propagating waves required one surface actuator per acoustic wave. The amplitude and phase of the actuators was determined through the solution of a set of complex linear equations. Kousen (ref.1) was also able to minimize the sound generation through a least-squares minimization procedure when the number of actuators was less than the number of propagating acoustic waves.

It is also possible to control the noise externally with cancellation techniques that position speakers in the engine inlet or duct casing (ref. 4). Thomas et al.(ref. 5) applied a three channel active control system to reduce fan noise radiating from the inlet of a JT15D turbofan engine. Microphones placed outside the inlet in the acoustic far-field were used for the error signals. An array of 12 horns and 24 loudspeakers mounted on the circumference of the inlet was used to generate the control sound field. A feed-forward adaptive filtered-x LMS algorithm was used. The 28 blade rotor was excited by 28 rods mounted upstream of the rotor that generated a plane wave spatial mode. With the 3 error microphones placed outside the engine, noise control was achieved within a 30° arc. However, there was an overall increase in noise.

Smith et al (ref. 6) experimentally demonstrated that multiple radial modes can be controlled by the use of multiple circumferential control source arrays. The experiment was conducted on an Pratt and Whitney JT15D engine. Four propagating radial modes of first circumferential order were generated. It was shown that better attenuation was obtained in this case than that obtained with a single array. Secondly, they also showed that an optimized control system with a single control array can yield better results than a multiple array case. Finally, experimental results show that control over a desired sector of the sound field is feasible and requires less control effort than global attenuation of the acoustic field.

A preliminary approach to active noise control considered the reduction of the unsteady forces acting on the stator. This reduction in the unsteady lift translates into a decrease in noise generation. This was demonstrated by Simonich et al.(ref.7) on an isolated airfoil with a moveable trailing edge flap. The flap represented the active aerodynamic element of the system. The flap was actuated by a servo motor and its motion controlled to reduce the unsteady lift generated by a periodic disturbance from a gust generator. The peak-to-peak acoustic dipole pressure was reduced by a factor of two and the sound pressure level was reduced by 10 dB over portions of the spectrum.

Minter, Hoyniak and Fleeter (ref. 8), Minter and Fleeter (ref. 9), and McCarthy and Fleeter (ref. 10) demonstrated active control of propagating spatial modes in a 16 blade/3 stator configuration. Both studies used near-airfoil source control and in-duct spatial mode measurements. Minter, Hoyniak and Fleeter used piezoelectric crystals to actuate airfoil surface pistons and oscillating flaps to realize maximum noise reductions of 6 dB upstream and 8 dB downstream. McCarthy and Fleeter utilized a speaker-dipole arrangement around each stator to generate additional control propagating pressure waves which interact with those generated by the rotor-stator for near source control of either the upstream or the downstream going acoustic wave. Maximum reductions of 17 dB upstream and 15 dB downstream were obtained.

Present Investigation

Objectives

The objective of this program was to prove the UTC concept for active noise control of rotor/stator interaction noise at the source. The goal was to demonstrate the simultaneous cancellation of one upstream and one downstream acoustic mode in the Purdue low speed, 2-D rotor/stator cascade facility. This demonstration was performed jointly with Purdue University.

Problem Formulation

UTC provided pretest support in the following areas: evaluation of the application of the approach in the Purdue geometry using computer simulation to predict required actuator amplitudes and locations for maximum noise cancellation, assessment of the acoustic quality of the Purdue annular cascade by acoustic radiation modeling, design of two different actuation schemes, fabrication of an actuated vane set and measurement of installed actuator performance prior to concept demonstration testing. All other aspects of the test were the responsibility of Purdue.

This report describes the effort that was made at UTRC to develop an in blade acoustic source using miniature speakers. A variety of different speakers were evaluated, however, in the end, the best of them had marginal performance. Therefore, it was decided to

develop an actuator which could be mounted outside of the vane and have the sound ported into the vane. The development of this actuator is also detailed in this report.

During the course of the experiment, the actuator requirements were determined using a linearized flow code, LINFLO. In addition to the current experiment, specifications were also required for the follow on 3-D test at NASA Lewis. These actuator requirements are also outlined in this report.

An effort was spent analyzing the acoustic characteristics of the Purdue Annular Cascade facility to determine it's merit as a test bed for aeroacoustic testing. Prior to these tests, it had only been used to examine aerodynamic phenomena.

Finally, the test at Purdue is described. This test was carried out by Scott Sawyer, a Ph.D. student of Prof. Sanford Fleeter. The results and descriptions of the experiment were provided by him.

Purdue Annular Cascade Acoustic Assessment

Radiation predictions for the Purdue thin annular rig baseline case indicate that noise is cutoff at the exit plane and in regions of the inlet at the nominal rig operating speed. Significant reflections occur in the inlet and the nozzle which will impact the ability to effectively measure mode amplitudes in the duct.

Inlet and aft radiation code predictions were made for the Purdue thin annular rig for an m = 2 mode (16 blades, 18 vanes) over a speed range of 700 - 1300 rpm. For this calculation, axial Mach number was kept constant (0.15 Mn) at the fan exit guide vane (FEGV) leading edge plane. All predictions were done with a hard wall duct. The aft plenum was not modeled, but an approximate flange was created, and the baffle was swept forward where the sides of the aft plenum begin. In addition, constant area annular duct cutoff ratio predictions were made at the FEGV leading edge, inlet plane (in the circular duct), and exit plane (where the duct meets the aft plenum).

Results indicate that noise is cutoff at the exit plane, and in the inlet near the centerbody leading edge for the m = 2 mode at a rig speed of 800 rpm. At about 1000 rpm, the m = 2 mode becomes cuton throughout the entire rig. As a result, reflections in the inlet and nozzle are quite significant. Reflections from the nozzle are the most important for this mode over the entire speed range.

It was anticipated that reflections such as these will have an important impact on the ability to effectively measure and control the mode amplitudes in the duct.

One possible solutions to this problem is to run with 15 or 17 vanes instead of 18 vanes. This gives a circumferential mode order, m = 1 which is cuton at 800 rpm. Inlet and aft radiation predictions have been made for this mode as well over a speed range of 800 -

1000 rpm. Results indicate that reflections from the nozzle continue to be at least somewhat important until the rig reaches a speed of about 1000 rpm.

Internally Mounted Actuators

Experimental Setup

The performance of a speaker is highly dependent on the type of environment in which it is located. The output of a speaker in an open chamber where the sound from the front of the speaker and interact with the out of phase sound from the rear of the speaker is vastly different from the performance in an enclosure. Likewise the size of the enclosure and sizes and types of vents also influence the output sound levels and spectral characteristics.

Early tests were all performed with the speakers mounted in a four foot square plywood baffle. The purpose of the baffle was to prevent the sound from the back of the speaker from interfering with the sound from the front of the speaker. The baffle represents an idealized case. In the Purdue rig, the speakers need to be mounted in the vanes and some sort of enclosure must be provided.

To evaluate the effect of the enclosure on the speakers performance, a small wooden enclosure was constructed with a 1.75 inch diameter, 1.75 inch deep cavity. The resulting 4.2 in^3 volume represents about 25% of total interior volume if the Purdue vanes were constructed of thin walls. (Since two speakers must be mounted in each vane, only 50% of the volume is available for each speaker and some space must be used for dividers, supports and wall thickness. To examine the effect of varying the enclosure volume, five wooden plug inserts were used to vary the volume from 1.2 to 4.2 in^3.

A large speaker enclosure was also built for testing the frequency response of miniature speakers. Enclosures of this type are typically used by speaker manufacturers to report specifications. It was therefore used to compare measured spectra to manufacture's claims. Since sound from the back of the speakers is prevented from interfering with the sound coming from the front of the speakers, the maximum sound levels are achieved using this setup.

Amplifier Evaluation

The frequency response of the 20 watt Radio Shack PA amplifier which was used to test the candidate speakers was evaluated for frequency response. White noise was input into an 8 ohm resistor at 0.1 watt of power and frequency response of the amplifier output was examined. From Figure 1, it was determined that the frequency response of the amplifier was flat to within ±2 dB over the range of 100 Hz to 10 kHz. Below 100 Hz, the response dropped drastically.

Rainbow Actuators

Hard Ceramic Material

The acoustic performance of seven hard ceramic Rainbow actuators were measured. Each of the samples was fabricated with a slightly different processing technique to see what effect this had on performance. The sound pressure level measured 1 cm away is shown in Figure 2. In general, the sound output level was relatively smooth with frequency and did not exhibit the resonant behavior which was shown in earlier displacement testing. The sound pressure amplitude increased with increasing frequency and showed a broad resonance near 700 Hz. The sound pressure level of each sample varied considerably, as much as 35 dB at resonance. At 200 Hz, the amplitudes varied from about 60 dB to 84 dB.

Two soft ceramic, 1.25 inch diameter Rainbow actuators were also tested and are shown in Figure 3. The variation between the two samples tested was much less, varying by only about 4 dB over a 50 to 500 Hz range. The actuator produced 92 dB at 200 Hz.

Rainbow actuators appear to have slightly less output at 267 Hz (BPF of the Purdue rig) than the best miniature speakers tested to date. The effect of a small enclosure of the size required to install the speakers inside the Purdue stators significantly reduces the sound output level compared to mounting the same speakers in a baffle.

The sound pressure output from a 2 inch diameter, soft piezoelectric Rainbow actuator mounted in a plywood baffle was measured. The results are shown in Figure 4. For a 213 Hz sine wave signal, the voltage was varied from 25 to 125 Vrms. The sound pressure level and the harmonic distortion rose slowly with increasing voltage. The peak output level at 213 Hz was 98 dB at 1 cm with a driving voltage of 200 Vrms and a DC offset of 175 volts. This is about the maximum voltage which could be applied without active cooling of the actuator.

The total harmonic distortion (THD) of Rainbow actuators in a large enclosure at 213 Hz has been measured for 0.015 inch thick actuators with two different diameters, 1.25 and 2.0 inches. Results are shown plotted along with other speakers in Figure 5. For both actuators, the THD increases with increasing SPL. The 1.25 inch diameter Rainbow achieved a peak SPL of 95 dB (at 1 cm) with a corresponding THD of 75%. The 2 inch Rainbow demonstrated a peak SPL of 111 dB at 50% THD. It was concluded that the Rainbows tested in commercially available sizes were not suitable for the current demonstration experiment. It should be pointed out that the Rainbows achieve their peak performance at resonance points of their natural frequencies. The resonance points of the 1.25 and the 2 inch diameter, 0.015 inch thick Rainbows are 2.3 and 1.2 Hz respectively. It may be possible to design Rainbows with optimized diameters and thickness to achieve peak performance at the lower frequencies of the current demonstration experiment.

Rainbow Actuator Structural Study

In order to better understand the performance of Rainbow actuators, a structural study was undertaken. A summary of the results is given here. A more detailed description is provided in the Appendix. From the previous actuator feasibility study, it was determined that the largest displacements of Rainbow actuators occurred at resonance. The resonance frequency was a function of the wafer diameter and thickness. Finite element methods were used to calculate the first several natural frequencies of three different sizes of Rainbow actuators under a variety of boundary conditions. Comparisons to test data indicate that the lowest frequencies are strong functions of the boundary condition along the outer edge of the actuator. By modeling the boundary conditions with vertical and rotation springs to simulate the flexible mounting material, reasonable correlation was found between test and analysis. However, different spring constants were required for each Rainbow actuator size. This structural modeling study indicates that the resonance of Rainbow actuators is strongly influenced by the type of edge mount.

The effect of hard and soft edge mounting of Rainbow actuators was investigated to see what effect mounting had on actuator displacement. Three samples of 1.25 inch diameter Rainbow actuators were mounted using the standard RTV mount used in previous studies which had RTV around the complete outer diameter. A fourth actuator was hard mounted using an epoxy around the complete diameter and a fifth was soft mounted using a three point RTV mount. The displacement was measured as the frequency was swept from 150 to 800 Hz. The results are shown in Figure 6. Some difference was noted in the displacement of the "identical" standard mounted actuators. The epoxy mounted actuator had displacements about 50% less than the standard mount. At low frequencies, the tri-mount actuator was comparable to the standard mount, but at higher frequency it had somewhat less displacement This test indicates that the complete RTV mount may be close to optimum.

The effect of enclosure volume on sound pressure level for a 1.25 inch diameter, 0.015 inch thick, soft Rainbow actuator was examined. Compared to a compliant, conventional speaker with soft mounts, the Rainbow ceramic is very stiff. It was therefore not expected that enclosure volume would have much of an effect. This proved to be true. These results are shown in Figure 7. A slight effect of enclosure volume was noted above 200 Hz. The maximum difference in SPL was about 5 dB. At 213 Hz, however, the output was only 85 to 90 dB. This ruled out the Rainbow as a candidate for this application.

Miniature Speakers

A search was performed for miniature speaker manufacturers. Catalogs were obtained and manufacturers were contacted. All the "off the shelf" speakers in the 1 inch diameter size suitable for insertion into stator vanes have resonant frequencies in the 700 to 800 Hz range. The speaker output typically drops 18 dB per octave below resonance. Since the BPF for the Purdue rig is 267 Hz, the output of these speakers may be too low for our

purpose. Three manufacturers were located who offer small speakers with flat, low frequency characteristics and resonance in the 200 to 300 Hz range. The difficulty with these speakers is that the manufacturers require a minimum purchase of 1,000 to 2,500 units and have delivery times of from one to three months. However, small samples could often be obtained from manufacturers.

The frequency amplitude characteristics of several candidate miniature speakers were evaluated in the laboratory. Each speaker was mounted in a four foot square plywood baffle and tested in an anechoic chamber. A half inch, low frequency response microphone was mounted 1 cm from the speaker. The speakers were typically tested at their maximum rated power with a swept sine wave signal. Seven speakers were tested. Of these, only 5 were probably small enough to be mounted inside a stator vane. The best candidate, a model JP302N by JEMA, produced 99 dB at 200 Hz. However, several samples of this speaker failed mechanically during very limited endurance testing at power levels as small as one third of the rated power (0.3 watts).

The displacement of the JEMA SP302N speaker was measured using the non contact measurement system developed in the first phase of this task. With a white noise input signal of 2 Vrms a mild resonant peak was observed at 90 Hz. This is somewhat lower than the manufacturer's claim of a resonant frequency of 180 Hz.

An alternate source of high quality miniature speakers is in stereo headphones. The speakers in these devices are about the right size for our application and the manufacturers claim a flat frequency response. The results for the Koss headphones are shown in Figure 8 and the Sony headphones in Figure 9. The maximum output is limited since they are intended to be operated very close to the ear. The maximum power for most headphones is only 50 to 100 mWatts. Three different models of headphones (two Sony's and one Koss) were evaluated for frequency response. All three had very flat responses over the 100 to 1000 Hz range of measurement. The best varied by 5 dB and the worst only 10 dB over that range. The highest output level was obtained from the Koss MAC/5. At 200 Hz, the sound pressure level was 102 dB at 1 cm.

Overnight endurance testing was performed on all three samples with a 213 Hz sine wave signal at the maximum rated power of each headphone. No failures were observed for any headphone.

Effect of Cavity Volume on Speaker Resonant Frequency

The effect of mounting a 1 inch diameter speaker into an enclosure was examined. Compared to a semi-infinite baffle, mounting a speaker into a closed enclosure has the effect of raising the resonant frequency. Since in our design, the objective was to produce rather low frequencies from very small speakers, the less the resonant frequency is raised, the better. Therefore the largest possible enclosure should be used to keep the resonance frequency, and the low frequency response of the speaker as low as possible. If the entire Purdue stator vane were hollow, it would have a volume of 2.9×10^{4} m^3 and would raise

the resonance frequency only 2.1%. However, if the vanes are solid and a reasonable sized cavity is used for a speaker enclosure with a volume of 1.0×10^5 m^3 (for example, a 1.25 inch diameter by .5 inch deep hole), the resonance frequency will increase by 44%.

Theoretical Analysis of Piston in Baffle

Based on earlier Task 5 measurements of the surface displacement of a miniature speaker which showed peak to peak amplitudes on the order of .01 inches, it was assumed that this amplitude would be sufficient for the Purdue rig tests which are at relatively low frequency and amplitude compared to a gas turbine engine. However, an analysis was performed to predict the required amplitude of a cylindrical piston in an infinite baffle at various frequencies to simulate a speaker. The analysis was limited to low frequencies ($ka < 1$) and far field ($r \gg a$). The unsteady pressure is described by:

$$p = \frac{\rho \omega U_0}{2\pi r}$$

The results in Figure 10 show that for a given sound pressure level, as the frequency decreased, the amplitude requirements increase dramatically. The analysis showed that at 1 kHz, it only takes ±0.023 inch displacement to produce a 100 dB sound pressure level (at a 4 foot distance). At 200 Hz, it requires a surface displacement of ±0.57 inches to produce the same sound pressure level.

Unimorph

The sound pressure level of a Radio Shack unimorph was measured in the baffle board and is shown in Figure 11. For a 15 Vrms signal, the device output 74 dB at 200 Hz. The performance at higher frequencies was much better, reaching 120 dB at a resonance of 920 Hz and 124 dB at 2.56 kHz. It appeared to be a poor candidate for the current test.

Measured Effect of Volume on Speaker Performance

The speaker from the Koss MAC/5 headphone was used to evaluate the performance of the wooden enclosure. A plot of sound pressure level vs frequency for a white noise input is shown in Figure 12. As expected from loudspeaker theory, as the volume decreased, the resonant frequency increased from 737 Hz to 2.2 kHz, with the output dropping drastically below resonance. A comparison to open space response and mounting in the baffle board is shown in Figure 13. The effect of the enclosure was also be raise the level at the resonance point about 10 dB above the baffle alone case. Below about 400 Hz however, the output leveled off at about 65 dB. This may have reached the noise floor for this experiment.

Helmholtz Resonator

A device which can be used to obtain higher sound pressure output at a given frequency is a Helmholtz resonator. The performance of such devices is dependent upon the throat diameter, throat length and cavity volume. A Helmholtz resonator was designed to fit inside the Purdue vanes. The interior volume of the vane must be divided into four regions to accommodate the Helmholtz resonator: a speaker volume and Helmholtz resonator volume for both the upstream and the downstream modes. For the resonator to be enclosed in the vane, the volume must be less than about 4 in^3. For a reasonable throat length, this restricts the throat diameter to about 0.1. Using these parameters, a model was fabricated and tested. It did not perform to expectations. One reason may have been that the throat diameter is very small, and viscous losses could be expected to be high.

Although the sound power output of individual speakers appear to be quite small, it must be remembered that there will be a total of 36 speakers installed in the rig. Based on the combined output of 36 speakers the sound level will be 15.5 dB higher than an individual speaker, and this may be within the amplitude required of the actuators.

Sound pressure level tests of miniature speakers in enclosures of the volume permitted by the size of the Purdue vanes, indicates a reduction in SPL by 6 to 9 dB compared to levels in large enclosures. Venting the back of the speakers increases the SPL by 3 dB.

Speaker Tube

The speaker concept uses a large, powerful woofer to generate sound external to the vane and pipe the sound in through a tube. A flat plate with a tube mounted perpendicular to it was attached to the face of a 12 inch woofer. The entire assembly was hung from springs in a large sound proof enclosure. (This mounting method was used to prevent speaker vibrations from generating sound on the enclosure walls.) Sound was led out of the enclosure through a .75 inch diameter tube. This diameter was selected as being about the largest diameter tube which would fit into the vane. Two different tube lengths were tested, 7.75 and 13.75 inches. The woofer was driven by a 50 watt swept sine from 25 to 1000 Hz. The results are shown in Figure 14. As expected, a large drop off in level (20 dB) was observed as the frequency increased from 25 to 50 Hz. At BPF (213 Hz), the output sound pressure level 1 cm from the tube end was 109 and 107 dB for the short and the long tubes respectively. Background noise levels measured with the tube plugged were about 18 dB lower. This is somewhat better than the performance of the best miniature speakers installed in a small enclosure. However, the performance of this concept in a vane may be less due to bending losses in the tube.

Required Amplitude

Noise levels measured by Purdue in their thin annular rig with the perforated plate rotor were 150 dB. This is far beyond the capability of miniature speakers which could be embedded into the vanes. With wakes from a real airfoil rotor, it appears that the sound power levels required is in the 110 dB range. It is possible to achieve this level with miniature speakers.

Harmonic Distortion

Six miniature speakers were tested in the large speaker enclosure, two Panasonics, two SPECOs and two RDIs. All of them were in the range of 1 to 1.5 inch diameter. Also tested in this enclosure was the Koss MAC/5 headphone speaker. The highest output measured 1 cm from the speaker at 213 Hz was the RDI HSP040BF at 112 dB. The RDI HSP-36SA output 108 dB and the Koss MAC/5 output 106 dB. The frequency response of the RDI speakers were not as flat as the Koss. The required operating frequency of 213 Hz is below the resonance frequency of both speakers. The total harmonic distortion for the highest output speaker (RDI HSP040BF) was 20% for this test condition. There may be a trade off required between low distortion and high output. A maximum acceptable distortion limit was chosen as 10% THD. The sound pressure level of several speakers with 10% THD is shown in Figure 15.

It was noticed that all of the headphones examined had vents on the back of the ear enclosure which were much larger than would be required for atmospheric pressure equalization. It was hypothesized that these were designed in to provide higher output. Substantial levels of sound come out of the vents. Test results are shown in Figure 16. The levels were found to be about 10 dB less than those from the front of the speakers.

To test the effect of a vent on the output of a speaker in a small enclosure, a .25 inch diameter hole was placed in the center of the back plate of the small wooden enclosure used previously. For the Koss MAC/5 speaker, adding the vent increased the output at 213 Hz about 3 dB to 97 dB. However, this is still about 9 dB less than that achieved in the large enclosure. See Figure 17.

The RDI HSP-40BF speaker determined above to have the largest SPL in the large enclosure was also tested in the small enclosure. The results are shown in Figure 18. At 213 Hz, the output varied from 104 to 108 dB depending on enclosure volume. This is about a 6 dB reduction from the large enclosure results.

Diaphragm displacement measurements indicate that commercially available miniature speakers may be able to achieve the amplitude requirements predicted by the LINFLO simulation for complete cancellation for real airfoil wakes in the Purdue rig. The diaphragm of miniature speakers move as rigid pistons at low frequencies, indicating they

are efficient unsteady volume sources. Perforated plates can be used as covers to preserve the aerodynamic flow over vane mounted speakers since they have negligible effect on sound transmission from the speakers. The maximum achievable sound pressure levels of miniature speakers will be limited by the allowable level of harmonic distortion. The loudest speakers may not be the best actuators.

There are two key requirements that a successful actuator must have for this demonstration: high output and low distortion. The highest output from speakers also generally occurs at the highest distortion as well. To better gauge the performance of the candidate speakers and actuators, data was acquired by driving the speakers with a 213 Hz sine wave at a range of voltages. Each actuator was mounted in a large speaker enclosure The total harmonic distortion (THD) was plotted vs the sound pressure level. Most of the speakers had 2-3% THD at their lowest operating levels and rapidly increased with increasing SPL. The two speakers with the highest output levels, the Koss MAC/5 and the RDI HSP-40BF had THD of 22% and 16% respectively at their maximum SPL levels (111 and 106 dB at 1 cm from the speaker). A representative plot of harmonic distortion vs frequency for the Koss MAC/5 headphone speaker is shown in Figure 19.

Above about 10% distortion, the output of the speakers is no longer sinusoidal in character but often appears triangular in wave form. At a limit of 10% THD, the Koss speaker had the highest output (102 dB).

Effect of Volume on Diaphragm Displacement

To better compare the speaker performance to the actuator requirements specified by the LINFLO analysis, measurements of the speaker diaphragm displacement were performed. An RDI HSP-40BF speaker was mounted in a small wooden enclosure and inserts were installed to vary the cavity volume from 1.2 to 4.2 in^3. Displacement measurements were obtained at two locations on the speaker diaphragm, the center and 12.64 mm off center. It was not possible to obtain measurements at other locations due to diaphragm corrugations in other locations which dispersed the light from the non-contact measurement sensor. These results are shown in Figures 20 and 21.

Measurements of displacement were acquired from 150 to 1150 Hz. The variation in displacement with cavity volume and frequency was complex, with regions of resonance's at some frequencies. In general, the displacements decreased with frequency from l0 to 25 mils at 200 Hz to 0.2 to 1.8 mils at 1000 Hz. At 213 Hz, the displacements at the center and off center were close to the same for small cavity volumes. They averaged about 15 mils. This indicates that the diaphragm was moving as a rigid piston at these frequencies.

A test was conducted to gauge the performance of the speakers in minimal cavities. An RDI HSP-40BF speaker was mounted in a small wooden board of the same thickness as the maximum thickness of the Purdue vane. The speaker displacement was measured with and without vent holes along the span and with zero and with minimal clearance

behind the speaker. A plot of the results are shown in Figure 22. As expected, the displacement at 213 Hz (26 mils) was highest for the case with the vented, minimal cavity. The smallest displacement (11 mils) was observed for the un-vented, zero clearance case. Based on the actuator requirements predicted by LINFLO, it appears likely that these speakers can achieve the displacement requirements.

Effect of Covers on Speaker Output

In the current design philosophy with speakers mounted into the vanes, the speakers must be covered so that there is not a cavity in the vane surface which would disrupt the air flow over the vanes. In order to preserve a reasonably aerodynamic surface on the vanes, it is suggested that the vanes be covered with a perforated plate. This will allow the air to pass over the speakers and yet not restrict the sound out of the speakers. A test of two candidate perforated plates was performed. An RDI HSP-40BF speaker was mounted in a 4.21 in^3 enclosure. A microphone was mounted 1 cm above the speaker. Samples of perforated plates were placed between the speaker and the microphone. One sample had .010 inch diameter holes and the other 0.015 inch. Both had approximately 30% open area. The speaker was driven with a sweep sine wave from 150 to 1150 Hz. A plot of the results is shown in Figure 23. No substantial difference was noted in the spectrum between the case with no plate and the perforated plate cases. Therefore, the perforated plate had a negligible effect on sound transmission.

Triple Speaker Mounting in Vane Cavities

A possible vane speaker mounting scheme was investigated. Two different speaker models were trial mounted in a vane and tested. There is sufficient space to mount three of the miniature speakers across the 6 inch span. In order to achieve the equivalent unsteady volume that was predicted from the 2-D LINFLO analysis, three speakers must have approximately 50% higher displacement than predicted for the 2-D strip of the same chordwise length as the speaker diameter. Three holes equal to the speaker diameter were machined 3/4 of the way through the airfoil at the point of maximum thickness (approximately 40% chord). A .25 inch diameter combination access/vent hole was drilled along the span to lead the wires out of the vane. The speakers were wired in parallel and driven from a single amplifier.

Frequency response sweeps were obtained for the Koss MAC/5 and the RDI HSP-40BF speakers. These are shown in Figure 24 and 25 respectively. For both speakers at low frequencies, the SPL of the vented speakers was higher than the un-vented speakers. At 213 Hz, the increase was as large as 7 dB for the RDI speakers and 3 dB for the Koss speakers. The performance of the vented speakers was dependent on mounting position. The inboard speaker was about 1.5 dB louder than the center speaker. The outboard speaker was about 1.5 dB lower than the center. For un-vented speakers, the variation in speaker output with position was considerably smaller.

Dipole vs Monipole Mounting

As has been demonstrated previously in this study, small speaker back cavity volumes reduce the sound pressure levels of speakers compared to their performance in large enclosures. A test of the acoustic performance of three Koss MAC/5 speakers installed as dipoles in the Purdue vane was performed. (The speakers were open on both the upper and the lower surface of the vane and were wired in parallel.) The dipole mount produced about 6 dB higher levels at 267 Hz compared to the output obtained from the same speakers mounted in vented cavities in the vane. The absolute level measured 1 cm away was 105 dB at 267 Hz (BPF at 1000 rpm). This was only about 2 dB less output than the level produced when the speaker was mounted in an optimum mounting environment, a very large enclosure. Therefore the dipole mount will be used to produce the highest output levels from the speakers. Speakers mounted open to the upper and lower surfaces of the vanes in a dipole mounting arrangement produce an output almost equal to that obtained if the speakers are mounted in an optimal enclosure.

In the dipole mounting arrangement, more sound is produced from the front of the speakers than the rear due to blockage by the magnet and speaker frame. A comparison of the output from the front and the rear of the speaker with and without the back covered with tape is shown in Figure 26. The difference between the front and the rear output was measured at 5.5 dB at both 213 and 267 Hz.

The surface displacement of the Koss MAC/5 speaker mounted in the Purdue vane was measured as a function of frequency for three different configurations: open front and back (dipole mount), back taped, and back taped with a vent. The results are shown in Figure 27. The corresponding displacements for the three cases at 267 Hz were 14, 11, and 13 mils peak respectively. The maximum achievable displacement drops rapidly with increasing frequency as shown in Figure 28. This is in contrast to acoustic sweeps, where SPL increases with frequency in this part of the spectrum. This effect is due to the fact that in order to produce the equivalent SPL at low frequencies, larger and larger displacements are required.

Push Pull Mounting

One method used to obtain high output from speakers in enclosures is to mount two speakers in a tube and wire them out of phase. This arrangement is known as push-pull mounting. For a dipole speaker mount in the vane, this arrangement is possible in the current geometry. Using Koss MAC/5 speakers, two different mounting arrangements were tested and compared to a single dipole mounted speaker in the vane. The first push-pull arrangement mounted the speakers with the speaker fronts facing the outside. The second arrangement had the speaker backs facing outside.

Results of these tests are shown in Figure 29. The speakers were tested both in phase and out of phase. As expected, the output from the speakers connected out of phase was significantly less than with the speakers connected in phase (7.5 dB for front facing

speakers and 20.5 dB for back facing speakers). The front facing out of phase push pull mount achieved 2 dB higher output at 267 Hz than a single dipole mounted speaker, while the back mounted push-pull mount had 3.1 dB less output. The latter result may be due to the blockage caused by the speaker magnet and supports on the back of the speaker.

Effect of Differential Diaphragm Pressure on Speaker Performance

One concern of using miniature speakers in a wind tunnel flow is the effect of angle of attack and subsequent pressure difference across the speaker. Based on Sawyer and Fleeter's measurements of steady differential pressure reported in AIAA 94-2953, the maximum pressure difference is about 8 inches of water for a 25 degree angle of attack. The effect of static pressure difference on speaker performance was investigated for two speakers with different diaphragm compliance. The speakers were mounted on the top of a one gallon container and the displacement was measured as the pressure in the container was varied above and below atmospheric. Figure 30 and 31 show the displacement at 267 Hz vs diaphragm differential pressure and displacement vs frequency for different differential pressures for the Koss headphone speaker. Figures 32 and 33 show the corresponding results for the RDI speaker.

As expected, the performance of the speakers decreased as the pressure was increased or decreased about ambient, since the voice coil is moved out of the field magnet. The speaker with the stiffer diaphragm, RDI Model HSP-40BF achieved a wider range of operation (±8 inches water) than the speaker with the more flexible diaphragm, Koss MAC/5 ±2 inches water). At 267 Hz, the peak displacement of the RDI speaker increased from 6 mils at -8 inches water to a peak of 15.5 mils at 2 inches of water and then fell to 4 mils at 8 inches of water. As the frequency was varied from 150 up to 1150 Hz, the peak displacement decreased and the difference in displacement between positive and negative pressures also decreased. These tests indicated that the RDI speakers are better candidates for use in wind tunnel flows.

Externally Mounted Actuators

Externally Mounted Compression Driver Actuator Design

In this part of the actuator study, an alternative concept to using vane mounted speakers as control actuators was developed. The concept uses compression drivers which are mounted externally to the stator vanes. Each compression driver is connected via a tube to an air cavity in the stator vane, from which the driver signal radiates into the working section of the experimental rig.

Initially it was intended that the relative dimensions of the tube connecting the driver to the vane cavity, and the vane cavity itself, would be selected such that the cavity and the tube formed a resonator which could be tuned to a desired frequency. The effect of such a

resonator can be seen in Figure 34, which shows a comparison of the acoustic output levels for a compression driver unit, and for the compression driver unit fitted with a stator vane incorporating a tube and cavity, for the same input signal power level. The sound pressure level is measured in an anechoic chamber at a distance of 1 m (39.37″) normal to the actuator. An 80 mm (3.15″) long tube of 10 mm (0.39″) diameter connected the compression driver to a 50 mm × 10 mm × 150 mm (2″ × 0.39″ × 6″) cavity which was machined in the stator vane. Figure 34 shows that at the target frequency of 267 Hz the measured sound pressure level is amplified by 12 dB with the stator vane configuration, compared to the compression driver alone. The frequency range over which the resonator is effective is also sufficiently broad to achieve the 267 Hz ± 10 % operating range specified for the experimental tests. The target frequency for the testing was determined previously, based on the geometry and the number of rotors and stators in the Purdue experimental rig (16 blades, BPF, 1000 rpm).

For the Purdue experimental rig the compression drivers would need to be mounted within the rig centerbody, and each stator vane would need to accommodate two independent cavities and connectors to two compression drivers. For the eighteen stator blades installed in the rig a total of 36 drivers is required, so that the upper and lower surfaces of each stator vane can be independently driven. The internal diameter of the rig centerbody is 940 mm (37″). An arrangement of the compression drivers within the centerbody of the experimental rig was determined for the type of compression driver selected for the application, an Atlas Soundolier PD-30T, based upon the size and number of compression drivers required and the available space in the centerbody. The orientation of the compression drivers is parallel with the longitudinal axis of the centerbody, necessitating a 90 degree bend in the connector from the compression driver to the stator vane. The connectors were designed such that the connectors are the same length for both the upper and lower surface actuators, so that the relative phase between the top and bottom surface actuators would be well matched. Because of the 90 degree bend in the connector tube and the need to use a number of components with differing internal diameters to construct the connector, it was decided to optimize the frequency response of the connector/cavity configuration experimentally.

A number of connector/cavity configurations were tested, for various combinations of tubing lengths, diameters, vane cavities, and 90 degree elbow types. Geometric constraints were imposed by the limited thickness of the stator vane, the maximum and minimum separation between the stator vane and the compression driver output coupling, and the size of the compression driver output coupling.

The source/connector/vane arrangement is shown in Figure 35, with detail of the stator vane shown in Figure 36, and detail of the compression driver to stator vane connector shown in Figure 37. The final design incorporated two cavities in the stator vane, one for the upper surface actuator and one for the lower surface actuator, with each cavity measuring 40 mm × 10 mm × 127 mm (1.58″ × 0.39″ × 5″). The connector was made from a number of common plumbing components, which were soldered together. The connector consisted of an 85 mm (3.3″) long, 8 mm (0.31″) internal diameter annealed

brass tube, joined to a 12.7 mm (0.5″) cap which was drilled to a common internal diameter with the brass tube, which was in turn joined to a 12.7 mm (0.5″) internal diameter rounded 90 degree elbow (Street EL) and a 31.8 mm (1.25″) cap, which was bonded to the compression driver output coupling with RTV silicone rubber adhesive sealant to form an airtight seal. A bonded, rather than a threaded, connector was used to attach to the compression driver output coupling so that the compression driver could be easily aligned for mounting within the centerbody.

Each of the stator vane cavities was covered with a micro-perforated screen which enabled the stator vane surface to have the correct airfoil form, and thus have minimal effect on the flow over the vane, while presenting minor resistance to the acoustic radiation from the cavity. The perforated screen had 0.25 mm (0.010″) diameter holes and 30% open area. The minimal resistance of the perforated screen in the frequency range of interest was verified by taking sound pressure measurements of the actuator with and without the perforated screen.

A computational study of active noise control applied to the Purdue experimental rig was performed for the actuator locations specified in the final design. A representative two-dimensional model was formulated and analyzed using the linearized unsteady analysis LINFLO. The LINFLO analysis is detailed in another section of this report, Active Noise Control Analysis of the Experimental Rotor-Stator Configuration at Purdue University.

Displacement requirements for the actuators were determined for complete cancellation of the generated tones, for actuators of piston length to chord ratio L/c = 0.276. The top (suction) surface actuator was located at a non-dimensional location $x_T/c = 0.224$ and the bottom (pressure) surface actuator was located at $x_B/c = 0.569$ for the analysis. The resultant displacements calculated for the three-dimensional actuators are 0.57 mm (0.02250″) for the top surface actuator and 0.24 mm (0.00996″) for the bottom surface actuator.

In the conversion from the two-dimensional analysis to the three-dimensional case, a uniform displacement over the actuator surface is assumed. The use of a two-dimensional analysis to calculate the actuator displacement requirements assumes that the actuator extends over the entire width of the stator vane. Hence it was desired that the real actuator extend over the total width of the stator vane for compatibility with the analysis. In practice, the actuator is 0.83 of the stator width.

Experimental testing

Experimental tests were conducted to determine if the externally mounted compression driver stator vane actuators could produce the required displacement levels predicted by the LINFLO computational analysis.

For the acoustic actuators it was not possible to directly measure the displacement of the actuator. Instead, an indirect measurement of the equivalent displacement of the actuator

was made by comparison with the acoustic output of a reference actuator. The tests were conducted in an anechoic chamber. The reference actuator was comprised of three RDI Model HSP-40 BF speakers mounted across the span of a stator vane. The three speakers were driven in parallel and in phase by a common voltage of 3.253 Vrms at an excitation frequency of 267 Hz. The displacement of the speaker diaphragms were measured using a non-contacting fiber-optic 88NE2 displacement sensor. In addition, the acoustic pressure was measured at a point 1 m (39.4″) normal to the speaker surface, in line with the stator vane centerline. It was thus possible to determine the acoustic transfer function from the actuator displacement to the acoustic pressure at the measurement location, at the particular excitation frequency. The measured peak displacement for this case was 0.22 mm (0.0085″) and the acoustic pressure 65.2 dB. The acoustic pressure measurement location 1 m (39.4″) from the source satisfies the criteria for being in the source far-field, for the source geometry and excitation frequency considered in this test. The radiating surface area of the three RDI speakers is approximately equal to the open area of the acoustic actuator. The stator vane containing the speakers was replaced at the same location with a stator vane fitted with the externally mounted compression driver actuator, which was driven at 25 W input power. The acoustic pressure measured at the same microphone location used to measure the reference actuator response was 86.5 dB. The equivalent displacement of the externally mounted compression driver actuator is found from the relation

$$s = \frac{\sqrt{\frac{2p_{rms}^2}{Z_a}}}{A_e \omega} \tag{1}$$

where

p_{rms} = acoustic pressure at measurement location for externally driven actuator
Z_a = acoustic radiation transfer function from actuator to measurement location
A_e = externally driven actuator surface area
ω = excitation frequency (rad/s)

The acoustic radiation transfer function is given by

$$Z_a = \frac{p_s^2}{Q_{rms}^2} = \frac{2p_s^2}{(A_s \omega s_s)^2} \tag{2}$$

where

p_s = acoustic pressure (rms) at measurement location for reference actuator
Q_{rms} = reference actuator volume velocity
s_s = reference actuator displacement

Using the measured values and the Equations (1) and (2), the equivalent displacement of the externally mounted actuator was found to be 1.3 mm (0.051″). This indicates that each of the externally driven actuators can produce an equivalent displacement greater than the maximum required by the prediction from the LINFLO analysis of 0.57 mm

(0.0225″). The response measured at the location 1 m (39.4″) from the actuator surface for the externally driven actuator is shown in Figure 38.

The externally driven actuator was also tested in a wind tunnel flow to investigate the influence of flow on the sound levels output by the compression drivers. The wind tunnel facility produced a flow of 38.1 m/s (125 ft/s) which is of the same order as the flow speed in the Purdue experimental rig of 45.7 m/s (150 ft/s). The sound pressure levels were measured at two points in the wind tunnel, one at a distance of 0.762 m (30″) normal to the actuator surface, and one at 0.826 m (32.5″) and an angle of 35 degrees to the normal. At both measurement locations the sound pressure level generated by a single actuator driven at 267 Hz was altered by less than 1 dB between the cases with and without flow. The tone generated by the actuator was also 20 dB above the sound pressure level produced by the wind tunnel. The acoustic pressure response measured at the microphone located normal to the actuator surface is shown in Figure 39, for the cases of the actuator operating with and without flow. A similar result is obtained at the other measurement location. The tests indicate that the externally mounted compression driver is not significantly affected by flow over the actuator surface for the flow speeds which are typically used in the Purdue experimental rig.

Matching Amplifier with Compression Driver

It was necessary to match the input of the compression drivers with the output of the amplifiers used with the Purdue Annular Cascade Research Facility, which are rated at 8 ohm 200 W. A number of tests were conducted with the amplifier output connected to the various input taps of the PD-30T compression drivers. The input electrical power and the acoustic output of the compression drivers were measured during the tests. It was found that exciting the compression drivers directly with the 8 ohm amplifier output resulted in the compression drivers becoming overheated, and melting of the compression driver winding occurred after very short periods (usually minutes). This was felt to be due to the fact that the standard implementation of the compression drivers is for music or white noise type inputs. The nominal 8 ohm 30 W driver rating thus needs to be de-rated for tonal excitation. The solution determined was to use voltage transformers to isolate the compression driver units so that the power and heat dissipation occurs in the transformers rather than in the compression driver coil.

A configuration was tested with the amplifier 8 ohm output connected to a separate 8 ohm to 70 V line transformer which is connected in series to the 70 V to 8 ohm transformer tap on the compression driver unit. The configuration was tested for a 3 hour period at 25 W input power with no noticeable degradation in the performance of the driver unit, and sufficient acoustic output levels to achieve the equivalent displacement levels required. The 8 ohm to 70V line transformer chosen for use in the tests was an Atlas Soundolier T-20.

Computational Study of Active Noise Control

The following section of the report contains the results of a computational study of active noise control at the source concepts on the Annular Cascade Research Facility at Purdue University. From the rotor-stator experimental set-up, a representative two-dimensional model is formulated and analyzed using the linearized unsteady analysis LINFLO. A set of actuator lengths, locations, and configurations is examined, where pairs of actuators are used to accomplish exact cancellation of the far-field propagating acoustic modes. Subsequently each actuator is used alone to perform a weighted least squares minimization of the total far-field sound power. Actuator displacement and power requirements are determined for both cases. It is observed that the computationally-determined actuator requirements lie near the boundary of current actuator technology.

Introduction

Blade rows in relative motion in an axial turbomachine produce discrete tone noise through wake/blade-row interactions (ref. 11). Inside a ducted turbomachine but in the acoustic far field of the blade rows the flow can often be described analytically as the superposition of a uniform mean flow and a series of unsteady vortical, entropic, and acoustic perturbations. The latter can be described by individual Fourier components of the unsteady disturbance field (ref. 12). The far-field modes either propagate without attenuation or decay exponentially as they move away from the blade row in the axial direction. The discrete tones in the turbomachinery noise spectrum result from the propagating acoustic modes generated by the wake/blade-row interactions.

Recent work in turbomachinery tone noise reduction generally followed two primary approaches. In anti-sound control, a set of tones identical but out of phase with the undesired noise are generated inside the machine. The intention is to generate tones that will result in a net sound amplitude of zero. By contrast, anti-source control endeavors to reduce the far-field noise by attacking it at its source, e.g., directly on the blades of the downstream blade row where the wake/blade interaction takes place. In ref. 13 and ref. 14 an attempt was made to combine these two approaches. The goal was to use actuators to generate anti-sound tones, but to do so using actuators on the blade surfaces themselves to take advantage of the proximity of the control to the noise source. An investigation of a representative, two-dimensional rotor-stator configuration suggested that the required actuator displacements for noise cancellation might lie within practical limits. An experimental study was thus required to test the assumptions inherent in the analysis and if possible to validate its conclusions.

The Annular Cascade Research Facility at Purdue University was chosen as an appropriate experimental rig for the active noise control tests. The facility has a hub-to-tip ratio high enough that its internal aerodynamics can be reasonably described by two-dimensional models. The following report contains an analysis of a rotor-stator

configuration in this rig, with the intent of determining actuator parameter requirements for significant far-field, tonal noise reduction. Section 2 below briefly summarizes the linearized unsteady aerodynamic analysis used (LINFLO) to determine the acoustic response of the stage. Section 3 then contains a description of the control approaches employed to minimize the far-field sound. Section 4 reports the results of the computational and analytical investigations. It is observed that for the experimental configuration of interest, the actuator requirements for effective noise cancellation lie near the limit of current actuator technology.

Aerodynamic Model

This section briefly describes the linearized unsteady flow analysis LINFLO (ref. 15, 16) which was used to determine the acoustic response of a stator row to incident vortical excitations.

The flow through the stator was considered to be a time-dependent, adiabatic, attached subsonic flow, with negligible body forces, of an inviscid non-heat-conducting, perfect gas. It was assumed that in the absence of unsteady excitation the mean flow is uniform at the inlet to the stator. The unsteady fluctuations in the flow arise from the entropic or vortical excitations at inlet, as well as the motions of control surfaces on the blades. All excitations are assumed to be of small amplitude, periodic in time, and periodic in the cascade or η-direction.

Control surface motions are modeled as prescribed blade motions of the form

$$\mathbf{R}_B(\mathbf{x} + mG, t) = \mathbf{Re}\{\mathbf{r}_B(\mathbf{x})\exp[i(\omega t + m\sigma)]\} \tag{3}$$

that are restricted to portions of the blade surfaces. Here R_B measures the displacement of a point on a blade surface relative to its mean or steady-state position, x is a position vector, t is time, r_B is a complex displacement amplitude vector, Re denotes the real part of a complex quantity and B denotes the reference (m = 0) blade surface. The incident disturbances are prescribed as functions of x and t which satisfy the field equations that govern the unsteady flow in the far field. Thus, small-amplitude entropic and vortical fluctuations relative to a uniform stream must be of the form

$$s_{-\infty}(\mathbf{x}, t) = \mathbf{Re}\{s_{-\infty}\exp[i(\mathbf{k}_{-\infty}\cdot\mathbf{x} + \omega t)]\}, \xi < \xi_- \tag{4}$$

and

$$\tilde{\zeta}_{-\infty}(\mathbf{x}, t) = \mathbf{Re}\{\zeta_{-\infty}\exp[i(k_{-\infty}\cdot x + \omega t)]\}, \xi < \xi_- \tag{5}$$

Here $s_{-\infty}$ and $\zeta_{-\infty}$ are the (prescribed) complex amplitudes of the entropic and vortical fluctuations $\tilde{s}_{-\infty}(\mathbf{x}, t)$, and $\tilde{\zeta}_{-\infty}(\mathbf{x}, t)$, respectively, far upstream ($\xi < \xi$-) of the stator. In

the present analysis, only vortical excitations are used to represent the effects of the rotor wakes.

The fluid motion is governed by a coupled set of nonlinear differential equations (i.e., the Euler equations) in continuous regions of the flow, a flow tangency condition at blade surfaces, and jump conditions at vortex-sheet unsteady wakes. In addition, information on the uniform flow conditions at inlet and exit and the entropic and vortical fluctuations at inlet must be specified. Since the unsteady excitations are assumed to be of small-amplitude, the time-dependent flow can be regarded as a small perturbation about an underlying mean or steady flow. This linearization can be performed by substituting relations analogous to that for the time-dependent fluid velocity, i.e.,

$$\tilde{\mathbf{V}}(\mathbf{x},t) = \mathbf{V}(\mathbf{x}) + \tilde{\mathbf{v}}(\mathbf{x},t)+\ldots \qquad (6)$$

where $\tilde{\mathbf{V}}(\mathbf{x},t)$ is the local mean velocity, and $\tilde{\mathbf{v}}(\mathbf{x},t)$ is the first-order (in ε) unsteady velocity into the full, time-dependent governing equations and collecting terms of like power in ε and neglecting terms of $O(\varepsilon^2)$ or higher. The first-order unsteady fluctuations that arise from the various independent modes of excitation are not coupled and hence, can be determined separately. Indeed, it is sufficient to determine unsteady flow solutions for each single harmonic (in t and η) component of a given disturbance. Solutions for arbitrary disturbances and arbitrary combinations of various disturbances can then be obtained by Fourier superposition.

The first-order or linearized unsteady flow properties caused by a periodic unsteady excitation at temporal frequency ω will be harmonic in time, e.g., $\tilde{\mathbf{v}}(\mathbf{x},t) = \mathrm{Re}\{v(x) \exp(i\,\omega\, t)\}$. In addition, the steady and, for an excitation at circumferential wave number $\kappa\eta = \sigma/G$, the first-order unsteady properties will satisfy the blade-to-blade periodicity conditions, e.g., $V(x + mG) = V(x)$ and $v(x + mG) = v(x) \exp(im\sigma)$, respectively. Thus, solutions to time-independent nonlinear steady and linearized unsteady flow problems are required only over a single extended blade-passage region of the cascade. In addition, since analytic far-field solutions can be determined (ref. 17), the numerical solution domain can be restricted further to a single extended blade-passage region of finite extent in the axial-flow direction.

The Steady Background Flow

As a consequence of the assumption of uniform mean flow at inlet, the steady background flow will be isentropic and irrotational. Thus, $V = \nabla\Phi$,

$$\nabla \bullet (\mathbf{q}\, \bar{\rho}\, \nabla \Phi) = 0 \tag{7}$$

and the fluid properties are related by

$$(M_{-\infty}\, A)^2 = \mathbf{q}\, \bar{\rho}^{\gamma-1} = (\gamma\, M_{-\infty}^2\, P)^{(\gamma-1)/\gamma} = 1 - \frac{\gamma - 1}{2}\, M_{-\infty}^2 (\nabla \Phi)^2 - 1 \tag{8}$$

where Φ, M, A, $\bar{\rho}$ and P are the steady velocity potential, Mach number, speed of sound propagation, density and pressure, respectively, and γ is the specific heat ratio of the fluid. Numerical procedures for determining two-dimensional steady potential flows through cascades have been developed extensively, e.g., see ref. 18 and ref. 19, particularly for flows with subsonic relative inlet and exit Mach numbers (i.e., $M_{\pm\infty} < 1$). The usual practice in such calculations is to solve the mass conservation Equation (7), subject to a prescribed (i.e., $V_{-\infty}$ and $\Omega_{-\infty}$) uniform inflow, flow tangency at blade surfaces, and a Kutta condition at blade trailing edges.

The Linearized Unsteady Flow

The system of field equations that govern the linearized unsteady perturbation of a potential mean flow can be cast in a very convenient form by introducing the velocity decomposition (ref.20, 21)

$$v = v^* + \nabla \phi = v_R + \nabla \phi^* + \nabla \phi \tag{9}$$

where the rotational velocity, v_R, is taken to be divergence-free far upstream of the blade row, ϕ^* is a convected or pressure-less potential (i.e., $\bar{D}\, \phi^*/Dt = 0$) which satisfies the condition $\nabla \phi^* \bullet n = - v_R \bullet n$ at blade and wake mean positions, and the unsteady pressure depends only upon the potential, ϕ, through the relation $p = - \bar{\rho}\, \bar{D}\, \phi/Dt$, where $\bar{D} / Dt = i\, \omega + \nabla \Phi \bullet \nabla$ is a convective derivative based on the mean-flow velocity.

The system of field equations that governs the linearized unsteady flow variables, s, v_R and ϕ is determined by substituting the velocity decomposition (Equation 9) into the linearized Euler equations. If the underlying mean flow is isentropic and irrotational, the unsteady equations reduce to

$$\frac{\bar{D}\, s}{Dt} = 0 \tag{10}$$

$$\frac{D}{Dt} (vR - s\, \nabla \Phi/2) + [(vR - s\, \nabla \Phi/2) \bullet \nabla]\, \nabla \phi = 0 \tag{11}$$

and

$$\frac{\overline{D}}{Dt}A^{-2}\frac{\overline{D}\phi}{Dt} - \frac{1}{\overline{\rho}}\nabla \bullet \mathbf{q}\left(\overline{\rho\nabla}\right) = \frac{1}{\overline{\rho}}\nabla\bullet(\rho v^*) \qquad (12)$$

These equations are coupled only sequentially; hence, they can be solved in consecutively to determine the complex amplitudes of the entropy (s), rotational velocity (vR) and velocity potential (ϕ), respectively.

Closed form solutions(ref. 20, 22) can be determined for the entropy and rotational velocity fluctuations in terms of the known conditions at inlet. Thus, the unsteady flow variables s, v_R and ϕ can be evaluated in terms of the drift and stream functions of the steady background flow.

The unsteady velocity potential, ϕ, is governed by the second-order partial differential Equation 12 along with conditions at the blade and wake surfaces and at the inlet and exit boundaries. This function can be found numerically as a solution of the field Equation 12 subject to the appropriate surface and far-field conditions. The flow tangency condition

$$\nabla\phi \bullet n = [i\,\omega\, r + (\nabla\Phi\bullet\tau)(\tau\bullet\nabla)\, r - (r\bullet\nabla)\nabla\phi] \bullet n \qquad (13)$$

applies at the mean blade surfaces (B_m), and the linearized unsteady pressure and normal velocity component are continuous across blade wakes (W_m), i.e.,

$$[[\ \overline{D}\,\phi/Dt\ ]] = 0 \qquad \text{and} \qquad [[\nabla\phi\ ]] \bullet n = 0 \qquad (12)$$

The velocity potential fluctuations in the far upstream and far downstream regions depend upon the prescribed excitation as well as on the acoustic and vortical response of the cascade. Analytic solutions for ϕ in the far field can be determined[17] which satisfy the requirements that acoustic response disturbances either attenuate with increasing axial distance from the blade row or propagate carrying energy away from or parallel to the blade row and that vorticity must be convected downstream. These solutions can be matched to a near-field numerical solution and thereby serve to complete the boundary-value problem for the unsteady potential. The vortical excitations determined by the rotor wake analysis can thus be imposed at the inlet of a single extended blade passage of the stator, and the resultant acoustic response can be calculated. The amplitudes of the propagating acoustic response modes that result become the targets of the active noise control analysis presented in the next section.

Control

The propagating far-field acoustic response waves make up the discrete tone noise at multiples of the blade passing frequency (BPF), and are the targets of the control analysis

given in this section. Note that for the purposes of the control analysis, all of the acoustic response waves are considered to be independent modes. The means, for instance, that the upstream and downstream moving acoustic response waves at BPF are considered as separate modes, even though both have the same frequency and interblade phase angle.

Actuator Implementation

Blade surface actuators are used to generate sound out of phase with the undesired acoustic responses. The actuators, or pistons, have been implemented into the LINFLO analysis as oscillating control surfaces on the suction and pressure surfaces of each blade. A general blade motion is represented by Equation 3. Control surfaces oscillate with prescribed translational displacements normal to the mean blade surfaces at a given frequency and interblade phase angle. For a set of K control surfaces, the complex amplitude of the displacement on the reference (m = 0) blade is given by

$$r_B(x) = \sum_{k=1}^{K} \mathbf{r}_k \left[U(x - x_{k,le}) - U(x - x_{k,te})\right] \qquad \textbf{(15)}$$

where $r_k = r_k e_N$ is the displacement of the kth piston with complex amplitude r_k, e_N is a unit vector normal to the blade surface, U is the unit step function, and $x_{k,le}$ and $x_{k,te}$ are the locations of the leading and trailing edges of the kth piston. Individual pistons are specified by choosing midpoint locations and lengths as a fraction of chord. The surface boundary condition routines in LINFLO then use the actuator midpoint locations and lengths to determine which surface mesh points lie within a given actuator, and these points are required to perform translational oscillations at the specified frequency and with the specified complex amplitude.

Control Algorithm

The unsteady aerodynamic equations governing small unsteady perturbations of a uniform mean flow can be solved to yield the wavenumbers and attenuation constants for all acoustic response disturbances[17]. The form of the acoustic response, i.e., the wavenumbers, attenuation constants, and propagation directions of each response wave, is independent of the means of excitation. The linearity of the unsteady equations for small amplitude excitations implies that superposition is valid, so if both an external excitation and a set of control surface oscillations act simultaneously, the net complex amplitudes of the acoustic response waves will be equal to the sum of the responses to both the excitations and the control oscillations. The control excitations can then in principle be "tuned" so that their corresponding acoustic response waves are of equal amplitude but 180 degrees out of phase with the undesired responses generated by the wake/blade-row interactions. In effect, the actuator surface motions act as sources of anti-sound to minimize the undesired noise.

Assume that there are N acoustic response modes and K independent control surfaces. The total acoustic response due to both a specified excitation and a set of control surface motions will contain contributions attributable to each. The complex amplitudes of the net propagating acoustic response modes can therefore be expressed as a vector pR such that

$$p_R = p_{R,exc} + p_{R,ctrl} = p_{R,exc} + A\, r \tag{16}$$

The N x K matrix A contains as its elements the complex amplitudes of each propagating acoustic response wave resulting from a unit amplitude oscillation of each control surface, and the vector r contains the complex amplitudes r_k of the control surface motions. If K = N, the matrix A in this equation is square and invertible. Consequently, a set of control surface amplitudes given by

$$r_{exact} = - A^{-1}\, p_{R,exc} \tag{17}$$

will yield $p_R = 0$. In this case, the net amplitude of each propagating acoustic response wave will be zero.

Should there be less actuators available than propagating acoustic response modes, then from a linear algebra perspective the error measures the amount that the undesired response vector lies outside the space spanned by the columns of the matrix A. Minimization of this error is done by forcing it to be perpendicular to the column space. (See Figure 40). The result of this process is to require that the actuator displacement amplitudes be found from

$$r_{lsq} = - (A^H A)^{-1} A^H\, p_{R,exc} \tag{18}$$

where the superscript H represents Hermetian. The elements r_k of r_{lsq} are the complex amplitudes of the control surface displacements.

A weighting matrix W can be introduced into Equation 16 to give

$$W\, p_R = W\, p_{R,exc} + W\, A_r\,. \tag{19}$$

In the present application the matrix W is chosen to be square, diagonal, and composed of real elements. The values specified on the diagonal represent the relative importance assigned to the individual modes, and are here specified to be the individual modal contributions to the far-field acoustic power. This weighted least squares solution is given by

$$r_{wlsq} = - (A^H W^T W A)^{-1} A^H W^T W\, p_{R,exc} \tag{20}$$

and minimizes the total far field acoustic power. Note that if the matrix A is invertible, then Equation 20 reduces to the solution given in Equation 17, and that the least squares

solution given in Equation 18 represents the case where the weighting matrix is chosen to be the identity matrix.

Actuator Power

The power required by the actuators in the control analysis is defined using the work per cycle quantity derived and presented in ref. [23]. The aerodynamic work per cycle, W, is defined as the work done by the fluid on a given blade over a period of its motion. According to linearized theory, a prescribed blade motion can be classified as stable, neutrally stable, or unstable depending upon whether the aerodynamic work per cycle is less than, equal to, or greater than zero, respectively.

Work per cycle can also be expressed in terms of the a so-called pressure-displacement function $w(\tau)$ over the mean blade surface,

$$W_{2D} = \oint_B w(\tau) d\tau \tag{21}$$

where for the actuator motions described above in subsonic flow $w(\tau)$ reduces to

$$w(\tau) = -\pi \, \mathrm{Im}\{p_B \, r^*\} \tag{22}$$

Here B and τ are the mean blade surface and its counterclockwise tangent vector, and p_B and r^* are the complex amplitude of the unsteady surface pressure and the complex conjugate of the actuator displacement amplitude.

The work per cycle quantity as defined results from a two-dimensional analysis and is thus integrated only along the chord, as opposed to the area of the actuator in three dimensions. Making the assumption that the two-dimensional aerodynamic response of the actuator does not change in the spanwise direction leads to the approximation for the three-dimensional work per cycle

$$W_{3D} = W_{2D} \, L \tag{23}$$

where L is the length of an assumed square actuator. Since power is defined to be the time derivative of the unsteady work and all unsteady quantities in the present analysis are taken to be periodic, the three-dimensional power is given by

$$P = \omega \, W_{2D} \, L = \frac{P^*}{\rho^*_{-\infty} V^{*3}_{-\infty} c^{*2}} \tag{24}$$

where the asterisks in this equation represent dimensional quantities. This is the expression used to compute the power required by the actuator oscillations.

Results

The stator cascade in the Purdue rig provided the model for the acoustic response calculations. This cascade has inlet and exit Mach numbers $M_{-\infty} = 0.15$ and $M_{+\infty} = 0.145$; inlet and exit flow angles $\Omega_{-\infty} = \Omega_{+\infty} = 0$ deg; zero stagger $\Theta = 0$ deg; and a gap-to-chord ratio G = 1.283. Table 1 contains the dimensional data from the Purdue Annular Cascade Rig, and the nondimensional quantities required by LINFLO that are derived from them. The conversion to dimensional quantities will also assume that the mean density is $\overline{\rho}$ = 0.0735 lbm/ft^3 = 1.1774 kg/m^3 and T = 539.67 R.

Dimensional Quantities	
Rotor Blades, N_B	16
Stator Vanes, N_V	18
Mean Radius, r^*	22 inches = 0.5588 m
Stator Chord, c^*_v	6 inches = 0.1524 m
Gap, G*	$2 \pi r^* / N_V$ = 7.679 inches = 0.1950 m
Axial Velocity, $V^*_{-\infty}$	159.6 ft/sec = 48.646 m/sec
Rotation Rate, Ω^*	
Ω^*_1, Case I	800 rpm
Ω^*_2, Case II	1000 rpm
Blade Passing Frequency, f^*	
f^*_1, Case I	213.3 Hz
f^*_2, Case II	266.67 Hz
Wheel Speed, V^*_W	
V^*_{W1}, Case I	153.59 ft/sec = 46.814 m/sec
V^*_{W2}, Case II	191.99 ft/sec = 58.519 m/sec
Derived and Nondimensional Quantities	
Interblade Phase Angle, σ	-2π NB / NV = -5.585
Gap/Chord Ratio, G	1.2821
Inflow Mach Number, $M_{-\infty}$	0.15
Reduced Frequency, ω	
ω_1, Case I	$2 \pi f^*_1 c_V / V^*_{-\infty}$ = 4.200
ω_2, Case II	$2 \pi f^*_2 c_V / V^*_{-\infty}$ = 5.250

Table 1: Purdue Rig Information Used in the LINFLO Calculations

The responses due to the upstream rotor were calculated using individual Fourier components of the rotational velocity in the rotor wakes at a nondimensional blade passing frequencies (BPF) $\omega = 4.200$ and $\omega = 5.250$ and an interblade phase angle $\sigma = -5.585$. At these frequencies one acoustic response mode propagated away from the blade row in each direction. The real part of the acoustic response field in Figure 41 shows the two propagating waves as they move away from the blade row in each direction. For a

unit vortical excitation, the acoustic response mode amplitudes are found to be $p_{-\infty}$ = (0.2000,-0.9686) and $p_{+\infty}$ = (-0.01970,-0.9059).

The active control analysis utilizes the responses of each acoustic response mode to unit amplitude excitations of each control surface to fill the control matrix A in Equation 17. These complex amplitude responses are given in Table 2. The last line in the table gives the response mode complex amplitudes when a unit amplitude upwash excitation is imposed at the upstream boundary. This last line, therefore, represents the target amplitudes for the active control analysis.

Excitation			Response	
Surface	Length	Location	Upstream Mode	Downstream Mode
Suction	0.1667	0.25	(2.338, 2.732)	(1.259, 2.098)
Suction	0.1667	0.408	(2.674, 1.975)	(1.260, 1.713)
Suction	0.25	0.25	(3.289, 3.969)	(1.749, 3.067)
Suction	0.25	0.408	(4.006, 2.926)	(1.902, 2.548)
Pressure	0.1667	0.25	(2.642, 3.821)	(1.647, 2.545)
Pressure	0.1667	0.408	(2.221, 3.379)	(0.8680, 2.494)
Pressure	0.25	0.25	(4.215, 5.361)	(2.718, 3.497)
Pressure	0.25	0.408	(3.352, 5.059)	(1.321, 3.739)
Unit upwash, v+ = (1.0, 0.0)			(0.6237,-1.286)	(0.5583, -1.273)

Table 2: Acoustic Mode Responses to Unit Excitations at $\omega = 4.200$

Table 3 contains the results of the active control analysis for complete cancellation of both acoustic response modes. The analysis has been applied in this table assuming a unit amplitude upwash excitation. Each box in the table contains two lines. The upper line has the amplitude and phase angle requirements for the suction surface actuator, and the lower line has the same information for the pressure surface actuator.

	Suction Surface, Length/Location							
Pres. Surf.	0.1667/0.25		0.1667/0.408		0.25/0.25		0.25/0.408	
Len./Loc.	Amp.	Phase	Amp.	Phase	Amp.	Phase	Amp.	Phase
0.1667/0.25	1.355	-0.3909	0.8009	-0.6004	0.8918	-0.3807	0.5398	-0.5874
	1.087	2.361	0.7520	1.828	1.023	2.369	0.7535	1.835
0.1667/0.408	2.617	1.519	4.512	-1.351	1.865	1.399	3.146	-1.323
	2.000	-1.687	4.036	1.493	2.037	-1.809	4.184	1.425
0.25/0.25	1.156	-0.3435	0.7373	-0.5146	0.7675	-0.3368	0.4966	-0.5020
	0.631	2.419	0.4711	1.924	0.5987	2.423	0.4716	1.931
0.25/0.408	2.645	1.521	4.415	-1.353	1.886	1.399	3.076	-1.325
	1.350	-1.682	2.637	1.404	1.375	-1.806	2.731	1.426

Table 3: Complete Cancellation of Unit Upwash Response, $\omega = 4.200$

The rotor wake information from Purdue stated that the first Fourier component of the upwash velocity had a nondimensional magnitude of 0.0077. Each amplitude entry in this table must therefore be multiplied by 0.0077 to get the appropriate actuator oscillation amplitude.

To get dimensional results, two factors are involved. First, all lengths in the LINFLO analysis are nondimensionalized with respect to stator chord, which according to Table 1 is 6 inches. Second, the LINFLO analysis is two-dimensional, so factors must be introduced to relate the LINFLO results to the three-dimensional experiment. Results of the two-dimensional analysis are defined per unit width. The Purdue Annular Cascade Rig has a large hub-to-duct ratio, a low Mach number, and a relatively low frequency, implying that two-dimensional assumptions are reasonable. The span of the stator vanes is large enough to hold three round speakers, each of which has a 1 inch or 1.5 inch diameter. If the span is assumed to be divided into three sections, each containing one speaker, the LINFLO analysis presumes that the aerodynamics is the same in each section. A correction is required for the fact that the actuators in the 2D model represent 3D square actuators in the experiment rather than the round speakers. It is assumed that the volume displaced between the square actuators and the speakers should be held constant. The volume displaced by the square piston is

$$V_{sq} = l^2 r_{sq} \tag{25}$$

where l is the length of the square and r_{sq} is its displacement, and the volume displaced by a cylinder

$$V_{cl} = \frac{\pi}{4} l^2 r_{cl} \tag{26}$$

This implies that to keep the volume constant, a displacement of

$$r_{cl} = \frac{4}{\pi} r_{sq} \approx 1.2732\, r_{sq} \tag{27}$$

is required for the three-dimensional speakers.

To convert the nondimensional displacements computed by LINFLO to the required three-dimensional dimensional amplitudes, it is necessary to multiply the results in Table 3 by 1.2732 times the chord length of 6 inches. These results are given in Table 4, where the displacement amplitudes given in inches.

	Suction Surface, Length/Location							
Pres. Surf.	0.1667/0.25		0.1667/0.408		0.25/0.25		0.25/0.408	
Len./Loc.	Amp.	Phase	Amp.	Phase	Amp.	Phase	Amp.	Phase
0.1667/0.25	0.07968	-0.3909	0.04711	-0.6004	0.05246	-0.3807	0.03175	-0.5874
	0.06394	2.361	0.04423	1.828	0.06017	2.369	0.04432	1.835
0.1667/0.408	0.1539	1.519	0.2654	-1.351	0.1097	1.399	0.1850	-1.323
	0.1176	-1.687	0.01828	1.493	0.1198	-1.809	0.2461	1.425
0.25/0.25	0.06800	-0.3435	0.04337	-0.5146	0.04515	-0.3368	0.02921	-0.5020
	0.03712	2.419	0.02771	1.924	0.03522	2.423	0.02774	1.931
0.25/0.408	0.1556	1.521	0.2597	-1.353	0.1109	1.399	0.1810	-1.325
	0.07937	-1.682	0.1551	1.404	0.08090	-1.806	0.1607	1.426

Table 4: Complete Cancellation, $v^+=(0.0077,0.)$, $\omega = 4.200$, 3D, Dimensional

The table suggests that actuator displacements of at least 20-40 mils are required to achieve complete cancellation of the far-field sound. Given the frequency range and size limitations for the speakers, this is close to the limit of what is possible with present technology. As an alternative, the possibility of minimizing the total sound power with a single actuator was explored.

Table 5 shows the 3D, dimensional displacements resulting from the weighted least squares minimization described in Section 3, along with the corresponding decreases in sound power level. Each length actuator was used at each position to minimize the far-field sound power, given $v^+ = (0.0077,0.)$ at the upstream boundary.

With an actuator of length of 0.25 located at 0.25 chord, the results show that displacements as small as 15 mils are sufficient to achieve a 22 dB decrease in the total far-field sound power.

Length	Location	Amplitude	Phase	ΔPWL
Suction Surface Actuator				
0.1667	0.25	0.02707	1.0630	-22.140 dB
0.1667	0.408	0.02951	1.2328	-19.893 dB
0.25	0.25	0.01884	1.0439	-22.188 dB
0.25	0.408	0.01977	1.2387	-19.933 dB
Pressure Surface Actuator				
0.1667	0.25	0.02130	1.0250	-22.315 dB
0.1667	0.408	0.02423	0.90253	-20.692 dB
0.25	0.25	0.01453	1.0979	-22.290 dB
0.25	0.408	0.01614	0.90663	-20.710 dB

Table 5: Weighted Least Squares Minimization, $\omega = 4.200$

Further analyses of the Purdue rig were conducted by D. Topol at Pratt & Whitney, which revealed that although the upstream and downstream acoustic response modes propagate unattenuated in the immediate vicinity of the rotor and stator, this is not the case in the inlet and exit plenums. The two plenums thus acted as highly reflecting boundaries for acoustic waves. It was decided, therefore, to examine the same system rotating at the higher frequency of 1000 rpm. Quantities relevant to this frequency are listed as "Case II" in Table 1. Tables 6, 9 and 10 are the analogs at the $\omega = 5.250$ frequency to Tables 2, 4 and 5 at $\omega = 4.200$.

Excitation			Response	
Surface	Length	Location	Upstream Mode	Downstream Mode
Suction	0.1667	0.25	(3.221, 1.921)	(1.778, 1.371)
Suction	0.1667	0.408	(3.401, 0.9845)	(1.608, 1.175)
Suction	0.25	0.25	(4.572, 2.802)	(2.525, 2.028)
Suction	0.25	0.408	(5.080, 1.449)	(2.414, 1.744)
Pressure	0.1667	0.25	(3.759, 3.345)	(2.194, 1.773)
Pressure	0.1667	0.408	(3.350, 2.698)	(1.448, 1.989)
Pressure	0.25	0.25	(5.740, 4.641)	(3.364, 2.333)
Pressure	0.25	0.408	(5.036, 4.033)	(2.186, 2.976)
Unit upwash, v+ = (1.0, 0.0)			(0.2000,-0.9686)	(-0.01970,-0.9059)

Table 6: Acoustic Mode Responses to Unit Excitations at $\omega = 5.250$

	Suction Surface, Length/Location							
Pres. Surf.	0.1667/0.25		0.1667/0.408		0.25/0.25		0.25/0.408	
Len./Loc.	Amp.	Phase	Amp.	Phase	Amp.	Phase	Amp.	Phase
0.1667/0.25	0.9609	-0.4864	0.4766	-0.7118	0.6320	-0.4743	0.3202	-0.7015
	0.7708	2.2110	0.4787	1.6471	0.7253	2.2178	0.4788	1.6519
0.1667/0.408	1.463	1.507	2.769	-1.381	1.048	1.418	1.895	-1.354
	1.056	-1.717	2.502	1.340	1.082	-1.811	2.548	1.362
0.25/0.25	0.8344	-0.4299	0.4494	-0.6326	0.5530	-0.4216	0.3019	-0.6226
	0.4566	2.273	0.3080	1.732	0.4329	2.276	0.3079	1.736
0.25/0.408	1.475	1.509	2.713	-1.384	1.058	1.419	1.856	-1.357
	0.7111	-1.712	1.637	1.340	0.7294	-1.807	1.668	1.361

Table 7: Complete Cancellation of Unit Upwash Response, $\omega = 5.250$

	Suction Surface, Length/Location							
Pres. Surf.	0.1667/0.25		0.1667/0.408		0.25/0.25		0.25/0.408	
Len./Loc.	Amp.	Phase	Amp.	Phase	Amp.	Phase	Amp.	Phase
0.1667/0.25	0.007399	-0.4864	0.003670	-0.7118	0.004866	-0.4743	0.002466	-0.7015
	0.005936	2.2110	0.003686	1.6471	0.005585	2.2178	0.003687	1.6519
0.1667/0.408	0.01126	1.507	0.02132	-1.381	0.008073	1.418	0.01459	-1.354
	0.008127	-1.717	0.01926	1.340	0.008334	-1.811	0.01962	1.362
0.25/0.25	0.006424	-0.4299	0.003461	-0.6326	0.004258	-0.4216	0.002325	-0.6226
	0.003516	2.273	0.002371	1.732	0.003333	2.276	0.002371	1.736
0.25/0.408	0.01136	1.509	0.02089	-1.384	0.008146	1.419	0.01429	-1.357
	0.005475	-1.712	0.01261	1.340	0.005617	-1.807	0.01284	1.361

Table 8: Complete Cancellation of Unit Upwash Response, $\omega = 5.250$, $v^+ = 0.0077$

	Suction Surface, Length/Location							
Pres. Surf.	0.1667/0.25		0.1667/0.408		0.25/0.25		0.25/0.408	
Len./Loc.	Amp.	Phase	Amp.	Phase	Amp.	Phase	Amp.	Phase
0.1667/0.25	0.05652	-0.4864	0.02803	-0.7118	0.03718	-0.4743	0.01884	-0.7015
	0.04534	2.211	0.02816	1.647	0.04266	2.218	0.02816	1.652
0.1667/0.408	0.08604	1.507	0.1629	-1.381	0.06167	1.418	0.1114	-1.354
	0.06209	-1.717	0.1471	1.340	0.06366	-1.811	0.1499	1.3616
0.25/0.25	0.04908	-0.4300	0.02644	-0.6326	0.03253	-0.4216	0.01776	-0.6226
	0.02686	2.273	0.01812	1.732	0.02547	2.276	0.01811	1.736
0.25/0.408	0.08678	1.509	0.1596	-1.384	0.06223	1.419	0.1092	-1.357
	0.04183	-1.712	0.09631	1.340	0.04291	-1.807	0.09809	1.361

Table 9: Complete Cancellation, $v^+=(0.0077,0.)$, $\omega = 5.250$, 3D, Dimensional

Figure 44 contains the real and imaginary parts of the unsteady surface pressure distributions on the suction and pressure surfaces, both with and without control applied. The associated pressure differences are shown in Figure 45.

The actuator power requirements for the complete cancellation cases shown in Table 9 are shown in Table 11. Each entry was computed from Equation 24 using the two-dimensional work per cycle calculation in LINFLO.

Length	Location	Amplitude	Phase	ΔPWL
Suction Surface Actuator				
0.1667	0.25	0.01819	1.0781	-20.555 dB
0.1667	0.408	0.01904	1.2376	-17.916 dB
0.25	0.25	0.01268	1.0617	-20.578 dB
0.25	0.408	0.01276	1.2419	-17.943 dB
Pressure Surface Actuator				
0.1667	0.25	0.01392	0.96821	-20.998 dB
0.1667	0.408	0.01579	0.87720	-18.774 dB
0.25	0.25	0.00952	1.0274	-20.974 dB
0.25	0.408	0.01053	0.88055	-18.792 dB

Table 10: Weighted Least Squares Minimization, $\omega = 5.250$

	Suction Surface, Length/Location							
Pres. Surf.	0.1667/0.25		0.1667/0.408		0.25/0.25		0.25/0.408	
Len./Loc.	Upper	Lower	Upper	Lower	Upper	Lower	Upper	Lower
0.1667/0.25	-0.8684	0.7312	0.05432	0.5906	-1.249	0.6779	0.01682	0.5893
0.1667/0.408	-1.053	-0.3591	-1.862	1.905	-2.253	-0.3470	-4.131	1.940
0.25/0.25	-0.7192	0.7533	0.05794	0.7629	-1.060	0.7157	0.02549	0.7605
0.25/0.408	-1.073	-0.6019	-1.723	2.679	-2.281	-0.5886	-3.864	2.724

Table 11: Power requirements for complete cancellation, $v^{+}=(0.0077,0.)$, $\omega =$ 5.250, 3D, Dimensional (Watts)

Negative numbers imply that power is going from the actuator into the fluid, and positive numbers are the opposite. Optimal cases appear to be those that require each actuator to withstand power on the order of 1 watt.

As an alternative to the weighted least squares power minimization, the control can focus on the integrated unsteady lift. Since this is a single quantity, it can be cancelled using a single actuator. If the source is compact relative to the generated acoustic wavelengths, this will result in a substantial reduction in the far-field sound.

Table 12 illustrates the results of applying this concept to the cascade in Case II. The suction surface actuators performing unsteady lift cancellation do indeed reduce the far-field noise by a moderate amount, but the pressure surface actuators increase the noise. In Table 13, the dimensional amplitudes of the suction surface actuators are presented. While the change in the total sound power is only 2-4 dB, the fact that the actuator displacement is only 7-11 mils might make this an approach worth pursuing.

Length	Location	Amplitude	Phase	ΔPWL
Suction Surface Actuator				
0.1667	0.25	0.18677	1.6460	-4.056 dB
0.1667	0.408	0.18776	1.9151	-2.926 dB
0.25	0.25	0.12864	1.6322	-4.006 dB
0.25	0.408	0.12386	1.9227	-2.916 dB
Pressure Surface Actuator				
0.1667	0.25	0.36752	-2.3578	+7.866 dB
0.1667	0.408	0.53039	-1.7950	+8.826 dB
0.25	0.25	0.23714	-2.3760	+7.527 dB
0.25	0.408	0.35591	-1.8081	+8.880 dB

Table 12: Unsteady Lift Cancellation, $v^+=(1.,0.)$, $\omega = 5.250$

Length	Location	Amplitude	Phase	ΔPWL
Suction Surface Actuator				
0.1667	0.25	0.01099	1.6460	-4.056 dB
0.1667	0.408	0.01087	1.9151	-2.926 dB
0.25	0.25	0.007567	1.6322	-4.006 dB
0.25	0.408	0.007286	1.9227	-2.916 dB

Table 13: Unsteady Lift Cancellation, $v^+=(1.,0.)$, $\omega = 5.250$, 3D, Dimensional

ANC Demonstration Experiment at Purdue University

Introduction

An experimental demonstration of the active noise control at the source concept was performed at Purdue University. An active noise source mounted on the stator vanes was used to generate a propagating spatial mode to interact with and cancel the upstream and downstream modes generated by rotor/stator interaction. Significant noise reductions were achieved simultaneously for the upstream and downstream propagating modes. The control system was demonstrated over a range of operating conditions.

Experimental Facility and Instrumentation

The demonstration experiment was performed on the Purdue Annular Cascade Research Facility. A schematic of the facility is shown in Figure 47. This test rig is an open loop draw through type of wind tunnel which is capable of test section velocities of 220 ft/sec. The flow is drawn through the facility by a 300 hp centrifugal fan located downstream of

the exit plenum. This facility is unique in that the flow through the rotor is set by a large fan downstream of the test section, so that the rotor speed can be set independently of the flow.

The rotor consisted of 16 one inch wide perforated plates mounted perpendicular to the flow direction. A schematic of the rotor is shown in Figure 48. These rotors were chosen since they generate a wide wake profile.

Acoustic instrumentation consisted of two arrays of 10 piezoelectric microphones with uniform circumferential spacing, mounted in static pressure taps in the outer wall of the inlet annulus (seen in Figure 47). The microphones had a nominal sensitivity of 1.5 V/psi and a natural frequency of 12 kHz. The microphones were calibrated in the rig and showed linear amplitude response and flat frequency response. Experimental error was estimated at 3% of the amplitude and 5° phase. For a ten microphone array, the Nyquist critical mode is 5. All spatial modes above this are aliased below the Nyguist mode.

The rig was configured with 16 perforated plate rotor blades and 18 stator vanes. The stator vanes were NACA 65A012 airfoils with a 15.24 cm (6.00 in) chord. Rotational speed was determined by an optical pickup.

The 16 rotor and 18 vane combination generates $k_\theta = n16 + m18$ spatial modes, where n is the rotor harmonic and m is an arbitrary integer. Therefore, spatial modes of $k_\theta = \cdots, -20, -2, 16, \cdots$ are generated at blade passage frequency. At twice blade passage frequency, the spatial modes are $k_\theta = \cdots, -22, -4, 14, \cdots$. For rotational speeds from 800 to 1000 rpm, only the $k_\theta = -2$ mode at blade passage frequency and the $k_\theta = -4$ mode at twice blade passage frequency will be cut-on. The interblade phase angle is -320° for the 16 blade/18 vane combination.

Data Acquisition and Signal Processing

The active noise control signals were generated using three, six channel analog output boards installed in a PC. The D to A converters were programmed to produce sinusoidal output signals at blade pass frequency, phase reference d to the output of the optical rotor shaft encoder. The interblade phase angle is set to the value determined by the rotor/stator interaction. The control signals were fed to power amplifiers and transformers (to match the impedance) which drove the compression drivers.

The microphone array signals were digitized using five analog to digital boards installed in an separate PC. This allowed simultaneous acquisition of twenty channels of data, synchronized by the shaft trigger signal. The microphone signals were ensemble averaged of 100 rotor revolutions to increase the signal to noise ratio.

The discrete frequency acoustic response is the superposition of spatial modes generated at multiples of rotor blade passage frequency. For this test, blade passage and twice blade passage are of primary interest. An array of microphones is required to determine the measured acoustic response as a function of both frequency and spatial mode. This

temporal-spatial transform is accomplished using two discrete Fourier transforms. The first determines the frequency content of the microphone signals, and the second determines the amplitude of spatial modes at each frequency. The spatial transform, operating on the temporal Fourier transform, is a function of frequency separates the forward and backward spinning modes.

Acoustic Results

A series of tests were conducted to demonstrate the viability and effectiveness of the noise control at the source concept. The axial flow velocity was fixed at 85 ft/sec and the rotor speed was varied from 800 to 1000 rpm. At blade passage frequency, the k_θ =-2 mode propagates both upstream and downstream. The active control system was designed to minimize the amplitude of this mode.

Figure 49 shows the measured amplitudes of the k_θ = -2 spatial mode as a function of rotor speed. The top graph shows the upstream microphone array and the bottom graph shows the downstream array. Two cases are shown, a baseline with the control off and the case with control on. The control system controls both the upstream and the downstream going waves simultaneously. Significant reduction was achieved over the entire range of operating conditions.

Another view of the noise reduction is shown in Figure 50. Here the simultaneous noise reduction is shown. This data was acquired from the previous plot by subtracting the control-on case from the control-off case. This figure demonstrates that reductions of over 10 dB were achieved over the entire operating range. Maximum reductions of 30 to 40 dB were demonstrated over selected regions.

Figure 51 shows the amplitude and phase of the control signals which were required to achieve simultaneous upstream and downstream control. As can be seen from the plot, the upstream and downstream control signals had similar phase and amplitude. This indicates that the drivers were acting more or less together.

Conclusions

The externally mounted compression driver stator vane actuator concept was shown to be feasible for the Purdue experimental rig tests. An arrangement of the thirty six compression drivers and connectors within the Purdue experimental rig centerbody was determined. Experimental tests indicate that the actuators are capable of producing equivalent displacements greater than the requirements predicted by a LINFLO analysis of the Purdue experimental rig configuration. The acoustic output of the actuators was also found to be unaffected by the presence of air flow representative of the Purdue experimental rig.

Wake/blade-row interaction noise produced by the Annular Cascade Facility at Purdue University has been modeled using the LINFLO analysis. Actuator displacements needed for complete cancellation of the propagating acoustic response modes have been determined, along with the associated actuator power requirements. As an alternative, weighted least squares minimization of the total far-field sound power using individual actuators has also been examined. Attempts were made to translate the two-dimensional aerodynamic results into three-dimensional actuator requirements. The results lie near the limit of present actuator technology.

The active noise control at the source concept was successfully demonstrated in a low speed 2-D test at Purdue University. Significant noise reductions were achieved over a range of operating conditions. Simultaneous reductions of 10 dB were obtained over most of the operating range, with significantly higher reductions demonstrated at some points. This was the first verification of simultaneous cancellation of two acoustic modes using actuators mounted on the stator vanes.

Appendix: Natural Frequencies of Ceramic Actuators

Finite element methods were used to calculate the first several natural frequencies of three different sizes of thin circular ceramic actuators under a variety of boundary conditions. Comparisons to test data indicate that the lowest frequencies are strong functions of the boundary condition along the outer edge of the circular geometry.

Conclusions and Recommendations

- Based on finite element models of 8 mil, 15 mil and 30 mil thick flat ceramic actuators, 1.25 inch in diameter, the lowest natural frequencies found from test do not match the analytical values assuming fixed, pinned or free boundary conditions.

- Introducing the appropriate curvature in the actuator models changes the frequencies significantly, but the predicted frequencies still do not match the test results.

- By modeling the boundary conditions with vertical and rotation springs to model the flexible material used in practice, reasonable correlation was found between test and analysis.

- The spring constants that provide correlation in the three cases do not match from case to case, suggesting sensitivity of the natural frequencies based on the manner in which the actuators are held.

Technical Discussion

Objective

The objective of this study is to determine if the natural frequencies of three different configurations of ceramic actuators can be accurately predicted using the finite element method.

Description of Finite Element Models

The ceramic actuators are 1.25 inch in diameter, with thickness of 8 mils, 15 mils and 30 mils. The actuators have a slight curvature, and the rise from edge to center was measured and found to be 19 mils, 20 mils and 14 mils for the 8, 15 and 30 mil thicknesses, respectively. Material properties were supplied by the vendor for the ceramic material.

The ceramic actuators are affixed to a metal specimen using some type of flexible epoxy around the outer diameter of the actuator. It was explained that a flexible connection was needed to eliminate cracking of the ceramic that occurs at a fully constrained boundary.

Finite element models using shell element formulation were constructed to model the actuators. The first three or four natural frequencies were found for a number of different boundary conditions. Both flat and curved geometries were analyzed. The boundary conditions considered include:

- Fixed: no vertical deflection or rotation
- Pinned: no vertical deflection
- Free
- Vertical spring with spring constant k_V
- Rotational spring with spring constant k_r
- Radial spring with spring constant k_{rad}

Results

Three tables are included which contain the frequencies determined by test and by analysis for the three geometries. A brief description of results in each table follows.

8 Mil Thick Actuator

Case	Frequency-1	Frequency-2	Frequency-3	Frequency-4
Test - 100V	**680.**	**1500.**	**1940.**	
Test - 225V	**680.**	**1420.**	**1930.**	
Flat - fixed	1109.	2419.	4314.	
Flat - pinned	537.	1509.	2780.	
Flat - free	578	979.	1338.	
Fixed	1590.	2632.	4583.	
Pinned	1031.	1845.	3600.	
Free	564.	1314.	1957.	
kv=50, kr=0	395.	576.	887.	1517.
kv=100, kr=0	527.	789.	1107.	1690.
kv=150, kr=0	612.	937.	1280.	1842.
kv=200, kr=0	**673**	**1048.**	**1423.**	**1978.**
kv=200, kr=50	759.	1051.	1474.	2168.
kv=200, kr=100	766.	1051.	1479.	2187.

Referring to the table, the first two lines contain the frequencies determined by test for two different voltages. There is some variation in frequency as a function of voltage, but this difference is not explored in this study. Note that the frequencies have units of Hz.

The next three lines contain analysis results assuming fixed, pinned and free conditions for a flat plate. The results in all cases do not correlate well with the test data.

The following three lines contain results assuming fixed, pinned and free conditions with the curvature incorporated into the model. In most cases, the frequencies have increased a significant amount when the curvature was included, but correlation with test data is not found.

The remaining lines of analysis results used a boundary condition consisting of a vertical and rotational springs of differing stiffnesses. The results for the case of 200 lb/in/in vertical stiffness and zero rotational stiffness (in bold in the table) indicates reasonable correlation with the test data. However, there seems to be an extra frequency predicted at 1048 Hz. Close scrutiny of the test data shows a jump in the amplitude of the response curve, although it is small.

15 Mil Thick Actuator

Case	Frequency - 1	Frequency - 2	Frequency - 3
Test - 100V	**880.**	**2430.**	
Test - 350V	**860.**	**2150.**	
Fixed	2404.	4493.	
Pinned	1384.	3017.	
Free	1053.	2455.	
kv=100, kr=0	418.	605.	1270.
kv=200, kr=50	759.	1051.	1474.
kv=200, kr=100	766.	1051.	1479.
kv=200, kr=0, krad=100000.	737.	1071.	1642.
kv=450, kr=200	868.	1261.	2094.
kv=450, kr=400	875.	1264.	2128.
kv=450, kr=600	878.	1265.	2141.
kv=450, kr=600, krad=100000.	**881.**	**1296.**	**2231.**

The table containing the results for the 15 mil thick case does not contain results for the assumption of a flat plate, since it was shown previously to be inaccurate not to include the curvature. Results again show that for fixed, pinned and free conditions at the boundary, the frequencies are too high compared to test data.

In this case, good correlation was found only when the boundary condition was modeled using springs. The best results occurred for a condition of a vertical spring of 450 lb/in/in, a rotational spring of 600 lb-in/rad/in and a radial spring of 100000. lb/in/in. As before, an extra frequency was located, in this case at 1296 Hz. Again, upon closer examination of the test data, a slight jump occurs at this point, but the amplitude is very small.

30 Mil Thick Actuator

Case	Frequency - 1	Frequency - 2	Frequency - 3
Test - 100V	**820.**	**1390.**	**3140.**
Test - 400V	**780.**	**1360.**	**3070.**
Fixed	4236.	8588.	16125.
Pinned	2121.	5626.	12101.
Free	2102.	3869.	4897.
kv=200, kr=0	427.	611.	2219.
kv=400, kr=0	595.	861.	2330.
kv=600, kr=0	719.	1051.	2435.
kv=800, kr=0	818.	1210.	2536.
kv=800, kr=100	831.	1317.	2783.
kv=800, kr=200	838.	1380.	2945.
kv=700, kr=400	**793.**	**1397.**	**3111.**

The results in this case follow closely with the two previous cases. The best correlation occurs when using a vertical spring of 700 lb/in/in and a rotation spring of 400 lb-in/rad/in. In this case, the first three frequencies from the analysis match reasonable well with the first three frequencies from test.

Conclusions

The results indicate that the boundary conditions determine the natural frequencies, and that for accurate prediction, a characterization of the stiffness parameters and geometry of the epoxy used to hold the actuators in place be made. Since the spring stiffness values are not the same from case to case, any variations in the amount of epoxy used or in the thickness and width of the epoxy should be noted and investigated. The epoxy itself could be modeled with finite elements, instead of using springs.

References

1 Kousen, K. A., "Multiple Mode Minimization of Wake/Blade-Row Interaction Noise Using a Single Actuator Per Blade," *AIAA Paper 96-1691*, October 1993.

2 Kousen, K.A. and J.M. Verdon, "*Active Control of Wake/Blade-Row Interaction Noise*," **AIAA Journal**, Vol. 32, No. 10, pp. 1953-1960, October 1994.

3 *Anti-Sound Arrangement for Multi-Stage Blade Cascade*, United States Patent Number 5,420,383, May 30, 1995.

4 Burdisso, R. A., R. H. Thomas, and C. R. Fuller, "Active Control of Spinning Acoustic Modes from Turbofan Engine," AIAA Paper No. 94-0361, January 1994.

5 Thomas, R. H., Burdisso, R. A., Fuller, C. R., and W. F. O'Brien "Preliminary Experiments on Active Control of Fan Noise From a JT15D Turbofan Engine," **Journal of Sound and Vibration**, Vol. 161, No. 3, 1993, pp. 532-537.

6 Smith, J.P; Burdisso, R.A.; and C.R. Fuller, "Experiments on the active control of inlet noise from a turbofan jet engine using multiple circumferential control arrays," AIAA Paper-96-1792, May, 1996.

7 Simonich, J., Lavrich, P., Sofrin, T., and Topal, D., "Active Aerodynamic Control of Wake-Airfoil Interaction Noise-Experiment," *AIAA Journal*, Vol. 31, No. 10, October 1993, pp. 1761-1768.

8 Minter, J.A., Hoyniak, D., and Fleeter, S., "Active Airfoil Surface Control of Wake Generated Discrete Frequency Noise," *AIAA Paper 94-2952*, June 1994.

9 Minter, J.A. and S. Fleeter, "Active control of turbomachine discrete frequency noise utilizing oscillating flaps and pistons," Proceedings of the 1st CEAS/AIAA Joint Aeroacoustics, Munich, Germany, CEAS-AIAA-95-030, Vol. 1, p. 195-204, June 12-15, 1995

10 McCarthy, S.M., and Fleeter, S., "Dipole Active Control of Wake-Blade Row Interaction Noise," *AIAA Paper 96-1783*, May 1996.

11 Tyler, J.M. and Sofrin, T.G., ``Axial Flow Compressor Noise Studies,"*SAE Transactions*, Vol. 70, 1962, pp. 309-332.

12 Verdon, J.M., ``The Unsteady Aerodynamic Response to Arbitrary Modes of Blade Motion,"*Journal of Fluids and Structures*, Vol. 3, No. 3, May 1989, pp. 255-274.

13 Kousen, K.A. and Verdon, J.M., ``Active Control of Wake/Blade-Row Interaction Noise Through the Use of Blade Surface Actuators," Contractor Report 4556, NASA, December 1993.

14 Kousen, K.A. and Verdon, J.M., ``Active Control of Wake/Blade-Row Interaction Noise," AIAA Journal, Vol. 32, No. 10, October 1994, pp. 1-4.

15 Verdon, J., Barnett, M., Hall, K., and Ayer, T., ``Development of Unsteady Aerodynamic Analyses for Turbomachinery Aeroelastic and Aeroacoustic Applications," Contractor Report 4405, NASA, October 1991.

16 Verdon, J.M., ``Review of Unsteady Aerodynamic Methods for TurbomachineryAeroelastic and Aeroacoustic Applications,"*AIAA Journal*, Vol. 31, No. 2, February 1993, pp. 235-250.

17 Verdon, J.M., ``The Unsteady Aerodynamic Response to Arbitrary Modes of Blade Motion,"*Journal of Fluids and Structures*, Vol. 3, No. 3, May 1989, pp. 255-274.

18 Caspar, J.~R., ``Unconditionally Stable Calculation of Transonic Potential Flow Through Cascades Using an Adaptive Mesh for Shock Capture,"*Trans ASME A: Journal of Engineering for Power*, Vol. 105, No. 3, July 1983, pp. 504-513.

19 Whitehead, D.S. and Newton, S.G., ``A Finite Element Method for the Solution ofTwo-Dimensional Transonic Flows in Cascades,"*International Journal for Numerical Methods in Fluids,* Vol. 5, No. 2, February 1985, pp. 115-132.

20 Goldstein, M.E., ``Characteristics of the Unsteady Motion on Transversely Sheared Mean Flows," *Journal of Fluid Mechanics*, Vol. 84, No. 2, 1978, pp. 305-329.

21 Atassi, H.M. and Grzedzinski, J., ``Unsteady Disturbances of Streaming Motions around Bodies," *Journal of Fluid Mechanics*, Vol. 209, December 1989, pp. 385-403.

22 Hall, K.C. and Verdon, J.M., ``Gust Response Analysis for Cascades Operating in Nonuniform Mean Flows,"*AIAA Journal*, Vol. 29, No. 9, September 1991, pp. 1463-1471.

23 Verdon, J.M., ``The Unsteady Aerodynamic Response to Arbitrary Modes of Blade Motion," Journal of Fluids and Structures, Vol. 3, No. 3, May 1989, pp. 255-274.

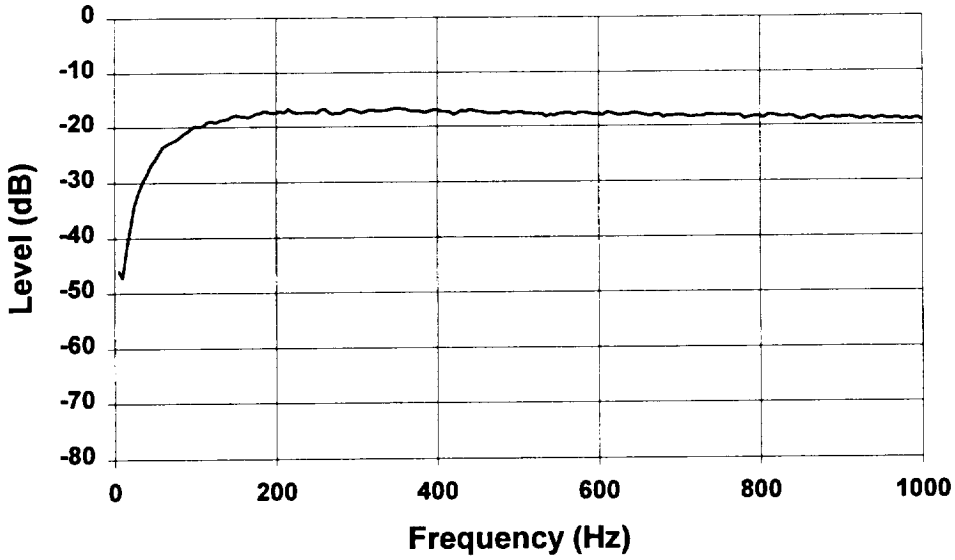

Figure 1 - Frequency Response of 20 Watt PA Amplifier (.1 watt white noise into 8 ohm resistor)

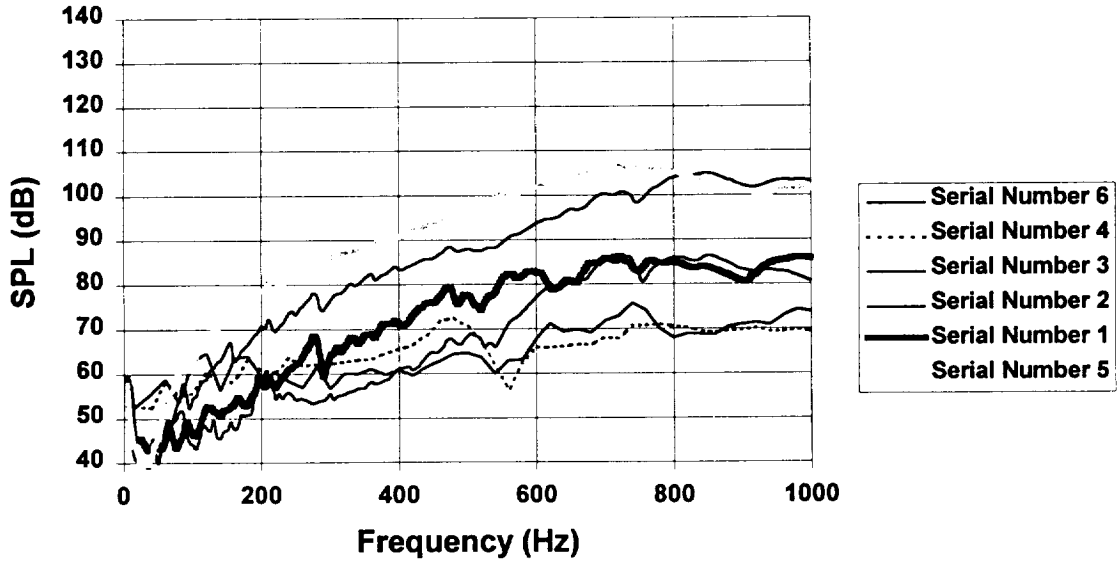

Figure 2 - Frequency Response of Various Samples of Hard Ceramic Rainbow, mounted in baffle board, 1 cm, 200 Vrms swept sine

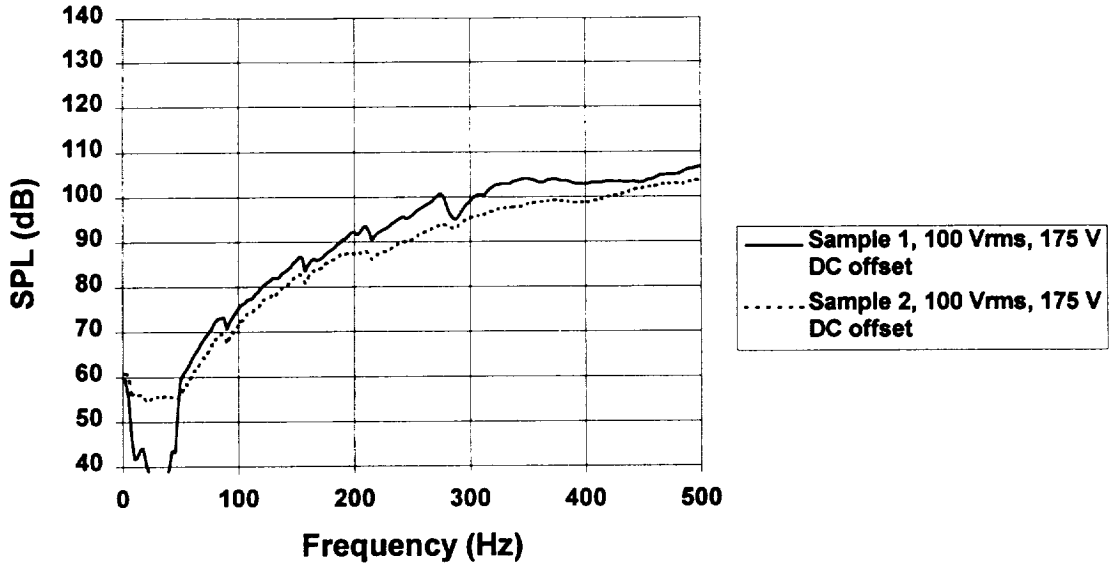

Figure 3 - Frequency Response of C3900 Piezoelectric Rainbow, mounted in baffle board, 1 cm

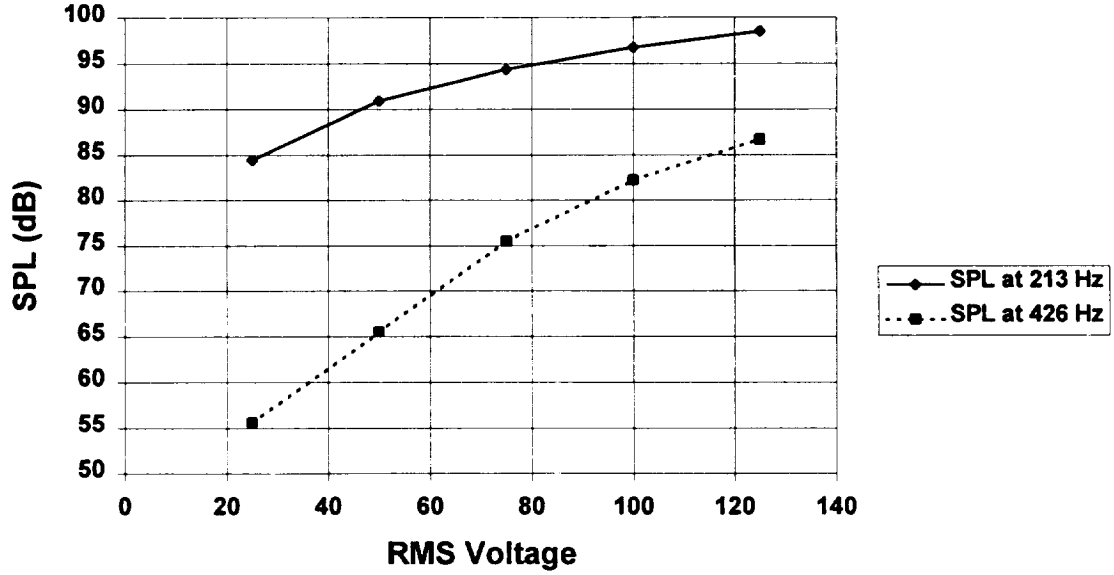

Figure 4 - Frequency Response of 2 inch diameter Rainbow, mounted in baffle board, 1 cm

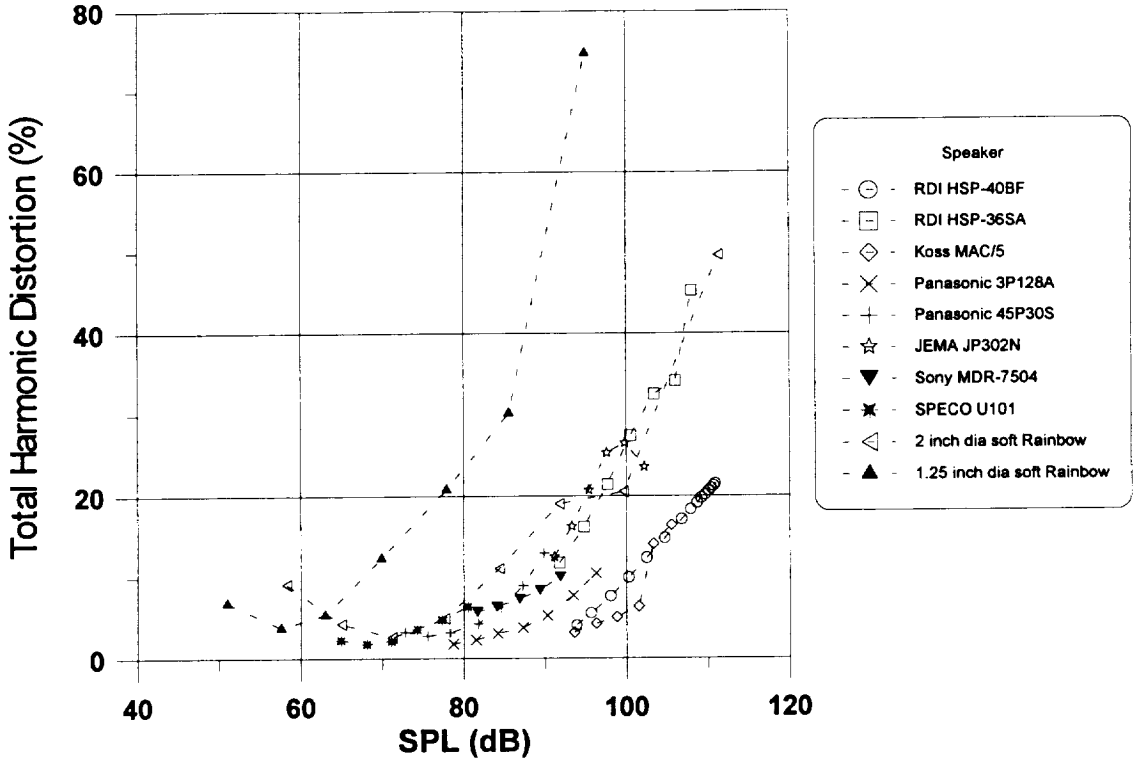

Figure 5 - Harmonic Distortion of Miniature Speakers, 213 Hz Sine Wave

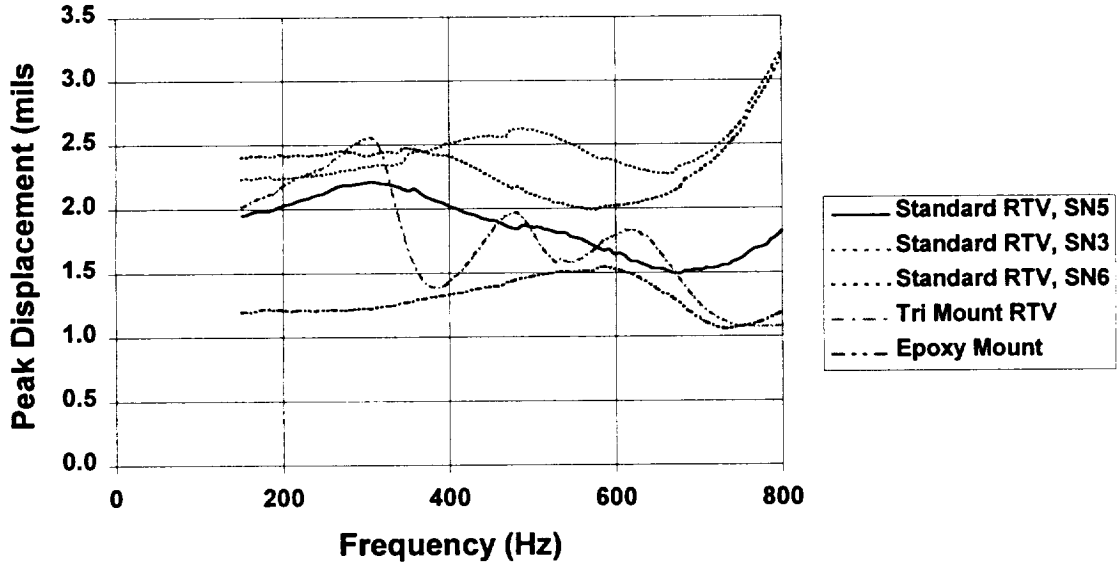

Figure 6 - Peak Displacement Response of 1.25 inch diamter Soft Rainbow, 175 Vdc offset, 90 Vrms

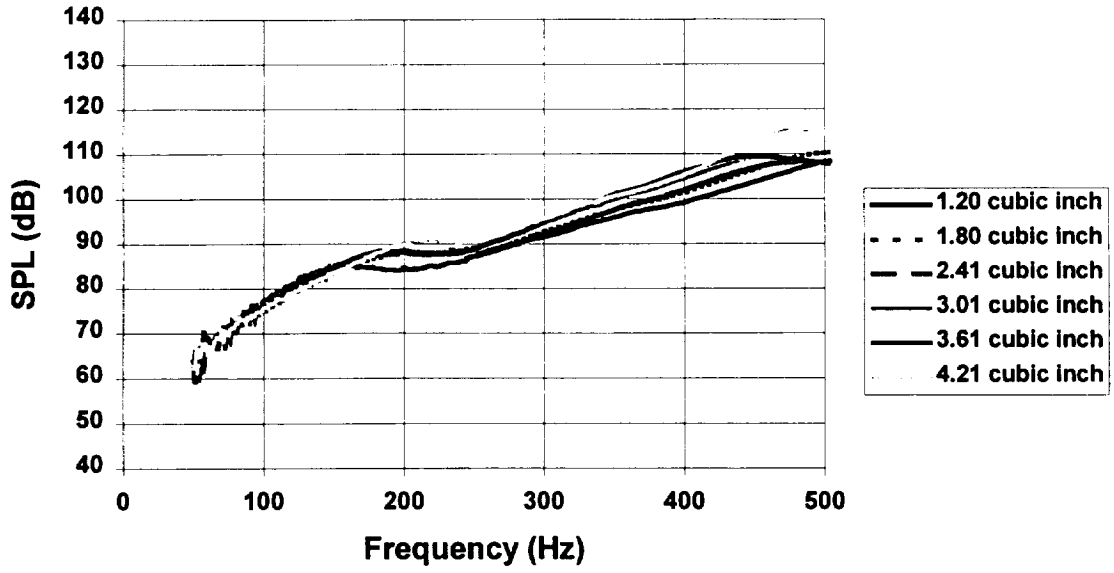

Figure 7 - Frequency Response of 1.25 inch diameter Soft Rainbow, 175 Vdc offset, 100 Vrms, 1 cm

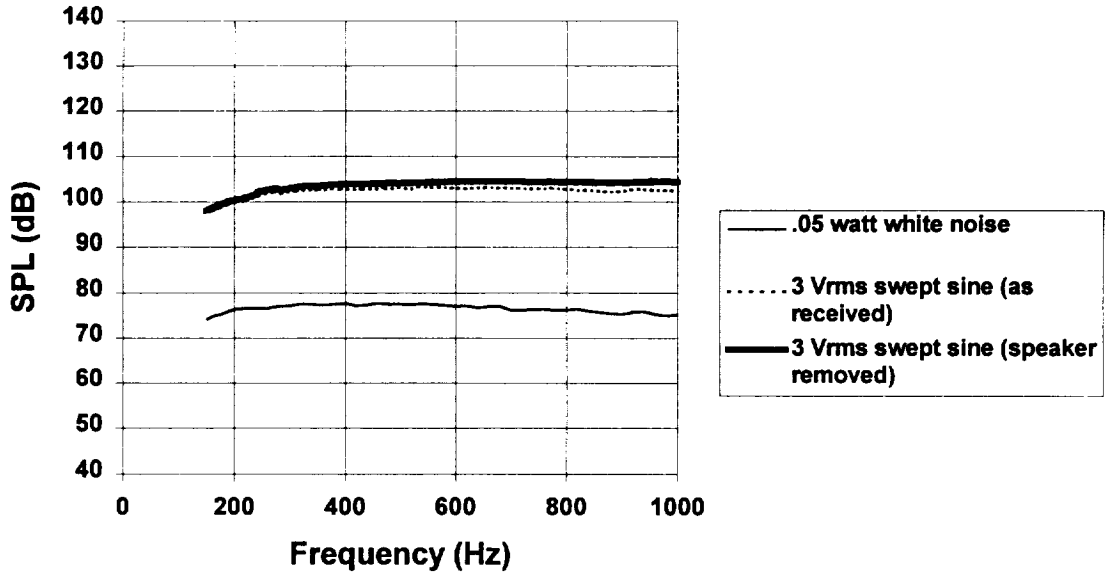

Figure 8 - Frequency Reponse of Koss MAC/5 Headphone Speaker, mounted in baffle board, 1 cm

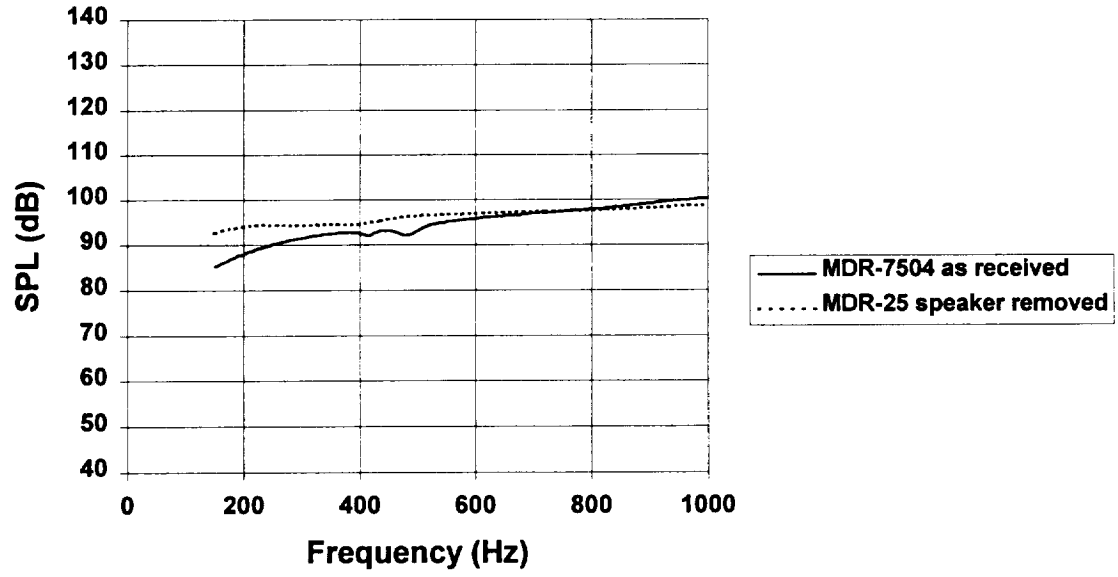

Figure 9 - Frequency Response of Sony Headphone Speaker, mounted in baffle board, .1 watt swept sine, 1 cm

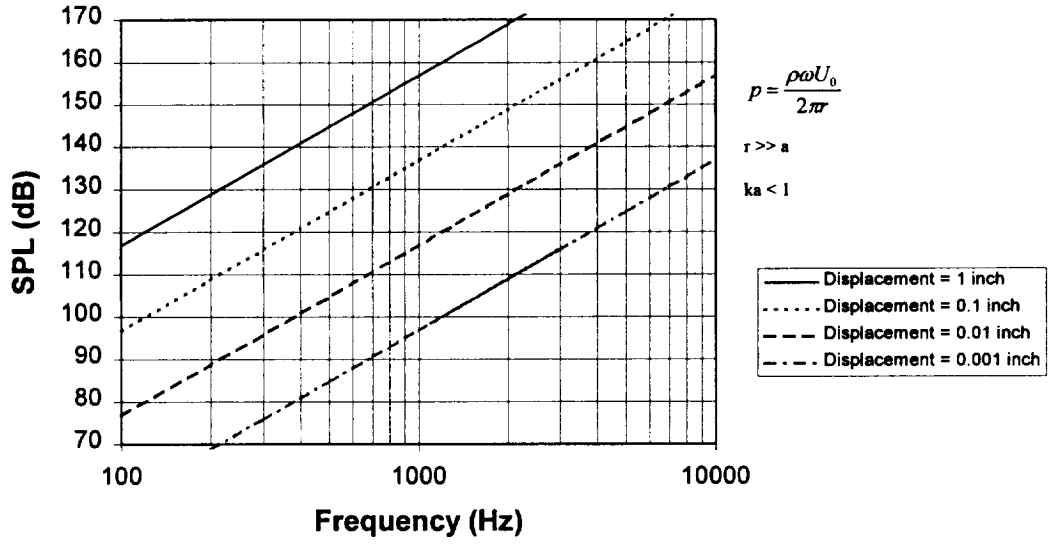

Figure 10 - Theoretical Prediction of Cylindrical Piston in Infinite Baffle, 1.25 inch diameter, r = 3 inches

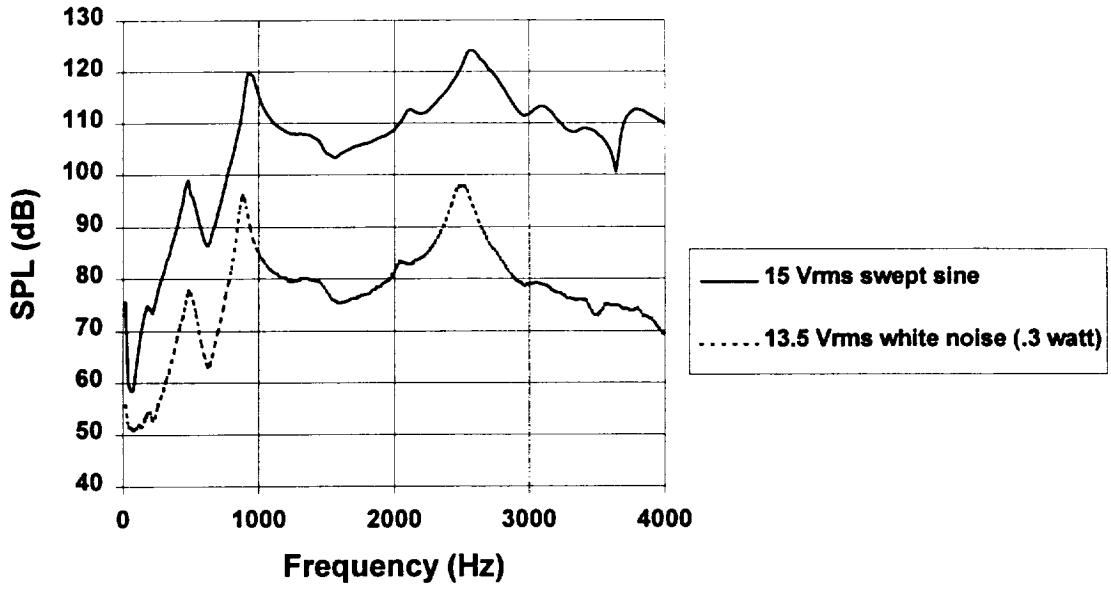

Figure 11 - Frequency Response of Radio Shack Unimorph, mounted in baffle board, 1 cm

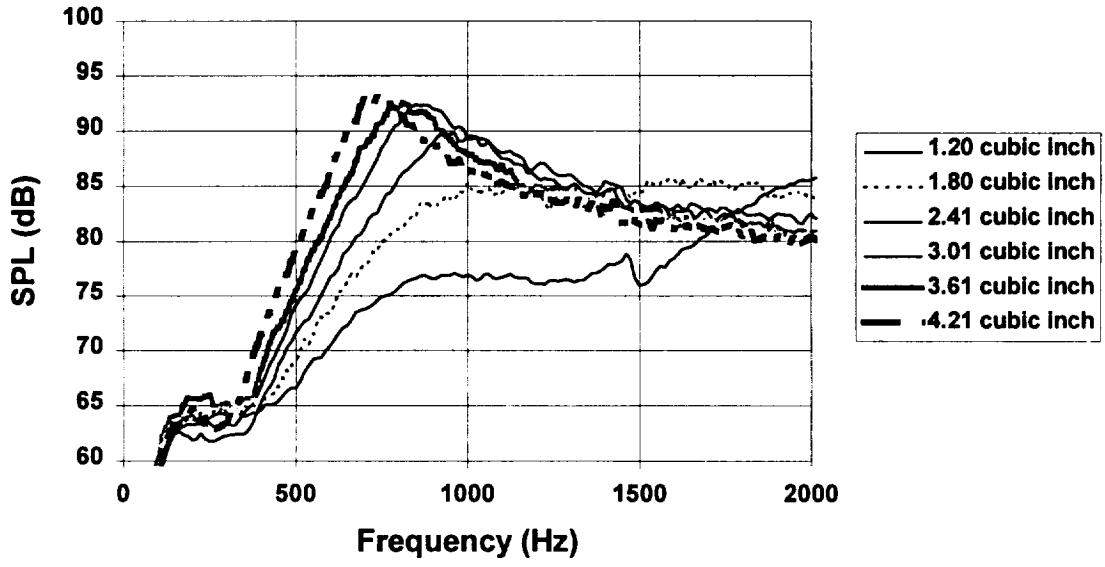

Figure 12 - Effect of Enclosure Volume on Koss MAC/5 Speaker Performance, .1 watt white noise, 1 cm mic distance

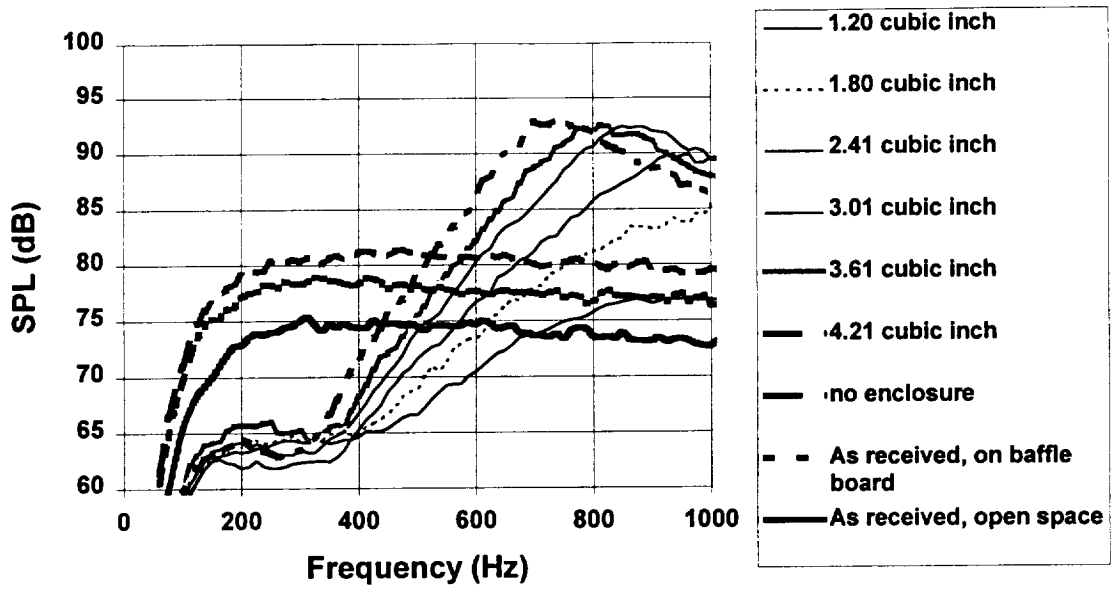

Figure 13 - Comparison of Koss MAC/5 Speaker Performance in Various Mounting Arrangements, .1 watt white noise, 1 cm mic distance

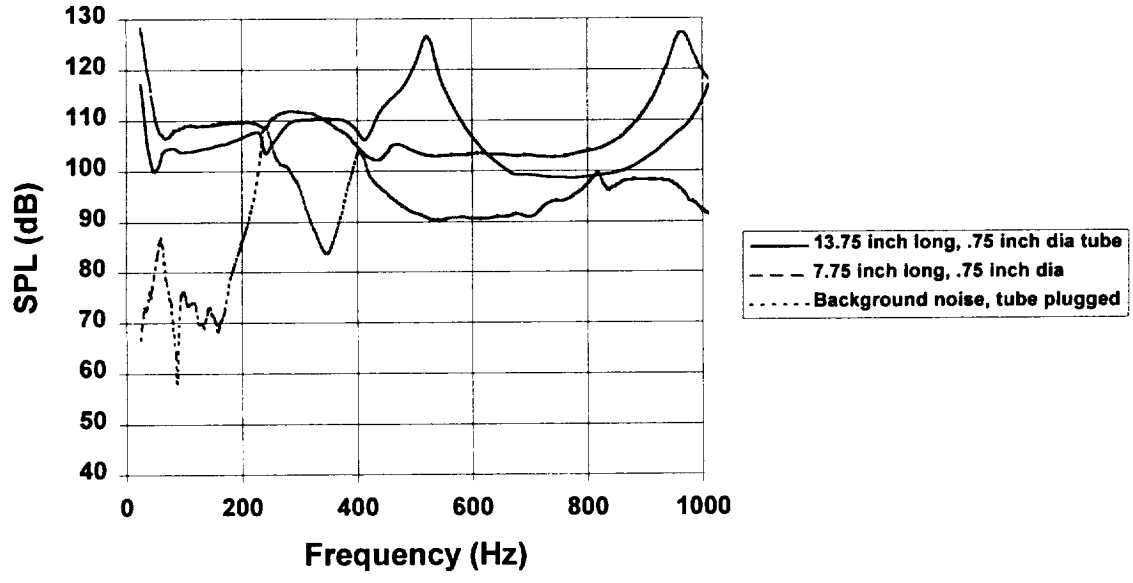

Figure 14 - Frequency Response of Woofer Coupled to Tube, spring mounted, 27.8 Vrms

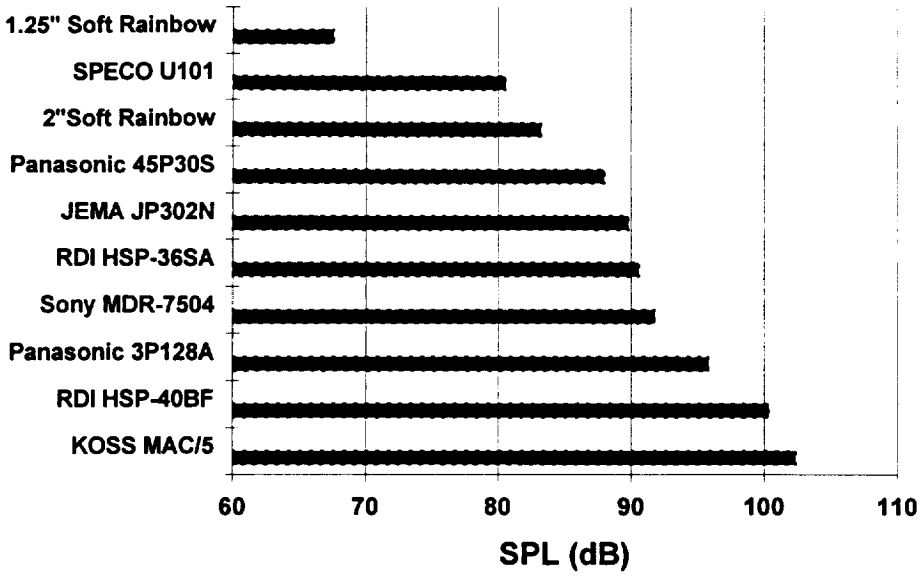

Figure 15 - Comparison of Different Speakers SPL at 10% THD

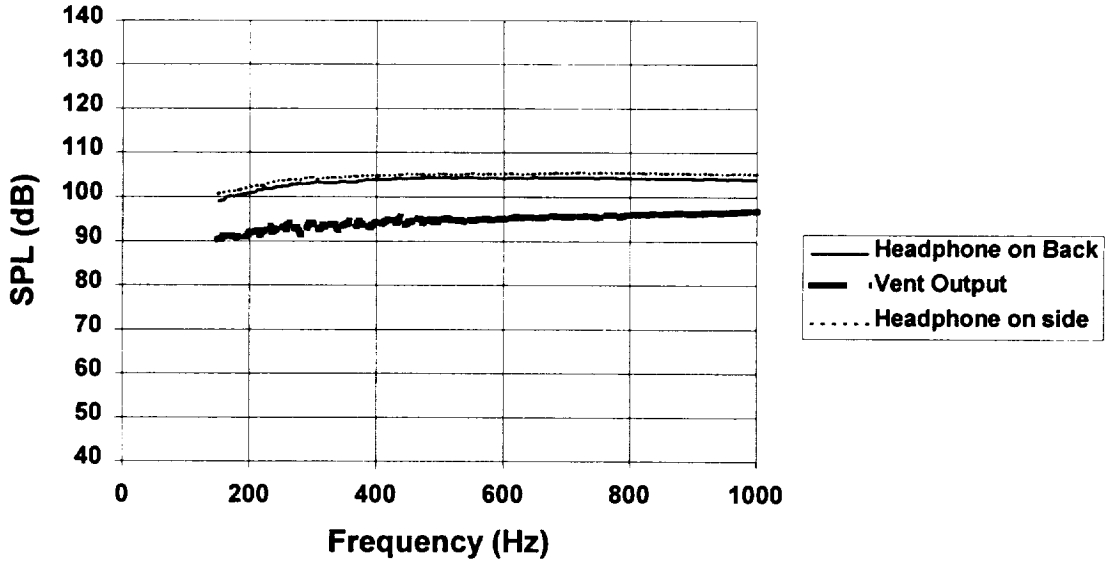

Figure 16 - Frequency Response of Koss MAC/5 Headphone, Open field, As received, 3 Vrms, 1 cm mic distance

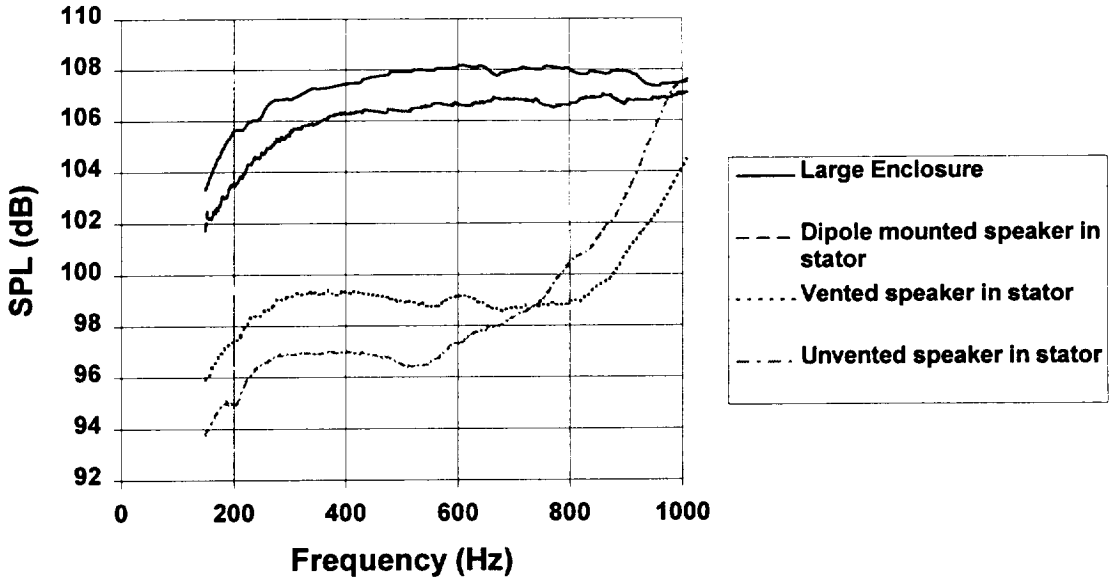

Figure 17 - Effect of Enclosure and Mountings on Performance of Koss MAC/5 Speaker

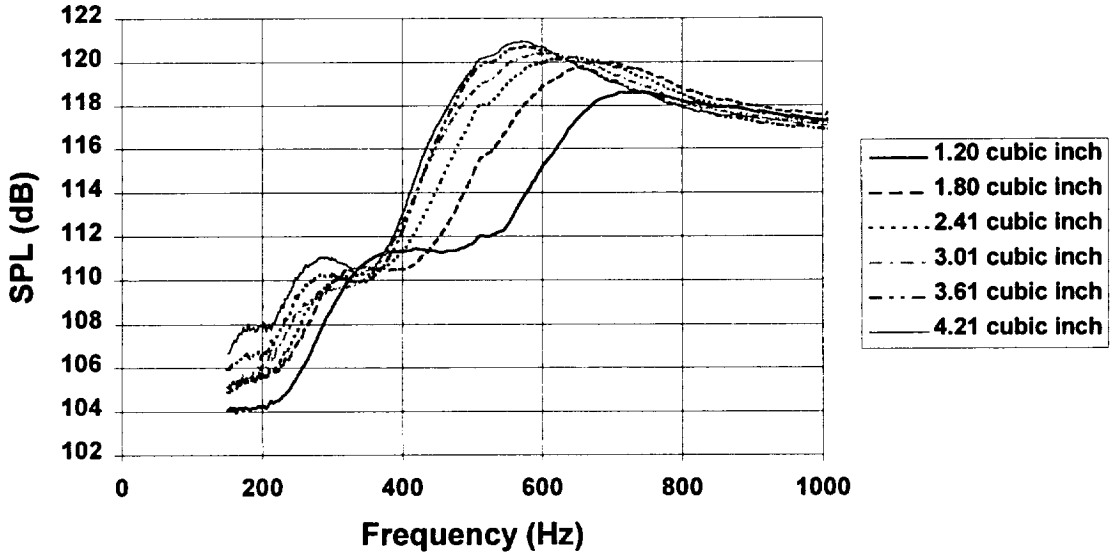

Figure 18 - Effect of Enclosure Volume on Performance of RDI HSP-40BF Speaker, 3 Vrms, 1 watt, .25 inch diameter vent, 1 cm mic distance

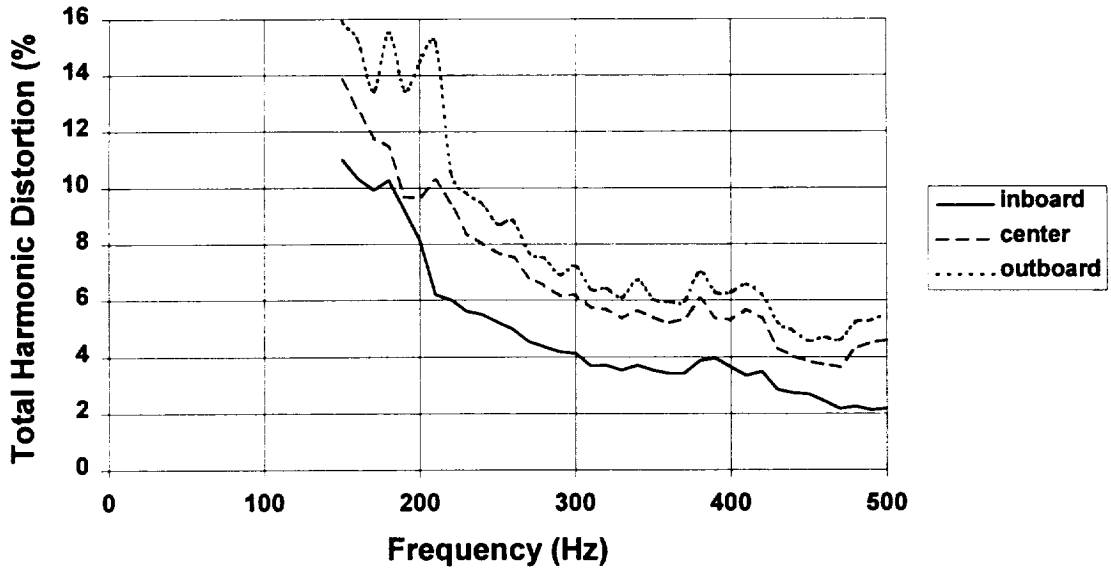

Figure 19 - Total Harmonic Distortion of Koss MAC/5 Speaker Mounted in Vane, 2.64 Vrms, vent open

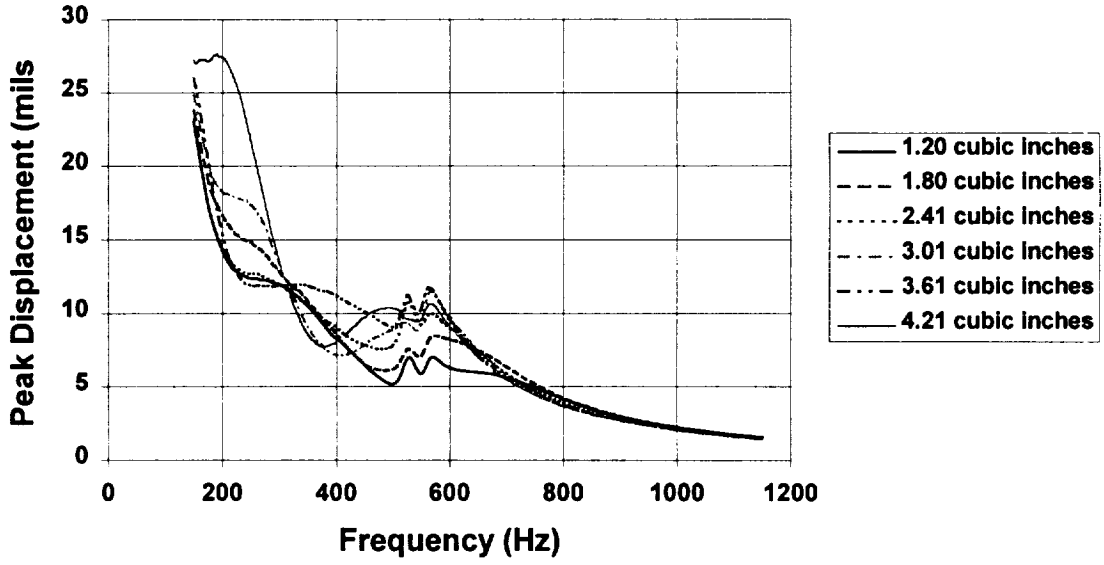

Figure 20 - Effect of Enclosure Volume on RDI HSP-40BF Speaker, 3 Vrms, Center Speaker

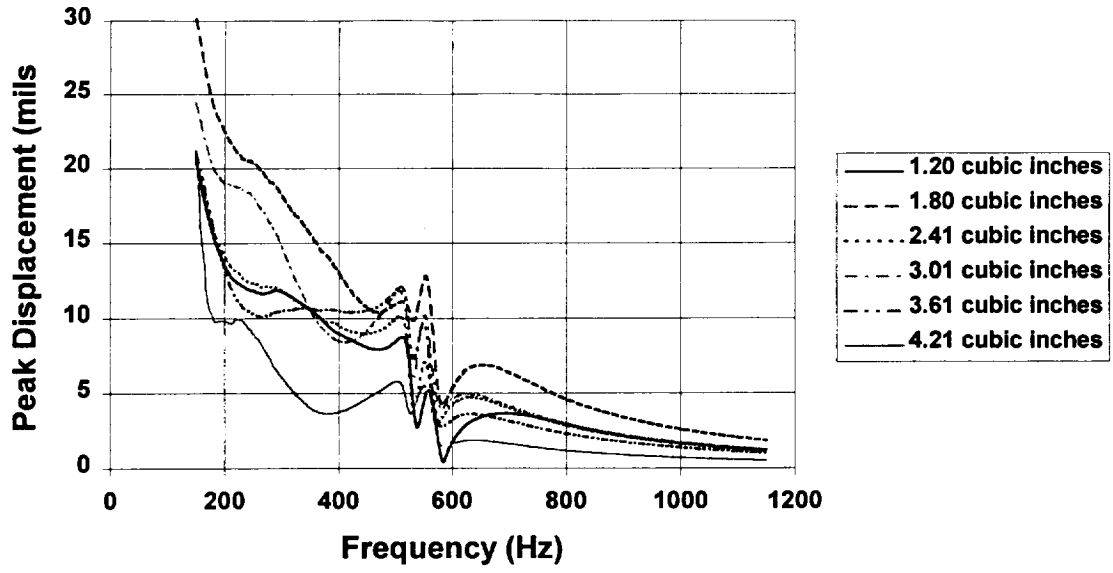

Figure 21 - Effect of Enclosure Volume on RDI HSP-40BF Speaker Displacement, 3 Vrms, 12.64 mm off center

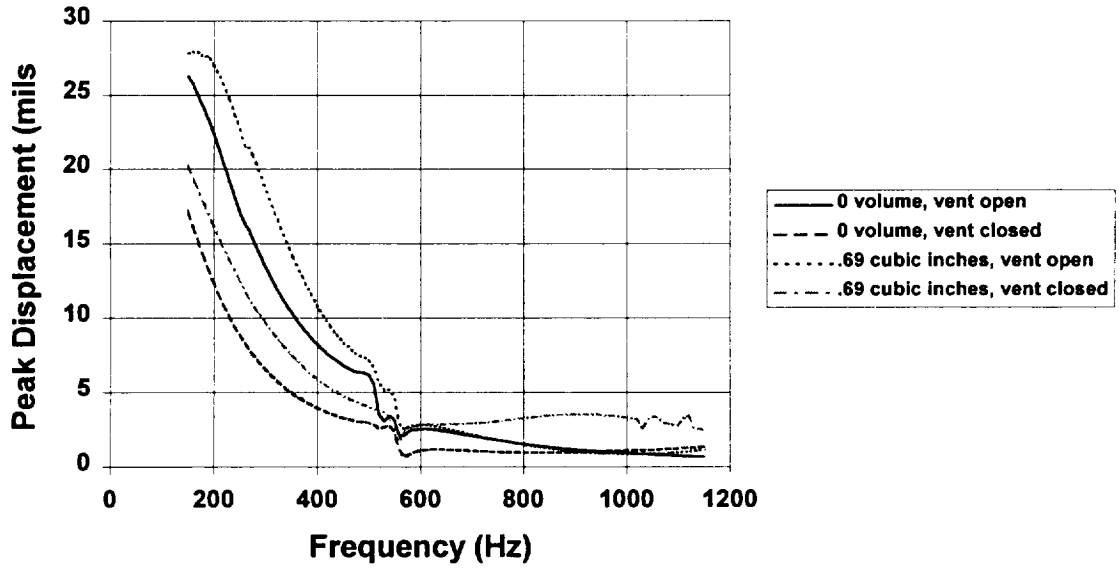

Figure 22 - Effect of Enclosure Volume on RDI-HSP-40DB Speaker Displacement, small board, 3 Vrms, center

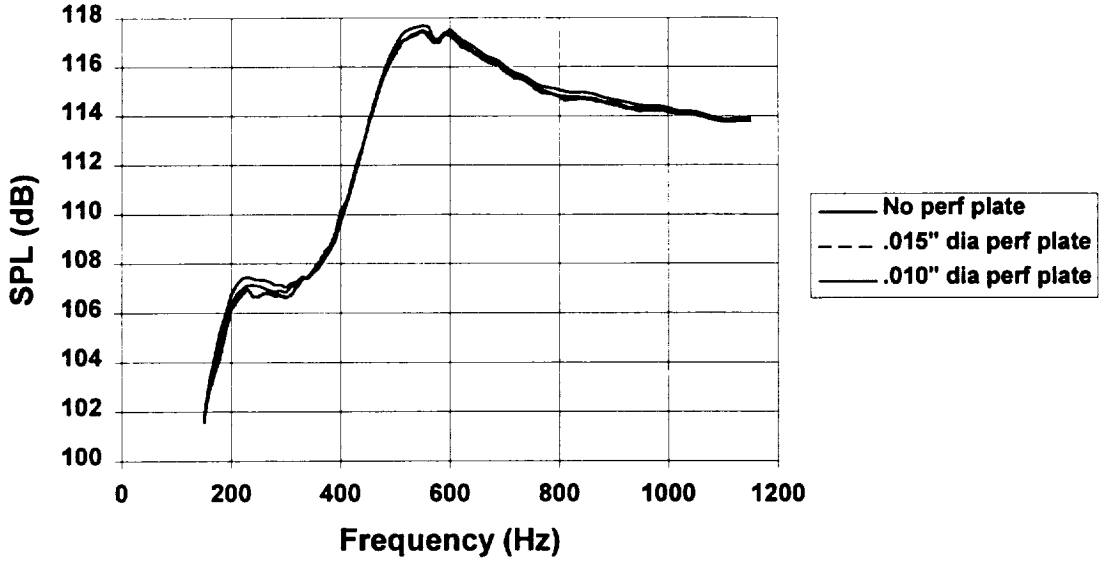

Figure 23 - Effect of Perforated Plate on Noise Transmission, RDI HSP-40BF, 4.21 in^3 enclosure volume, 3 Vrms

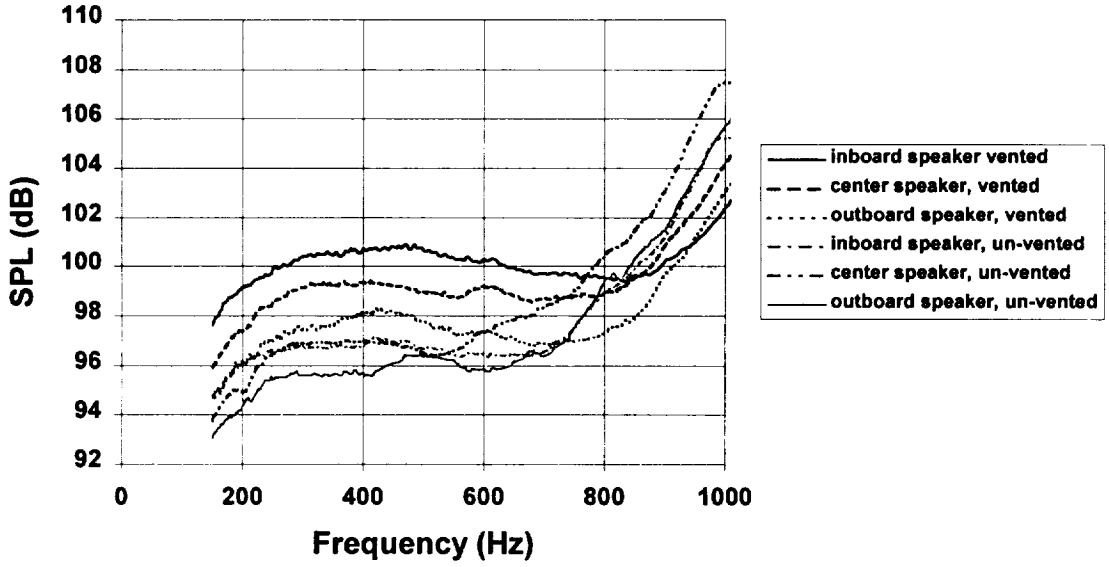

Figure 24 - Effect of Venting on Koss MAC/5 Speaker Performance, mounted in vane, 3 Vrms

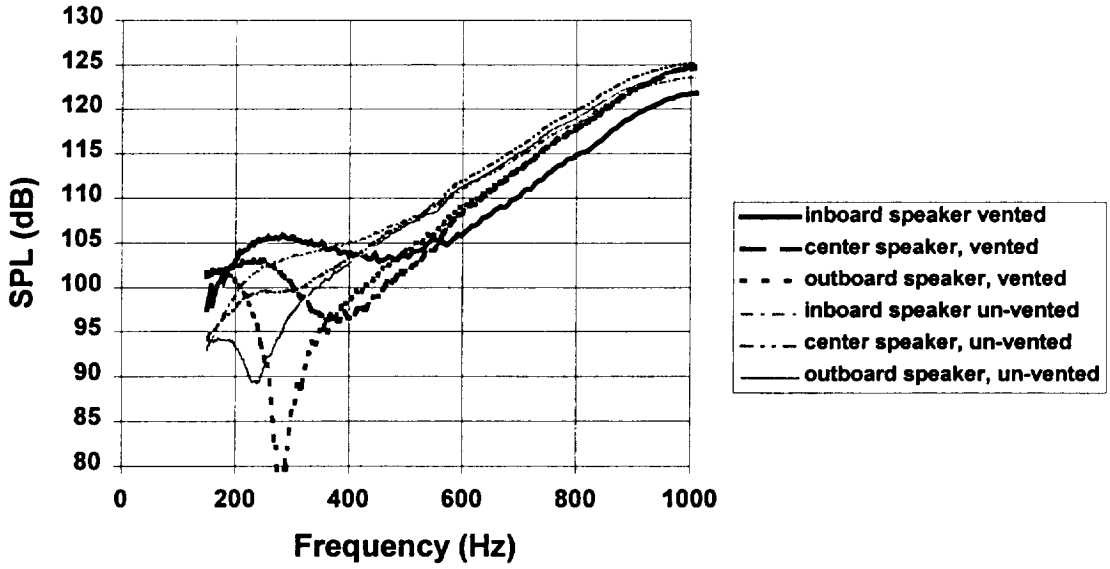

Figure 25 - Effect of Venting on RDI HSP-40BF Speaker Performance, 3 Vrms, 3 Watts, wired in parallel, mounted in vane, 1 cm mic distance

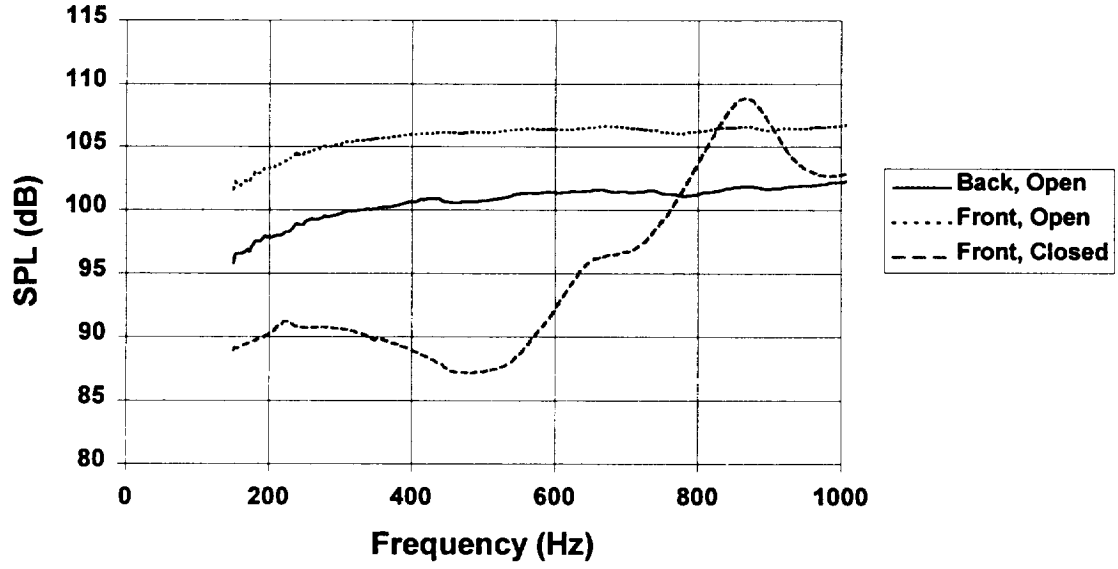

Figure 26 - Effect of Dipole Mounting on Koss MAC/5 Speaker Performance, Average of inboard, center and outboard speakers

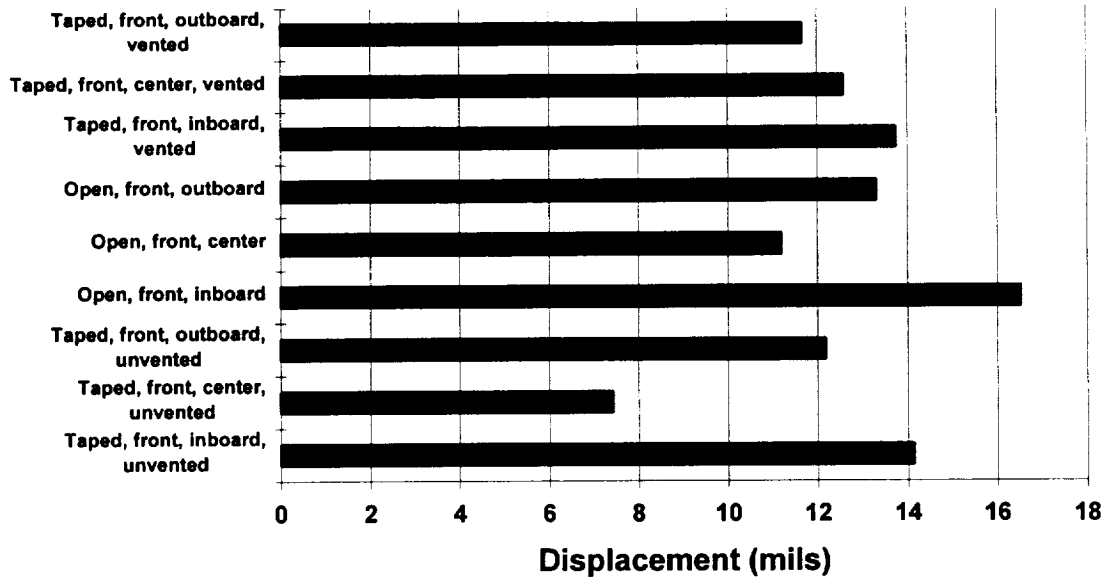

Figure 27 - Effect of Venting on Koss MAC/5 Speaker Displacement

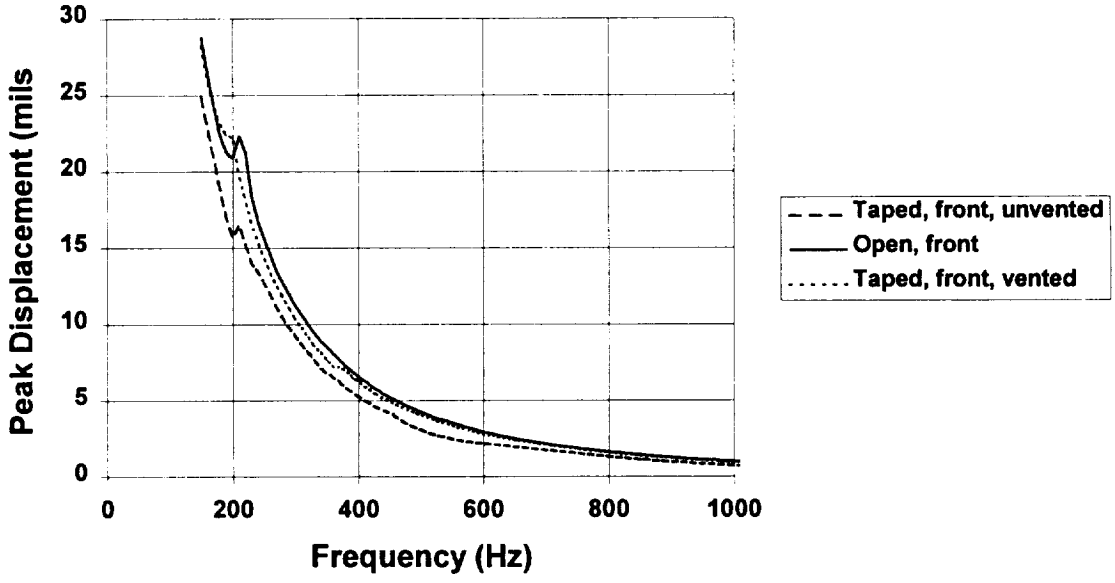

Figure 28 - Effect of Venting on Koss MAC/5 Displacement, Averaged inboard, center and outboard speakers

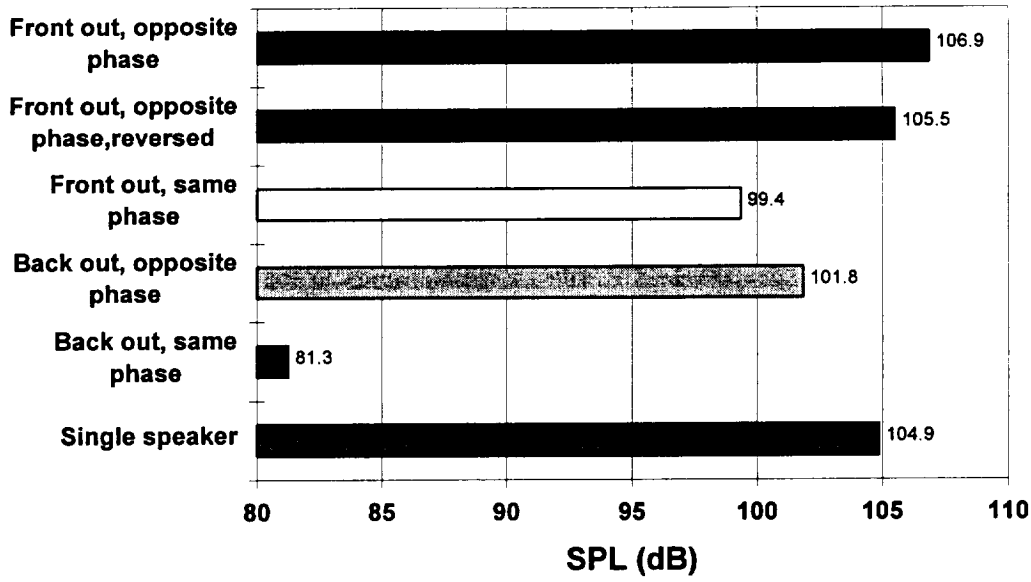

Figure 29 - Push-Pull Mounting Performance of Koss MAC/5 Speaker, 2.77 Vrms, .2 watt, 267 Hz

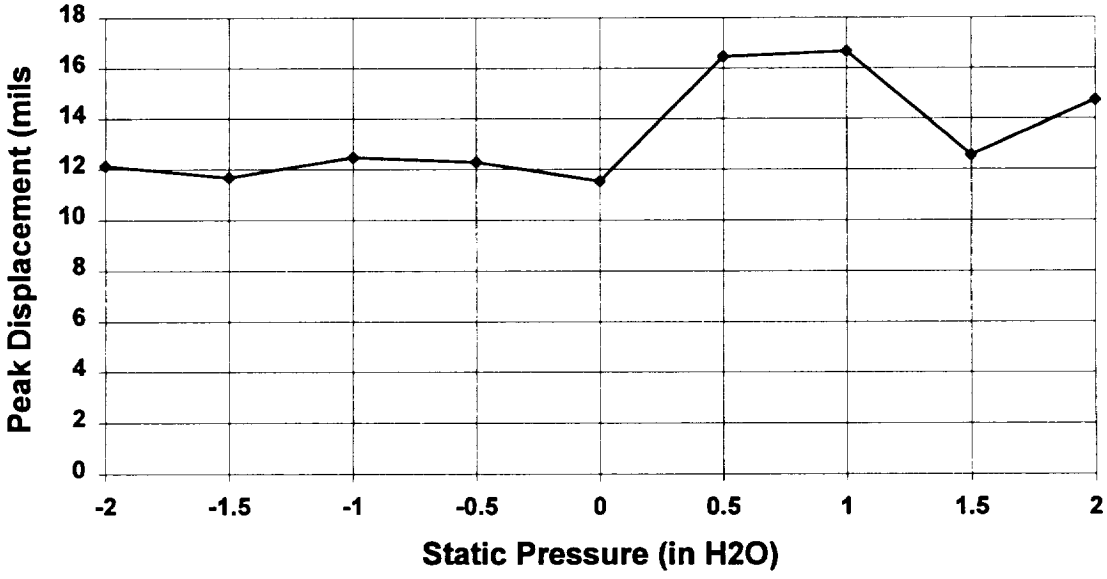

Figure 30 - Effect of Static Pressure on Koss MAC/5 Performance, 3.0 Vrms, 267 Hz

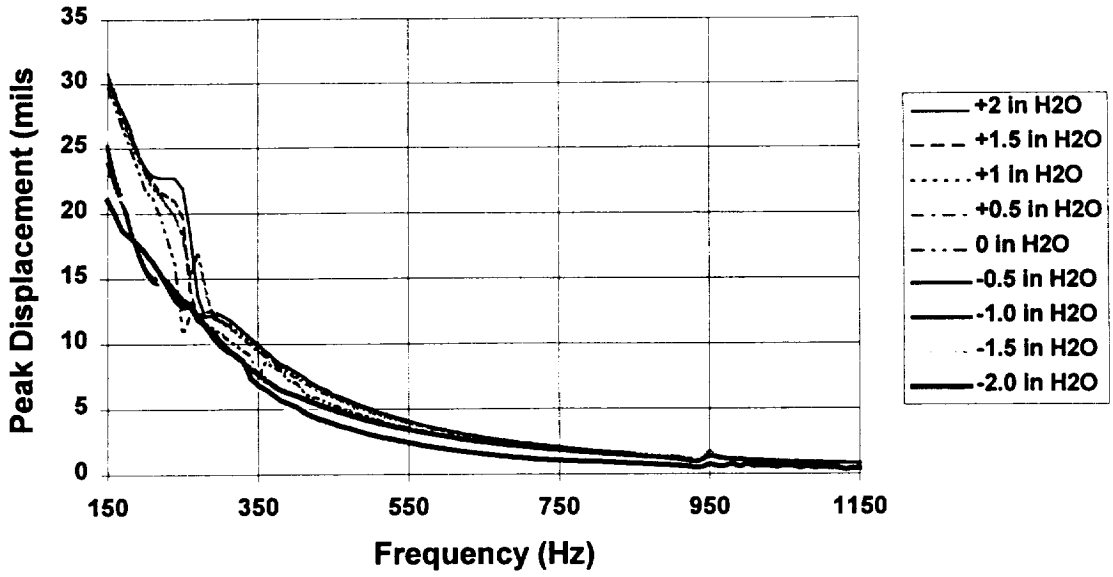

Figure 31 - Effect of Static Pressure on Displacement of Koss MAC/5 Speaker, 3 Vrms

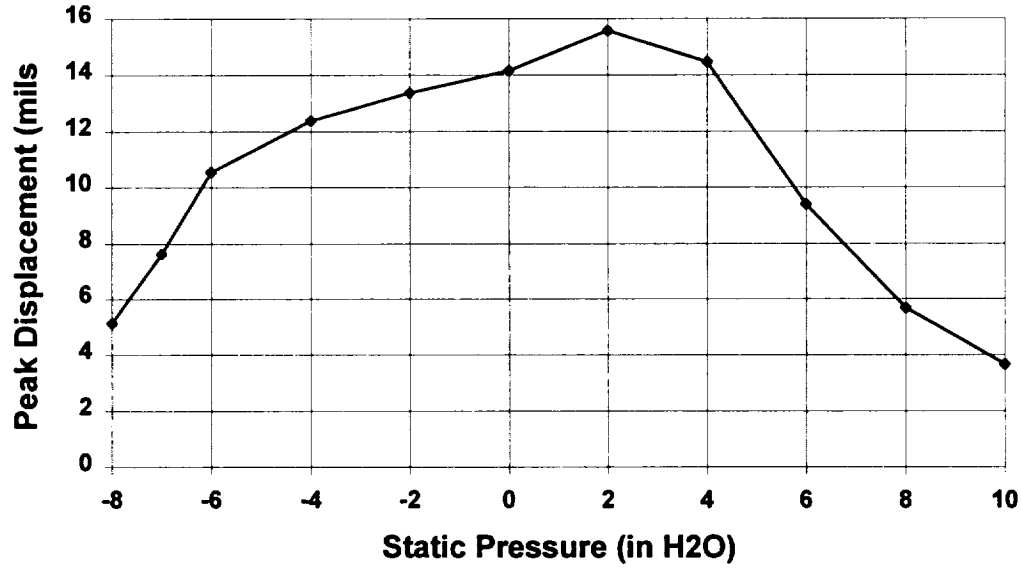

Figure 32 - Effect of Static Pressure on Displacement of RDI HSP-40BF Speaker, 3 Vrms, 267 Hz

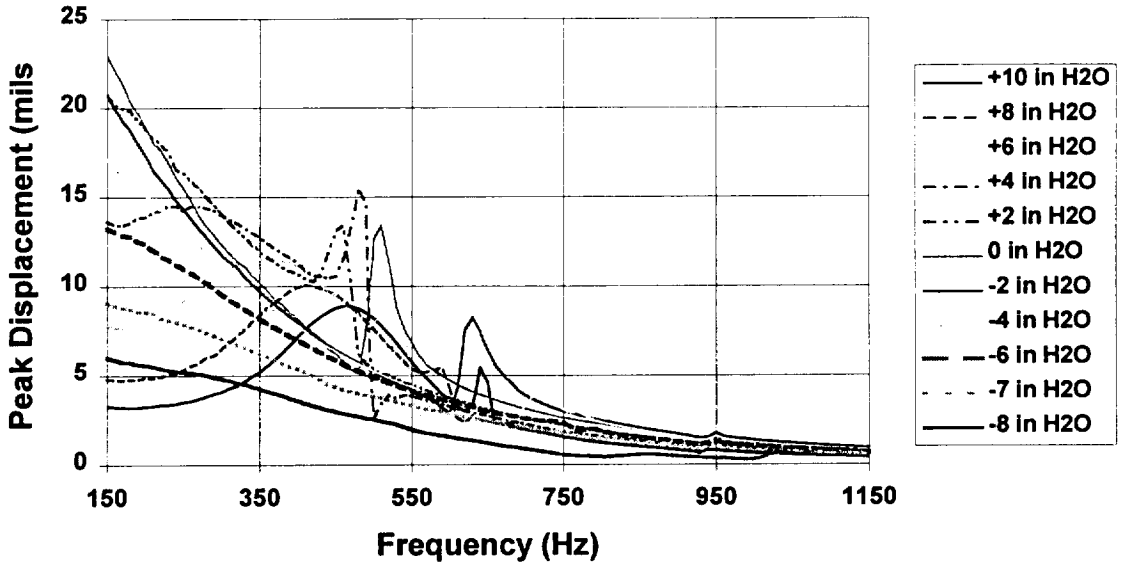

Figure 33 - Frequency Response and Effect of Static Pressure on Displacement of RDI HSP-40BF Speaker, 3 Vrms

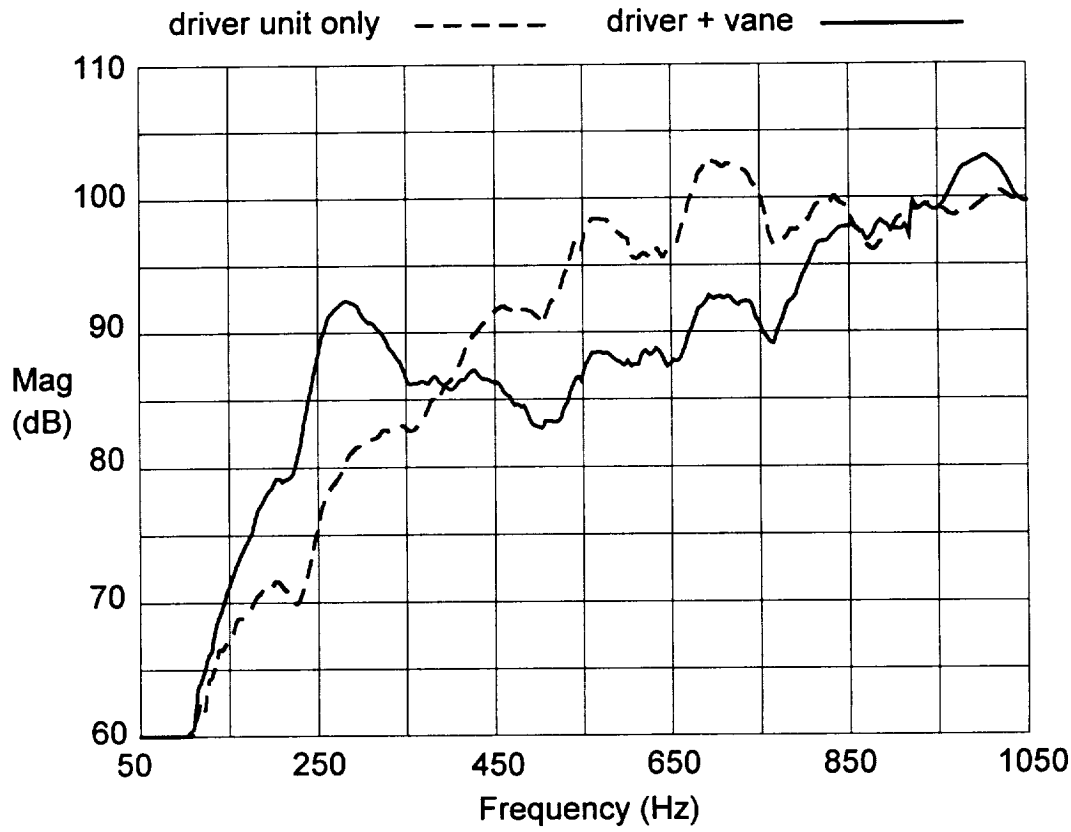

Figure 34 - Acoustic pressure measured at 1 m (39.4 inches) from actuator, for compression driver only and compression driver fitted with stator vane.

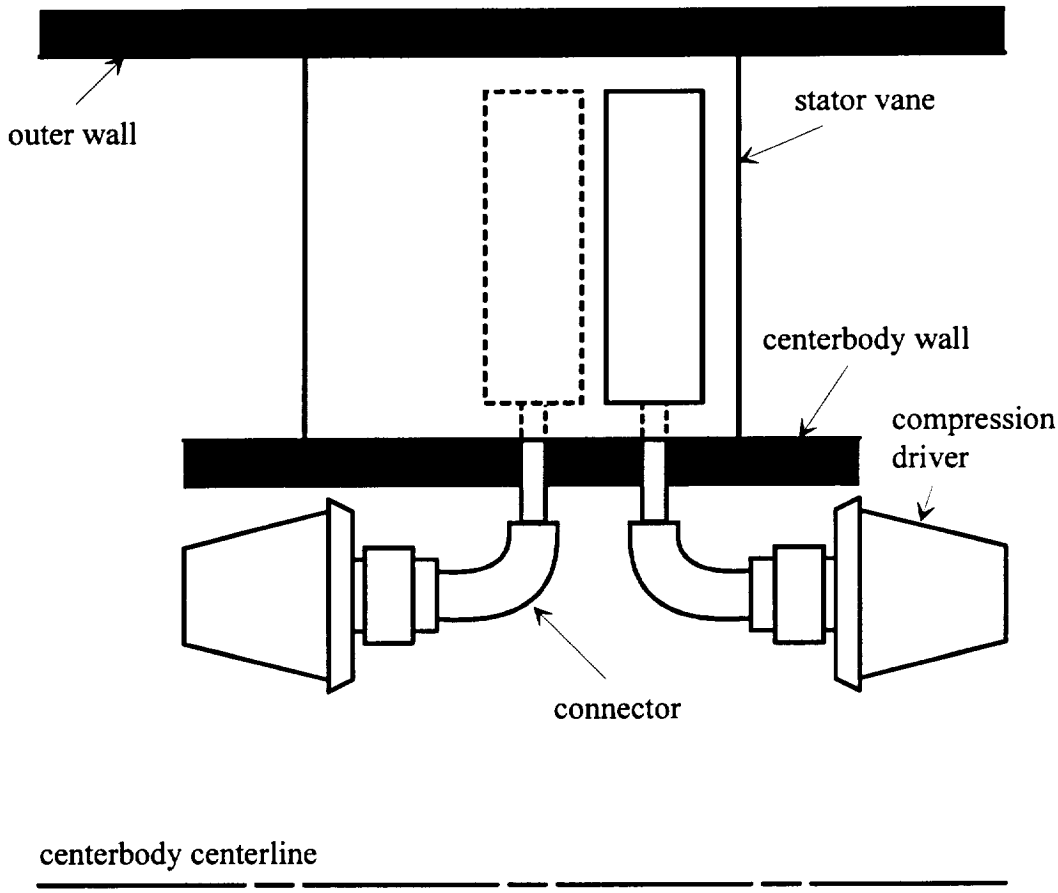

Figure 35 - Arrangement of externally mounted compression driver, stator vane, and compression driver to stator vane connector for Purdue experimental rig.

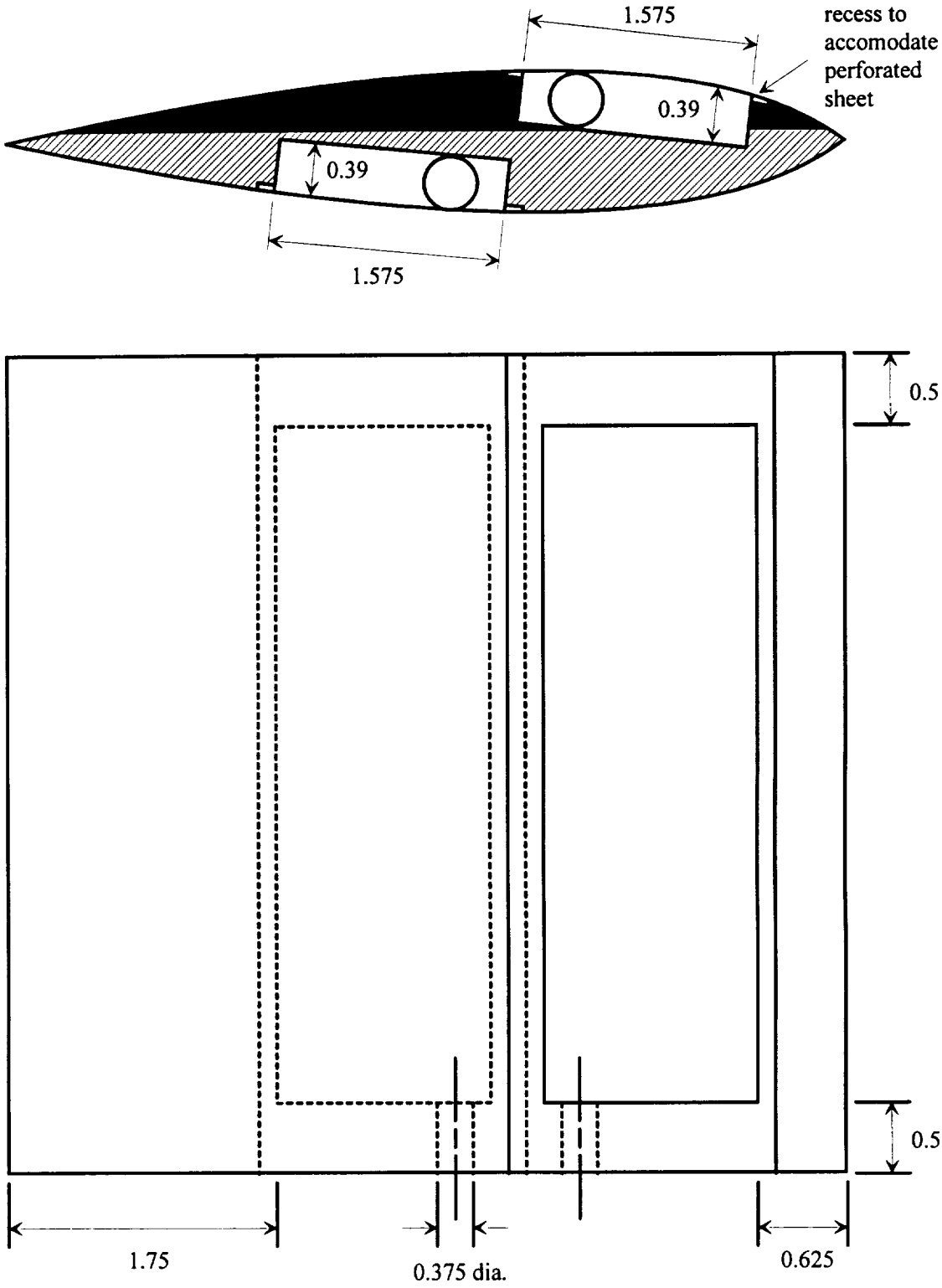

All dimensions in inches

Figure 36 - Detail of stator vane actuator arrangement.

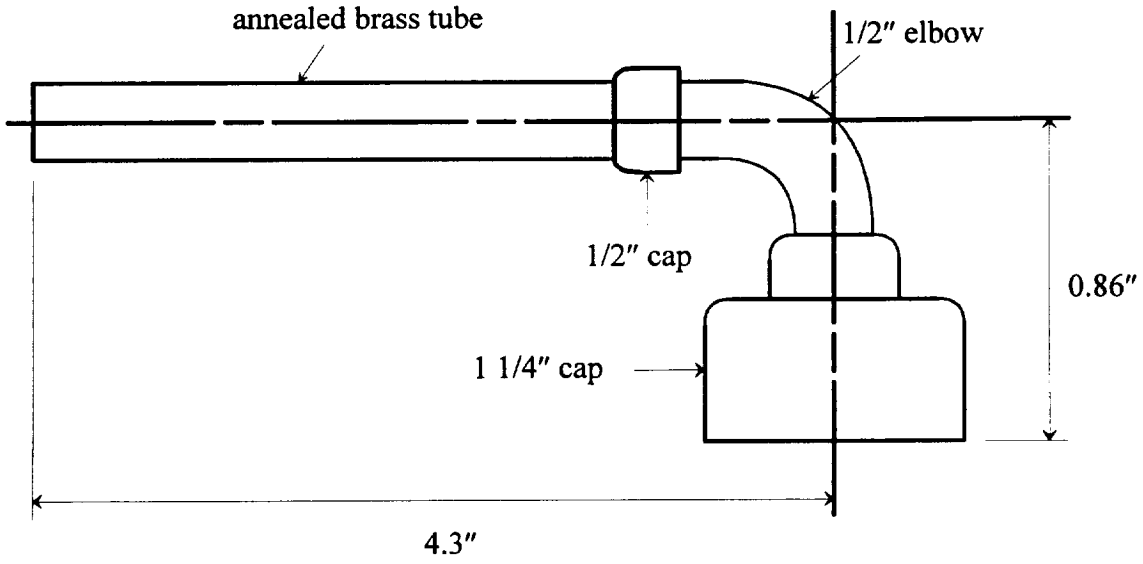

Figure 37 - Detail of compression driver to stator vane connector.

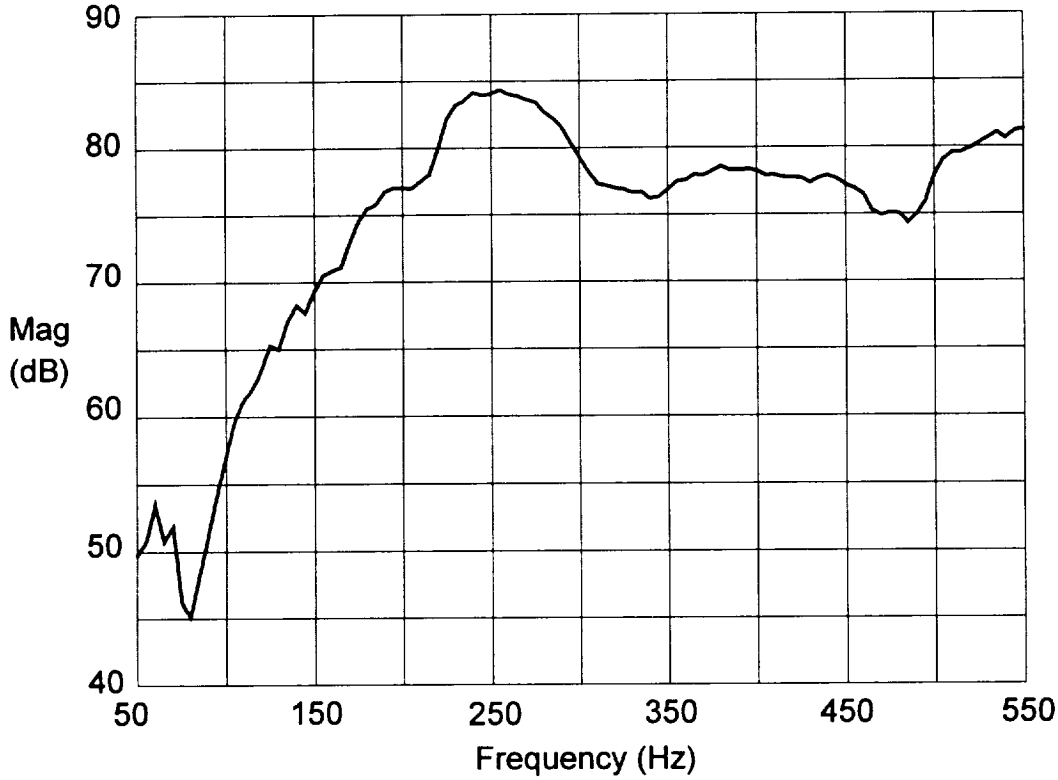

Figure 38 - Acoustic pressure measured at the location 1 m (39.4 inches) from the actuator surface for the externally driven actuator.

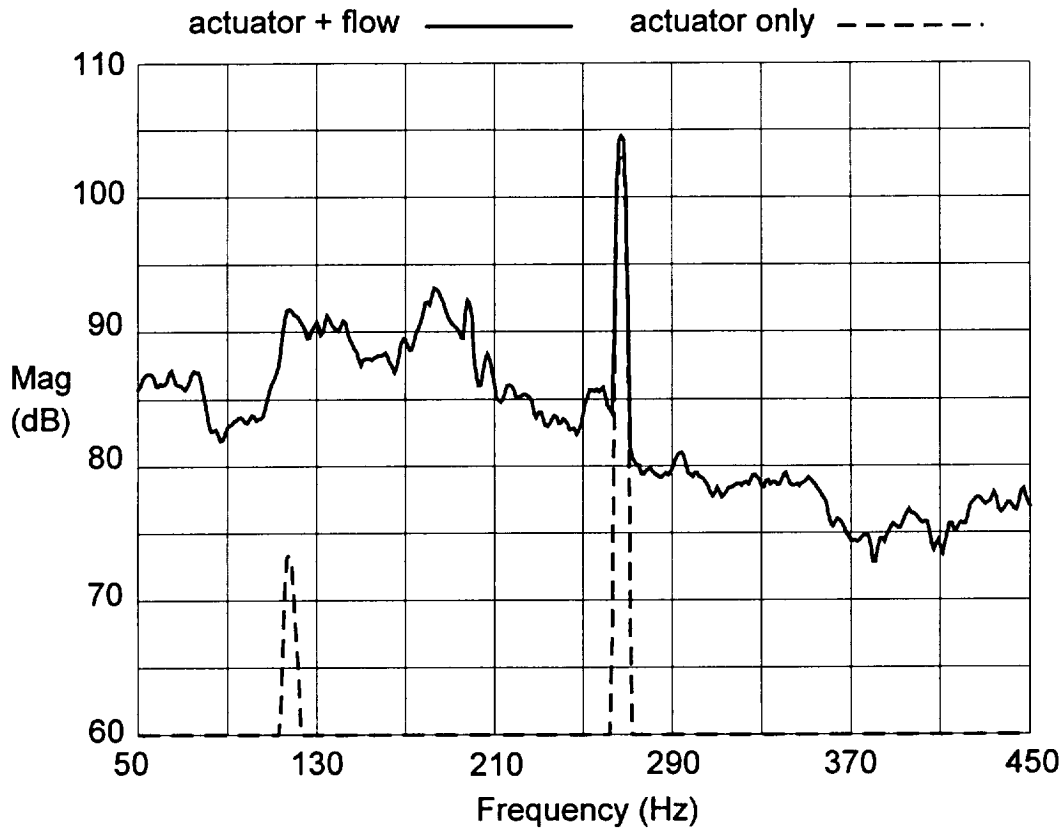

Figure 39 - Acoustic pressure measured at microphone located normal to the actuator surface, for the cases of the actuator operating with and without flow.

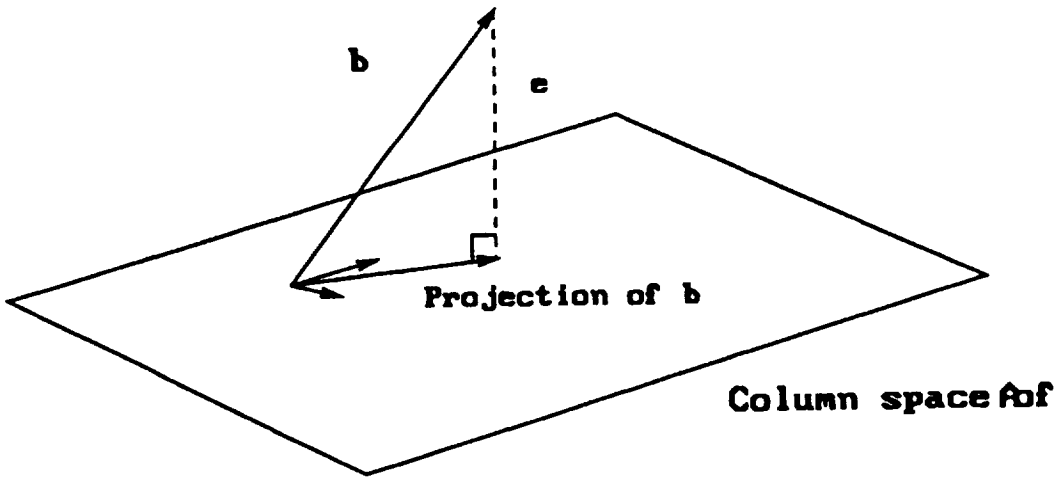

Figure 40 - Least Squares Procedure

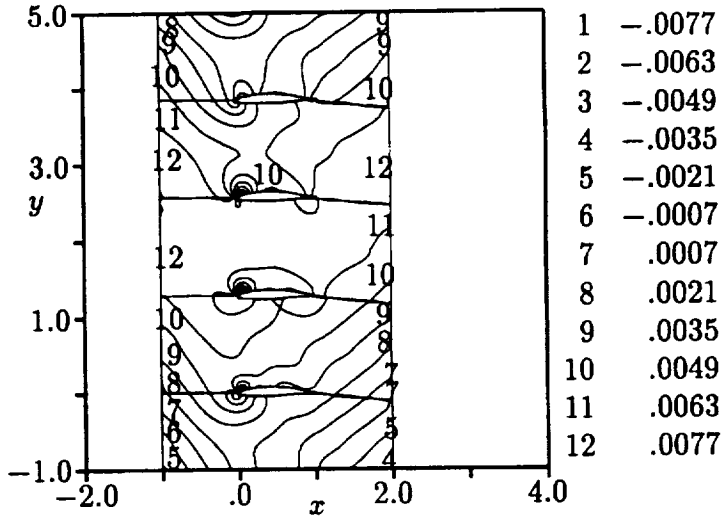

Figure 41 - Acoustic Field Without Control Applied

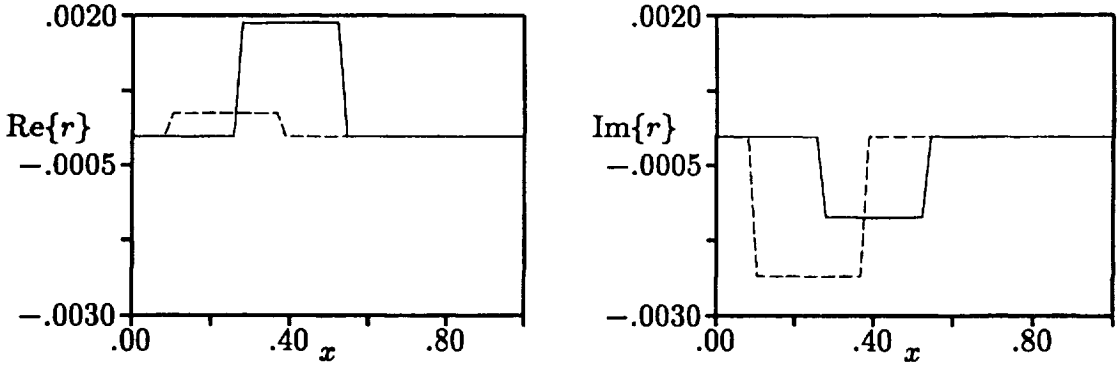

Figure 42 - Real and Imaginary Part of the Actuator Displacements for Complete Cancellation

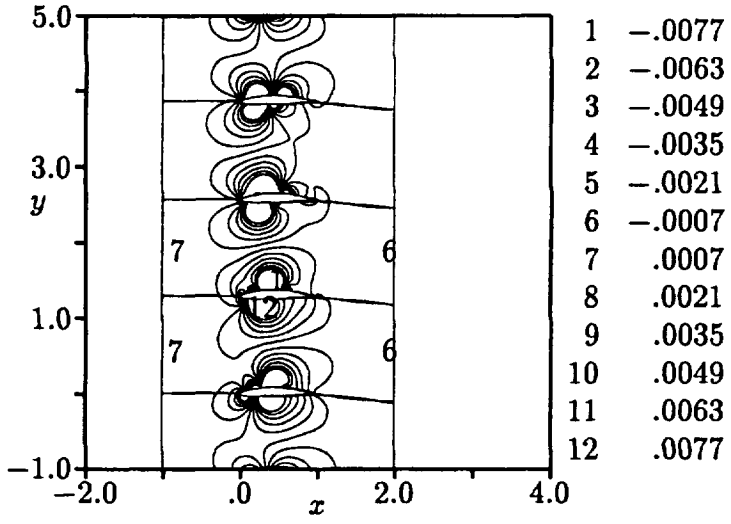

Figure 43 - Acoustic Pressure Contours with Control Applied

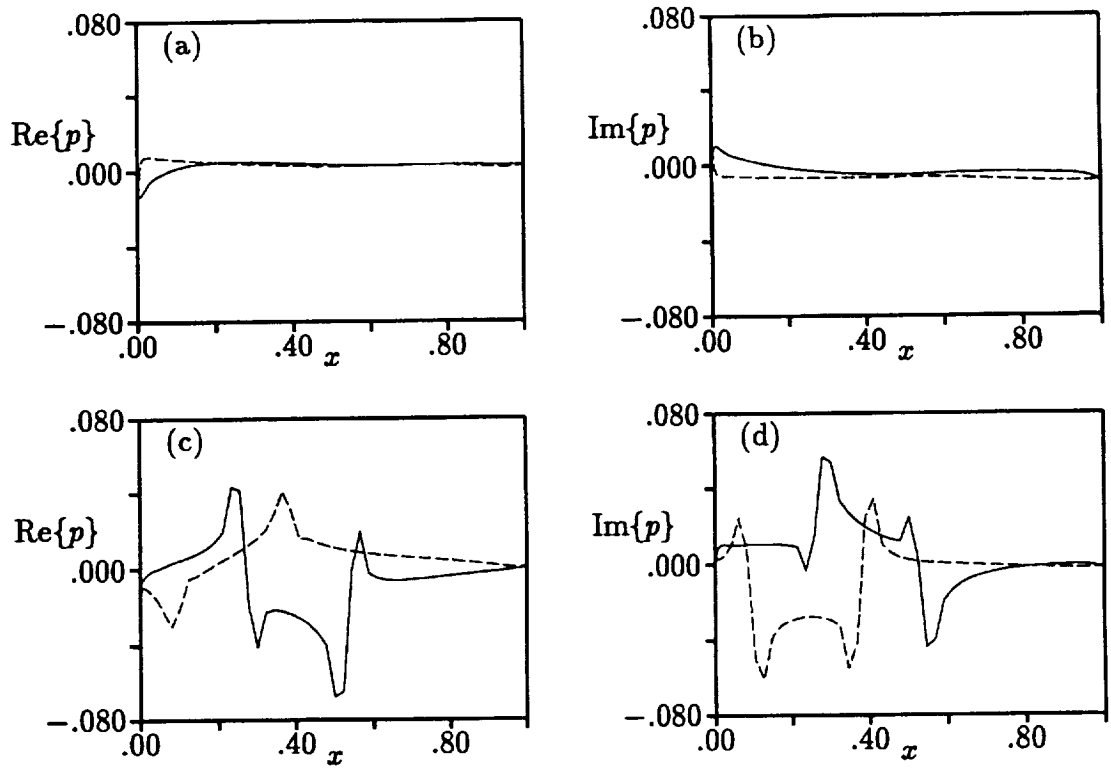

Figure 44 - (a) Real and (b) Imaginary Parts of the Surface Pressure with No Control. (c) Real and (d) Imaginary Parts of the Surface Pressure with Control

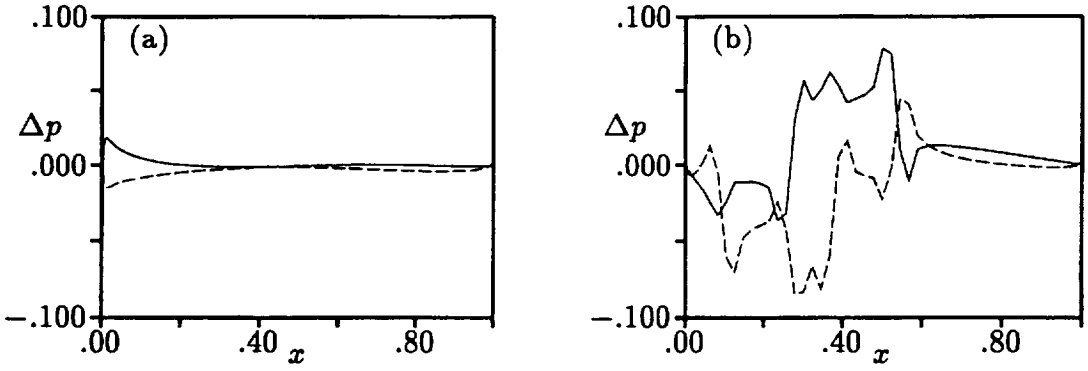

Figure 45 - Unsteady Pressure Difference (a) No Control and (b) With Control

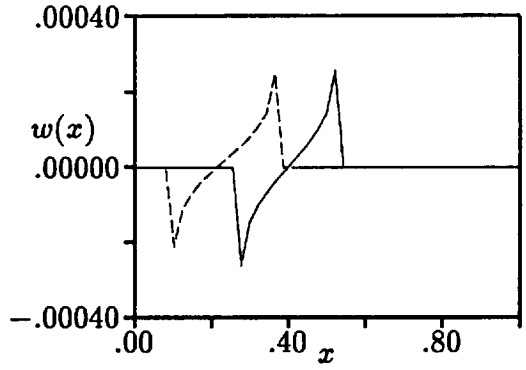

Figure 46 - Pressure Displacement Function for Controlled Case Above

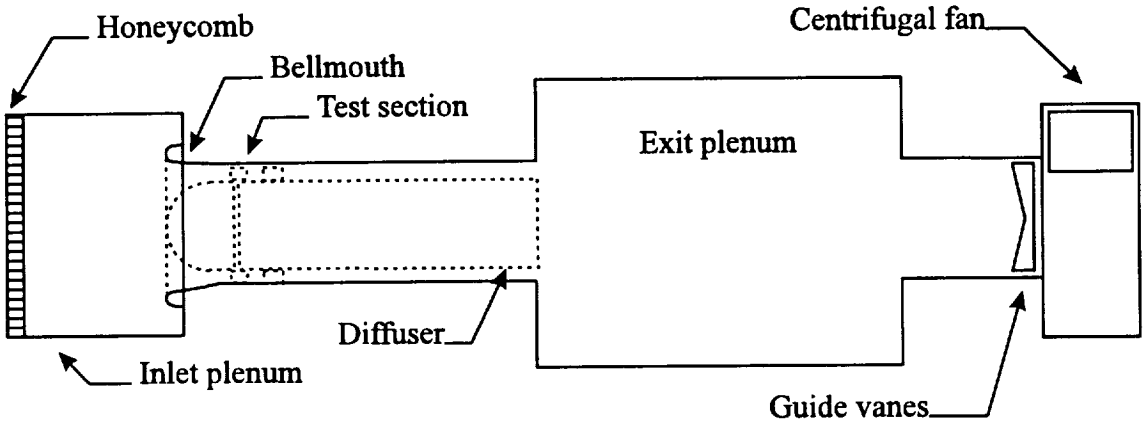

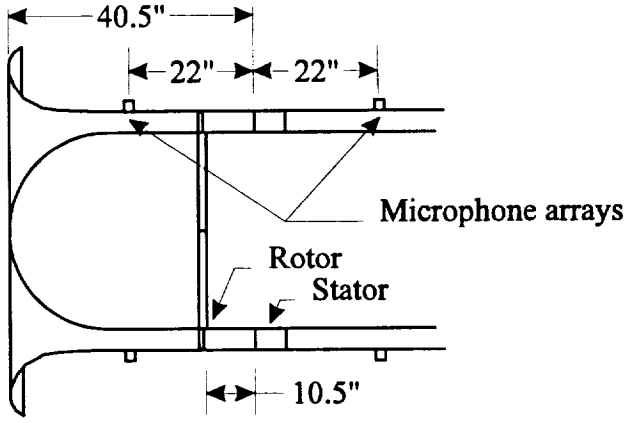

Figure 47 - Purdue Annular Cascade Facility

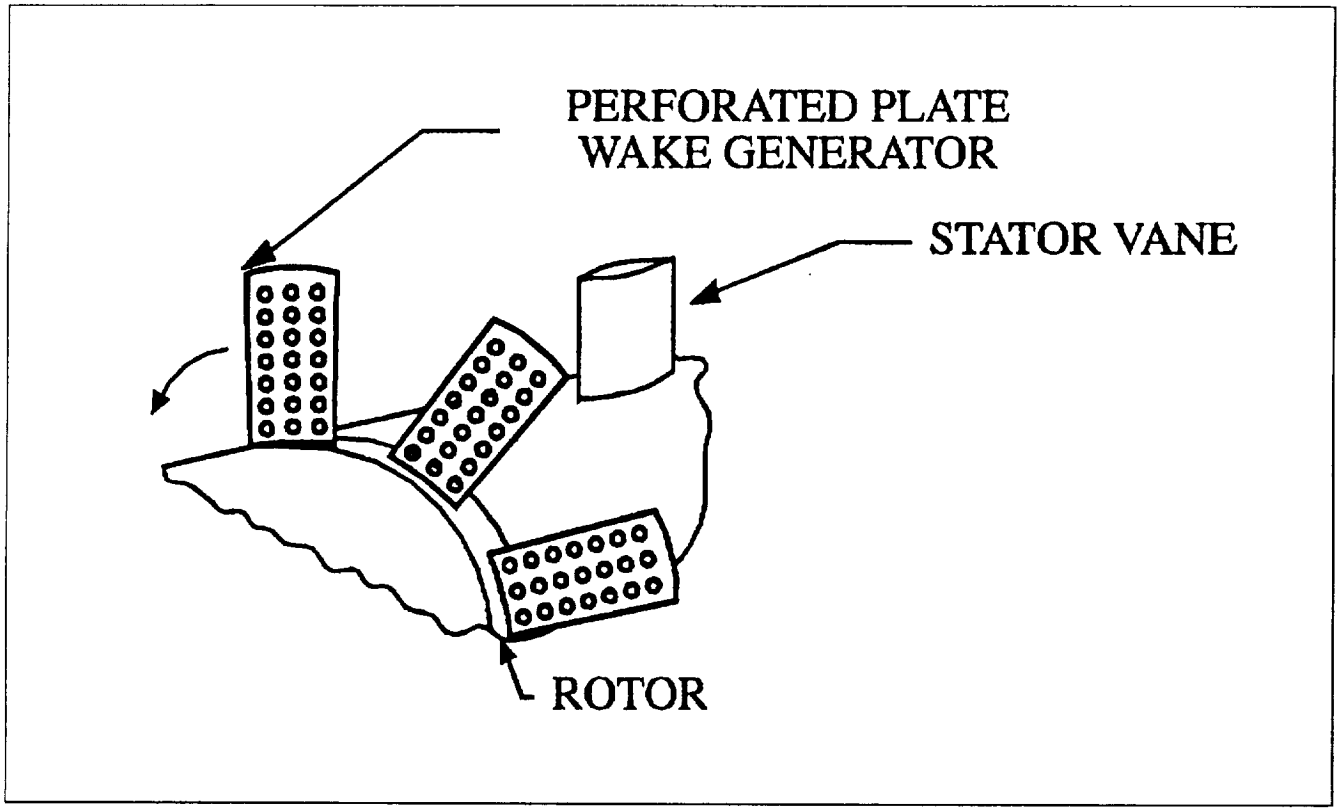

Figure 48 - Perforated Plate Rotor Mounted Perpendicular to Flow Direction

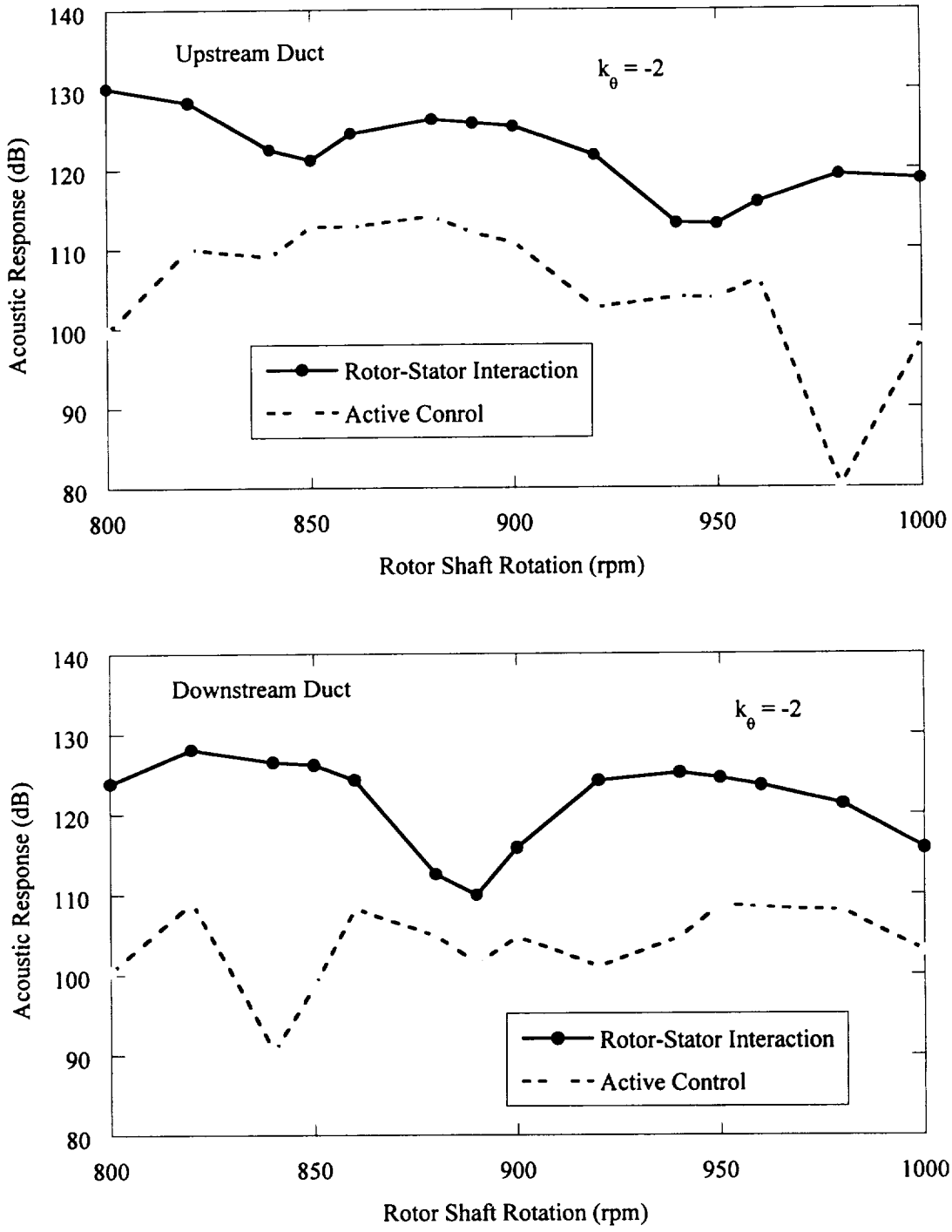

Figure 49 - Simultaneous control of upstream and downstream propagating discrete-frequency noise

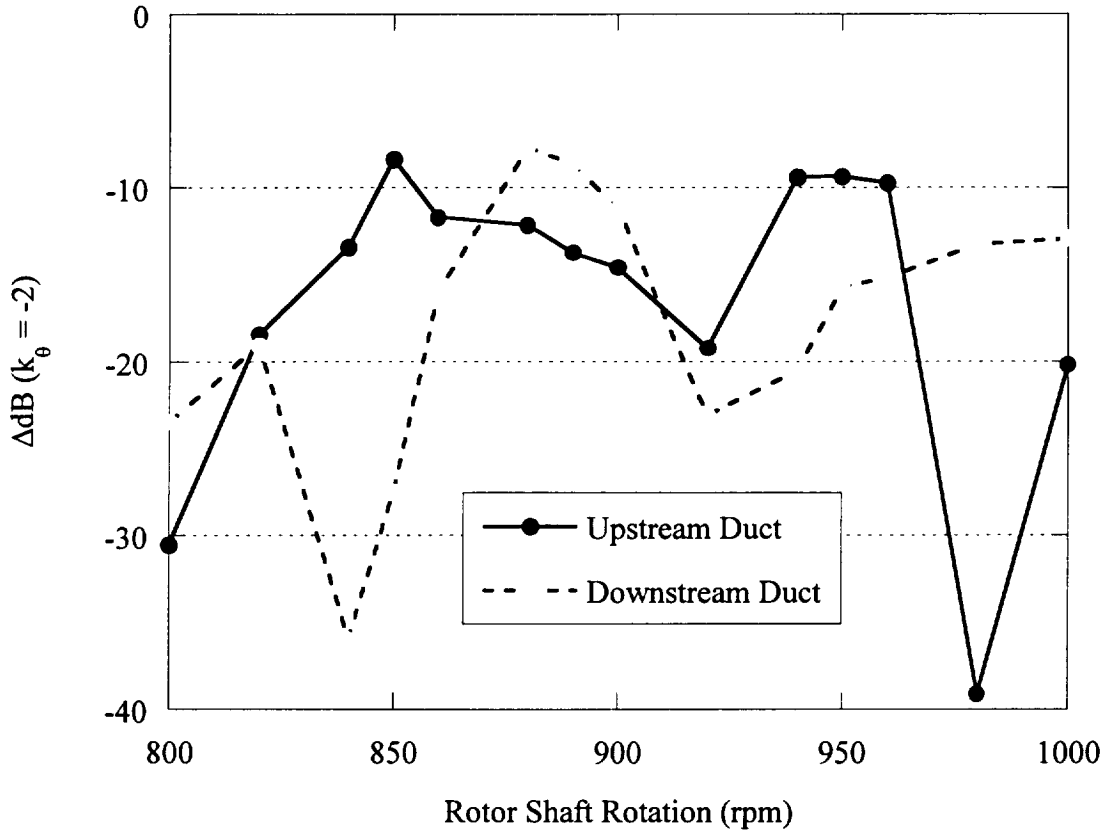

Figure 50 - Control authority demonstrated over a large range of operating conditions

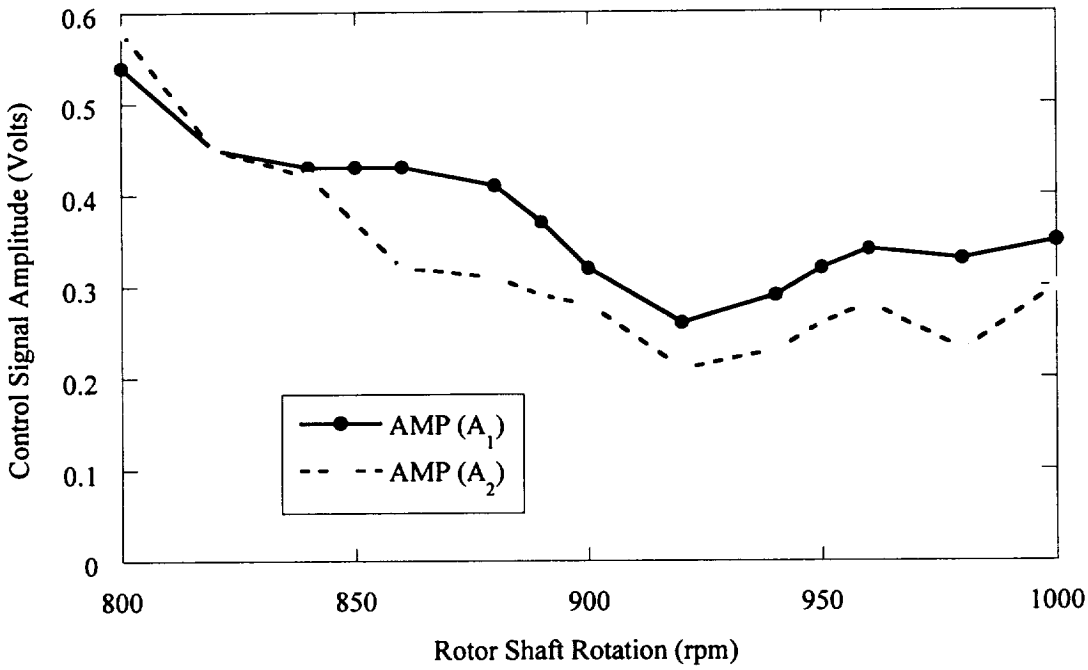

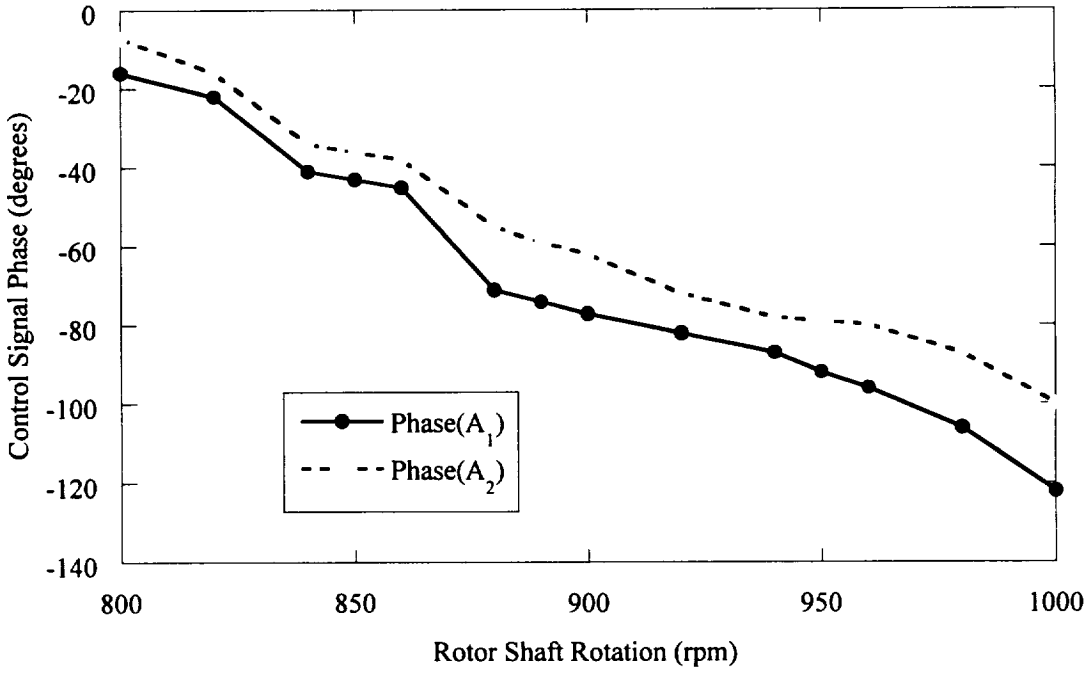

Figure 51 - Control signal voltage amplitude and phase as a function of rotor shaft rotation

REPORT DOCUMENTATION PAGE

Form Approved
OMB No. 0704-0188

1. AGENCY USE ONLY (*Leave blank*)	2. REPORT DATE	3. REPORT TYPE AND DATES COVERED
	September 1997	Final Contractor Report

4. TITLE AND SUBTITLE

Low Speed, 2–D Rotor/Stator Active Noise Control at the Source Demonstration

5. FUNDING NUMBERS

WU–538–03–11
C–NAS3–26618

6. AUTHOR(S)

John C. Simonich, Ken A. Kousen, Anthony C. Zander, Michael Bak, and David A. Topol

7. PERFORMING ORGANIZATION NAME(S) AND ADDRESS(ES)

United Technologies Research Center
East Hartford, Connecticut

8. PERFORMING ORGANIZATION REPORT NUMBER

E–10923

9. SPONSORING/MONITORING AGENCY NAME(S) AND ADDRESS(ES)

National Aeronautics and Space Administration
Lewis Research Center
Cleveland, Ohio 44135–3191

10. SPONSORING/MONITORING AGENCY REPORT NUMBER

NASA CR–204149

11. SUPPLEMENTARY NOTES

John C. Simonich, Ken A. Kousen, Anthony C. Zander, and Michael Bak, United Technologies Research Center, East Hartford, Connecticut; David A. Topol, Pratt & Whitney, East Hartford, Connecticut. Project Manager, Laurence J. Heidelberg, Structures and Acoustics Division, NASA Lewis Research Center, organization code 5940, (216) 433–3859.

12a. DISTRIBUTION/AVAILABILITY STATEMENT

Unclassified - Unlimited
Subject Categories 07 and 71

This publication is available from the NASA Center for AeroSpace Information, (301) 621–0390.

12b. DISTRIBUTION CODE

13. ABSTRACT ***(Maximum 200 words)***

Wake/blade-row interaction noise produced by the Annular Cascade Facility at Purdue University has been modeled using the LINFLO analysis. Actuator displacements needed for complete cancellation of the propagating acoustic response modes have been determined, along with the associated actuator power requirements. As an alternative, weighted least squares minimization of the total far-field sound power using individual actuators has also been examined. Attempts were made to translate the two-dimensional aerodynamic results into three-dimensional actuator requirements. The results lie near the limit of present actuator technology. In order to investigate the concept of noise control at the source for active rotor/stator noise control at the source, various techniques for embedding miniature actuators into vanes were examined. Numerous miniature speaker arrangements were tested and analyzed to determine their suitability as actuators for a demonstration test in the Annular Cascade Facility at Purdue. The best candidates demonstrated marginal performance. An alternative concept to using vane mounted speakers as control actuators was developed and tested. The concept uses compression drivers which are mounted externally to the stator vanes. Each compression driver is connected via a tube to an air cavity in the stator vane, from which the driver signal radiates into the working section of the experimental rig. The actual locations and dimensions of the actuators were used as input parameters for a LINFLO computational analysis of the actuator displacements required for complete cancellation of tones in the Purdue experimental rig. The actuators were designed and an arrangement determined which is compatible with the Purdue experimental rig and instrumentation. Experimental tests indicate that the actuators are capable of producing equivalent displacements greater than the requirements predicted by the LINFLO analysis. The acoustic output of the actuators was also found to be unaffected by the presence of air flow representative of the Purdue experimental rig. A test of the active noise control at the source concept for rotor/stator active noise control was demonstrated. This 2–D test demonstrated conclusively the simultaneous reduction of two acoustic modes. Reductions of over 10 dB were obtained over a wide operating range.

14. SUBJECT TERMS	15. NUMBER OF PAGES
Active noise control ducted fans; Engine noise aeroacoustics; Aircraft noise	80
	16. PRICE CODE: A05

17. SECURITY CLASSIFICATION OF REPORT	18. SECURITY CLASSIFICATION OF THIS PAGE	19. SECURITY CLASSIFICATION OF ABSTRACT	20. LIMITATION OF ABSTRACT
Unclassified	Unclassified	Unclassified	